Chapter 3: Observations: Ocean

Coordinating Lead Authors: Monika Rhein (Germany), Stephen R. Rintoul (Australia)

Lead Authors: Shigeru Aoki (Japan), Edmo Campos (Brazil), Don Chambers (USA), Richard Feely (USA), Sergey Gulev (Russia), Gregory C. Johnson (USA), Simon A. Josey (UK), Andrey Kostianoy (Russia), Cecilie Mauritzen (Norway), Dean Roemmich (USA), Lynne Talley (USA), Fan Wang (China)

Contributing Authors: Michio Aoyama, Molly Baringer, Nicholas R. Bates, Timothy Boyer, Robert Byrne, Sarah Cooley, Stuart Cunningham, Thierry Delcroix, Catia M. Domingues, John Dore, Scott Doney, Paul Durack, Rana Fine, Melchor González-Dávila, Simon Good, Nicolas Gruber, Mark Hemer, David Hydes, Masayoshi Ishii, Stanley Jacobs, Torsten Kanzow, David Karl, Alexander Kazmin, Samar Khatiwala, Joan Kleypas, Kitack Lee, Eric Leuliette, Calvin Mordy, Jon Olafsson, James Orr, Alejandro Orsi, Geun-Ha Park, Igor Polyakov, Sarah G. Purkey, Bo Qiu, Gilles Reverdin, Anastasia Romanou, Raymond Schmitt, Koji Shimada, Lothar Stramma, Toshio Suga, Taro Takahashi, Toste Tanhua, Sunke Schmidtko, Karina von Schuckmann, Doug Smith, Hans von Storch, Xiaolan Wang, Rik Wanninkhof, Susan Wijffels, Philip Woodworth, Igor Yashayaev, Lisan Yu

Review Editors: Howard Freeland (Canada), Silvia Garzoli (USA), Yukihiro Nojiri (Japan)

Date of Draft: 5 October 2012

Notes: TSU Compiled Version

Table of Contents

Executive Summary **3**
3.1 Introduction **6**
3.2 Changes in Ocean Temperature and Heat Content **6**
3.2.1 Background: Instruments and Sampling *6*
3.2.2 Upper Ocean Temperature *7*
3.2.3 Upper Ocean Heat Content *8*
3.2.4 Deep Ocean Temperature and Heat Content *9*
3.2.5 Conclusion *10*
Box 3.1: Change in Global Energy Inventory **10**
3.3 Changes in Salinity and the Freshwater Budget **11**
3.3.1 Introduction *11*
3.3.2 Global to Basin-Scale Trends *12*
3.3.3 Regional Changes in Salinity *13*
3.3.4 Evidence for Change of the Global Water Cycle from Salinity *14*
3.3.5 Conclusion *15*
3.4 Changes in Ocean Surface Fluxes **15**
3.4.1 Introduction *15*
3.4.2 Air-Sea Heat Flux *15*
3.4.3 Ocean Surface Precipitation and Freshwater Flux *17*
3.4.4 Wind Stress *18*
3.4.5 Changes in Surface Waves *19*
3.4.6 Conclusions *20*
3.5 Changes in Water-Mass Properties and Ventilation **20**
3.5.1 Introduction *20*
3.5.2 North Atlantic Deep Water (NADW) *20*
3.5.3 North Pacific Intermediate Water (NPIW) and Subtropical Mode Water (STMW) *21*
3.5.4 Southern Ocean *21*
3.5.5 Conclusions *22*
3.6 Changes in Ocean Circulation **22**

3.6.1 Observing Ocean Circulation Variability *22*
3.6.2 Wind-Driven Circulation Variability in the Pacific Ocean *23*
3.6.3 The Atlantic Meridional Overturning Circulation (AMOC) *24*
3.6.4 The Antarctic Meridional Overturning Circulation *26*
3.6.5 Water Exchange Between Ocean Basins *26*
3.6.6 Conclusion *27*
3.7 Sea Level Change, Including Extremes **27**
3.7.1 Introduction and Overview of Sea Level Measurements *27*
3.7.2 Trends in Global Mean Sea Level and Components *28*
3.7.3 Regional Patterns of Sea Level Change *30*
3.7.4 Observations of Accelerations in GMSL *31*
3.7.5 Changes in Extreme Sea Level *32*
3.7.6 Conclusions *32*
3.8 Ocean Biogeochemical Changes, Including Anthropogenic Ocean Acidification **34**
3.8.1 Ocean Carbon *34*
3.8.2 Anthropogenic Ocean Acidification *36*
Box 3.2: Ocean Acidification **37**
3.8.3 Oxygen *39*
3.8.4 Regional and Long-Term Trends in Nutrient Distributions in the Oceans *40*
3.8.5 Summary *40*
3.9 Synthesis **41**
FAQ 3.1: Is the Ocean Warming? **42**
FAQ 3.2: How Does Anthropogenic Ocean Acidification Relate to Climate Change? **44**
FAQ 3.3: Is There Evidence for Changes in the Earth's Water Cycle? **45**
References **47**
Figures **62**

Executive Summary

It is *virtually certain* that the upper ocean has warmed since 1971, when observations covering most of the global upper ocean became available. *Confidence* in this assessment is *high* based on the high level of agreement between independent observations of subsurface temperature [3.2], sea surface temperature [2.2.2], and sea level rise, which is known to include a substantial component due to thermal expansion [3.7, Chapter 13]. Largest warming is found near the sea surface (>0.1°C per decade in the upper 75 m), decreasing to about 0.015°C per decade by 700 m, for the time period 1971 to 2010. The surface intensification of the warming signal increased the thermal stratification of the upper ocean by about 4% (between 0 and 200 m depth) over that time period. Instrumental biases in historical upper ocean temperature measurements have been identified and mitigated, reducing a spurious decadal variation in temperature and upper ocean heat content present in analyses included in AR4. [3.2.2, Figure 3.1, FAQ3.1]

Upper ocean (0–700 m) heat content *very likely* increased at a rate between 74 [43 to 105] TW and 137 [120 to 154] TW for the relatively well-sampled 40-year period from 1971–2010. While not all published rates of energy gain agree within their statistical uncertainties, all are positive, and all are statistically different from zero. The largest difference between estimates comes from the treatment of areas with sparse data; the smaller trends are from estimates that assume no change in these regions. [3.2.3, Figure 3.2]

It is *likely* that the deep ocean has warmed below 3000-m depth since the 1990s. The global ocean has warmed at a rate of <0.01°C per decade below 4000 m over this time interval. It is *very likely* that the Southern Ocean has warmed throughout the full ocean depth since the 1990s, at a rate of about 0.03°C per decade. Warming of the global ocean below 4000 m and the Southern Ocean below 1000 m combined amount to a heating rate of 48 [21 to 75] TW between 1992 and 2005. Sparse sampling of the deep ocean means that there is less confidence in estimates of heat content change there than in the upper ocean. [3.2.4, Figure 3.3]

It is *virtually certain* that ocean warming dominates the global energy change inventory. Warming of the ocean accounts for more than 90% of the extra energy stored by Earth between 1971 and 2010; melting ice (including Arctic sea ice, ice sheets, and glaciers) and warming of the continents and atmosphere account for the remainder. [Box 3.1]

It is *very likely* that the mean regional pattern of sea surface salinity has been enhanced since the 1960s: saline surface waters in the evaporation-dominated mid-latitudes have become more saline, while the relatively fresh surface waters in rainfall-dominated tropical and polar regions have become fresher. Similarly, it is *very likely* that the interbasin contrast between saline Atlantic and fresh Pacific surface waters has increased. These patterns are *very likely* caused by an intensification of the water cycle as the lower atmosphere has warmed, reflecting the expected and observed increased water vapour content of the warmer air [2.5]. A similar conclusion was reached in AR4. The more recent studies, based on expanded data sets and new analysis approaches, have substantially increased the level of confidence in the inferred change in the global water cycle. [3.3.2, Figure 3.4, FAQ 3.3]

There is *medium confidence* that salinity has also changed in the ocean interior. The formation of salinity anomalies on density surfaces has likely resulted from changes in freshwater flux as recorded by changes in surface salinity and from the migration of surface density outcrops caused by surface warming (e.g., to regions of lower or higher surface salinity). [3.3.2–3.3.4, Figures 3.5 and 3.9]

Uncertainties in currently available surface flux products are too large to allow detection of the very small change in global mean net heat flux (order 0.5 W m^{-2} since 1971) expected from observed ocean heat content changes. The products cannot yet be reliably used to identify trends in the regional or global distribution of evaporation or precipitation over the oceans on the timescale of the observed salinity changes since the 1960s. There is *medium confidence* that wind stress over the Southern Ocean has increased since the early 1980s, based on agreement between atmospheric reanalyses, satellite observations and island station data. Mean significant wave height has *likely* increased since the 1950s over much of the mid-latitude North Atlantic and North Pacific, with winter season trends of 8 to 20 cm per decade, although confidence is limited by the lack of observations. Mean significant wave height (SWH) likely increased by up to 2.5–5%

per decade over much of the Southern Ocean since the mid-1980s, with the strongest changes between 80°E–160°W. [3.4, Figures 3.6–3.8]

Observed changes in water mass properties *likely* reflect the combined effect of long-term trends (e.g., warming of the surface ocean and changes in the hydrological cycle) and interannual-to-multidecadal variability related to climate modes like ENSO, NAO and SAM, but these observations are too sparse in space and time to distinguish trends from natural variability. Strong variability in the temperature and salinity of the source waters of North Atlantic Deep Water is observed, but there is *no evidence* of long-term trends in formation rates or transports. The observed weakening in the formation rate of Labrador Sea Water from 1997 to 2005 is *likely* related to the NAO. A freshening trend in the dense overflow waters in the North Atlantic, highlighted in AR4, reversed in the mid-1990s. Warming and lower oxygen observed in the North Pacific Intermediate Water *likely* reflect a reduction in ventilation. [3.5, Figure 3.9]

Recent observations have strengthened evidence for variability in major ocean circulation systems on time scales from years to decades. It is *very likely* that the subtropical gyres in the North Pacific and South Pacific have expanded and strengthened since 1993. It is about *as likely as not* that this reflects a decadal oscillation linked to changes in wind forcing, including changes in winds associated with the modes of climate variability. As found in AR4, there is no evidence for a long-term trend in the AMOC. There is also no evidence for trends in the transports of the Indonesian Throughflow, the Antarctic Circumpolar Current, or between the Atlantic and Nordic Seas. [3.6, Figures 3.10, 3.11]

It is *virtually certain* that globally mean sea level (GMSL) has risen at a mean rate between 1.4 to 2.0 mm yr^{-1} over the 20th Century and between 2.7 and 3.7 mm yr^{-1} since 1993 (99% confidence limits). This assessment is based on high agreement between multiple studies using different methods and independent observing systems (tide gauges and altimetry) since 1993. It is *likely* that GMSL rose between 1930 and 1950 at a rate comparable to that observed since 1993, possibly due to a multidecadal climate oscillation, as individual tide gauges around the world and reconstructions of GMSL show increased rates of sea level rise during this period. High agreement between studies with and without corrections for land motion suggests that it is *very unlikely* that estimates of the global average rate of sea level change are affected by land motion. [3.7.2, 3.7.3, Table 3.1, Figures 3.12, 3.13]

It is *very likely* that warming of the upper 700 m has been contributing an average of 0.6 [0.4 to 0.8] mm yr^{-1} of sea level change since 1971. It is *likely* that warming between 700m and 2000m has been contributing an additional 0.1 mm yr^{-1} [0 to 0.2] of sea level rise since 1971, and that warming below 2000 m has been contributing another 0.11 [0.01 to 0.21] mm yr^{-1} of sea level rise since the early 1990s. It is *virtually certain* that the ocean mass has increased, at a rate *very likely* in the range [0.8 to 1.6] mm yr^{-1} since 2005, based on high agreement between estimates based on satellite gravity measurements over the same six-year period and those computed from altimeter sea level measurements after removing steric variations. [3.7.2, Table 3.1, Figure 3.13]

Two out of three reconstructions of GMSL from tide gauge data extending back to 1900 or earlier indicate non-zero acceleration. Estimates range from 0.000 to 0.013 [–0.002 to 0.019] mm yr^{-2}, so it is *likely* that GMSL rise has accelerated since the early 1900s. It is *very likely* that the rate of mean sea level rise along Northern European coastlines has accelerated since the early 1800s and that the increased rate of sea level rise has continued into the 20th Century, as the signal has been observed in multiple long tide gauge records and by different groups using different analysis techniques. Many more long (> 60 year) tide gauge records around the world show the increased rate of sea level rise since 1900. Finally, it is *likely* that extreme sea levels have increased since 1970, and this is mainly attributable to rising mean sea level. [3.7.4, 3.7.5, Figure 3.14]

Based on high agreement between estimates using different approaches (e.g., oceanic carbon, nutrient, or tracer data), there is *very high confidence* that the global ocean inventory of anthropogenic carbon (C_{ant}) increased from 1994 to 2010. The C_{ant} inventory was estimated to be between 93–137 PgC in 1994, and 155 [125 to 185] PgC in 2010. The 2010 inventory corresponds to an annual global uptake rate of 2.3 [1.7 to 2.9] PgC yr^{-1}, in agreement with carbon uptake rates calculated from atmospheric O_2/N_2 measurements (2.5 [1.8 to 3.2] PgC yr^{-1}). [3.8.1, Figures 3.15, 3.16]

There is *very high confidence* that oceanic uptake of anthropogenic CO_2 has resulted in gradual acidification of seawater and decreasing pH (i.e., anthropogenic ocean acidification) in surface waters. The observed pH trends range between –0.0015 and –0.0024 per year. In the ocean interior, pH can also be modified by natural physical and biological processes over decadal time scales. [3.8.2, Table 3.2, Box 3.2, Figures 3.17, 3.18, FAQ 3.2]

Analyses of the limited oxygen observations available since 1960 show high agreement that oxygen concentrations have decreased over much of the open ocean thermocline since the 1960s. The rate of decrease was about 3–5 μmol kg^{-1} $decade^{-1}$, with strong regional differences. This is consistent with the expectation that warmer waters can hold less oxygen, and that warming-induced stratification leads to a decrease in the supply of oxygen to the thermocline from near surface waters. It is *likely* that the tropical oxygen minimum zones have expanded in recent decades. [3.8.3, Figure 3.19]

Taken together, the observations summarized in this chapter provide strong evidence that the physical and biogeochemical state of the oceans has changed during the past forty years. The consistency of the observed patterns of change with known physical and biogeochemical processes in the ocean enhances the level of confidence associated with this conclusion. [3.9, Figures 3.20, 3.21]

3.1 Introduction

The oceans influence climate by storing and transporting vast quantities of heat, freshwater, and carbon around the globe, and exchanging these properties with the atmosphere. The ocean has a large thermal inertia, both because of the large heat capacity of sea water relative to air and because ocean circulation connects the surface and interior ocean. More than three quarters of the total exchange of water between the atmosphere and the earth's surface through evaporation and precipitation takes place over the oceans (Schmitt, 2008). The ocean contains 50 times more carbon than the atmosphere (Sabine et al., 2004) and is at present absorbing one quarter of human emissions of carbon dioxide (Mikaloff-Fletcher et al., 2006; Le Queré et al., 2010), acting to slow the rate of climate change. The ocean also slows the rate of climate change by storing large amounts of heat. Changes in the ocean may result in climate feedbacks that increase or reduce the rate of climate change. The evolution of climate on time-scales from seasons to millennia is therefore closely linked to the ocean.

The large inertia of the oceans means that they naturally integrate over short-term variability and often provide a clearer signal of longer-term change than other components of the climate system. Observations of ocean change therefore provide a means to track the evolution of climate change. Such observations also provide a rigorous and relevant test for climate models.

Documenting and understanding change in the ocean remains a challenge because of the paucity of long-term measurements of the global ocean and because measurement techniques and sampling coverage have changed over time. Many of the issues raised in Box 2.1 regarding uncertainty in atmospheric climate records are common to oceanographic data. Despite the limited records, AR4 reported trends in ocean heat content, sea level, regional patterns of salinity, and biogeochemical parameters. The historical data sets at the heart of these conclusions are now being extended with much more comprehensive global observations. The Argo array of profiling floats is now providing year-round measurements of temperature and salinity in the upper 2000 m for the first time. The satellite altimetry record is now approaching twenty years in length. Longer continuous time series of important components of the meridional overturning circulation are being collected. While these recent data sets do not solve the problem of a lack of historical data, by documenting the seasonal and interannual variability they help estimate longer-term trends and their uncertainties from the incomplete observational record. Significant progress has also been made in reducing biases and errors in the historical measurements. The spatial and temporal coverage of biogeochemical measurements in the ocean has expanded. As a result of these advances, there is now stronger evidence for change in the ocean and our understanding of the causes of ocean change is improved.

This chapter summarizes the observational evidence of change in the ocean, with an emphasis on basin- and global-scale changes relevant to climate. Section 3.2 discusses observed changes in ocean temperature and heat content (sea surface temperature changes are covered in Chapter 2), the major contributor to global energy inventory changes (Box 3.1). Changes in ocean salinity and implications for the global water cycle are discussed in Section 3.3. Observed changes in ocean properties are related to changes in fluxes of heat, water and momentum (wind stress) across the air-sea interface (Section 3.4). Considering ocean changes from a water-mass perspective adds additional insight into the nature and causes of ocean change (Section 3.5). Evidence for changes in ocean circulation is considered in Section 3.6. Observations of sea level change are summarized in Section 3.7; Chapter 13 builds on the evidence presented in this and other chapters to provide an overall synthesis of past and future sea level change. Biogeochemical changes in the ocean, including ocean acidification, are covered in Section 3.8. Chapter 6 combines observations with models to discuss past and present changes in the carbon cycle. Section 3.9 provides an overall synthesis of changes observed in the ocean during the instrumental period. As in Chapter 2, the robustness of observed changes are assessed relative to sources of observational uncertainty. The issue of detection and attribution of ocean change, including the degree to which the observed changes are consistent with anthropogenic climate change, is addressed in Chapter 10.

3.2 Changes in Ocean Temperature and Heat Content

3.2.1 Background: Instruments and Sampling

Temperature is the most often measured subsurface ocean property. Historically, a variety of instruments have been used to measure temperature, with differing accuracies, precisions, and sampling depths. Both the mix of instruments and the overall sampling patterns have changed in time and space (Boyer et al., 2009), complicating efforts to determine and interpret long-term change. Since AR4 the significant impact of measurement biases in some of these instruments (the expendable (XBT) and mechanical bathythermograph (MBT)) on estimates of ocean temperature and upper (0–700 m) ocean heat content (hereafter UOHC) changes has been recognized (Gouretski and Koltermann, 2007). Careful comparison of measurements from the less accurate instruments with those from the more accurate ones has allowed some of the biases to be identified and mitigated (Gouretski and Reseghetti, 2010; Ishii and Kimoto, 2009; Levitus et al., 2009; Wijffels et al., 2008). One major consequence of this bias mitigation has been the reduction of an artificial decadal variation in upper ocean heat storage that was apparent in the observational assessment for AR4, in notable contrast to climate model output (Domingues et al., 2008). Data used in AR4 included substantial time-dependent XBT and MBT instrument biases that introduced a spurious warming in the 1970s and cooling in the early 1980s. Most ocean state estimates that assimilate biased data (Carton and Santorelli, 2008) also showed this artificial decadal variability while one (Stammer et al., 2010) apparently rejected these data on dynamical grounds. More recent estimates assimilating better-corrected data sets (Giese et al., 2011) also result in reduced decadal variability.

Recent estimates of upper ocean temperature change also differ in their treatment of unsampled regions. Some studies (e.g., Ishii and Kimoto, 2009; Smith and Murphy, 2007) effectively assume no temperature anomaly in these regions, while other studies (Lyman and Johnson, 2008; Palmer et al., 2007) assume that the averages of sampled regions are representative of the global mean in any given year, and yet others (Domingues et al., 2008) use ocean statistics (from satellite altimeter data) to extrapolate anomalies to sparsely sampled areas and estimate uncertainties. These differences in approach can lead to significant divergence in areal averages in sparsely sampled regions (e.g., the extra-tropical Southern Hemisphere prior to Argo), and as a result can produce different global averages. However, for well-sampled regions and times, the various analyses of temperature changes cited above yield consistent results, as do reanalyses (Xue et al., 2012).

Upper ocean temperature (hence heat content) varies significantly over multiple time-scales ranging from seasonal (e.g., Roemmich and Gilson, 2009) to decadal (e.g., Carson and Harrison, 2010), as do ocean data assimilation products using these data (e.g., Xue et al., 2012). Given the close relation between ocean warming and sea level rise, together with the evidence of decadal and longer time-scale variability in global sea level rise (see Section 3.7), it is *virtually certain* that upper ocean heat content also varies on these longer time-scales.

Sparse historical sampling coupled with large amplitude variations on shorter time and spatial scales raise challenges for estimating globally averaged temperature changes. However, an uncertainty analysis making use of well-resolved satellite sea-surface height data and exploiting its relation to UOHC indicates that the historical data set begins to be reasonably well suited for this purpose starting around 1970 (Lyman and Johnson, 2008). Uncertainty estimates from other UOHC studies (e.g., Domingues et al., 2008; Palmer and Brohan, 2011), with annual values that shrink as sampling improves around 1970, support this conclusion, so this assessment focuses on changes since 1971.

3.2.2 Upper Ocean Temperature

Zonally averaged upper ocean temperature trends from 1971–2010 show warming at nearly all latitudes and depths (Figure 3.1b), with the exception of four small bands of cooling. The warming is more prominent in the northern hemisphere, especially the North Atlantic (Figure 3.1a), a result robust with respect to different analyses, time periods, and bias corrections (e.g., Figure 3.10; Palmer et al., 2007). However, the greater volume of the Southern Ocean increases the contribution of its warming to global heat content. A maximum in warming south of 30°S is present but not as strong as in other analyses (e.g., Gille, 2008), likely because the data are relatively sparse in this location and because much of the Southern Ocean warming occurred between the 1930s and the 1970s. Another maximum is present at 25–65°N. Both extend to 700 m (Levitus et al., 2009, Figure 3.1b). The warming is broadly consistent with poleward displacement of the mean temperature field. The warming observed in the upper Southern Ocean is thought to be at least partly owing to southward shifts of the Antarctic Circumpolar Current that are in turn largely driven by southward

migration and intensification of the westerly winds (Böning et al., 2008; Gille, 2008; Sokolov and Rintoul, 2009). Other zonally-averaged temperature changes, for example cooling between 30°S and the equator (Figure 3.1b), are also consistent with poleward displacement of the mean field. That is, where the mean temperature field cools toward the pole, a poleward displacement would cause warming, and vice versa.

Globally averaged ocean temperature anomalies as a function of depth and time (Figure 3.1c) relative to a 1971–2010 mean reveal warming at all depths in the upper 700 m over the relatively well-sampled 40-year time-period considered. Strongest warming is found closest to the sea surface, and the near-surface record is consistent with independently measured sea surface temperature (Chapter 2). The global average warming over this period exceeds 0.1°C per decade in the upper 75 m, decreasing to 0.015°C per decade by 700 m (Figure 3.1c). Comparison of Argo data to Challenger expedition data from the 1870s suggests that warming started earlier than 1971 (Roemmich et al., 2012).

A time-series of globally averaged temperature difference from 0 to 200 m (Figure 3.1d) shows thermal stratification has increased by about 4% over the 40-year record. An increase in thermal stratification is widespread in all the oceans, except the Southern Ocean south of about 40°S, based on the Levitus et al. (2009) temperature anomaly fields.

[INSERT FIGURE 3.1 HERE]

Figure 3.1: a) Depth-averaged 0–700 m temperature trend for 1971–2010 (longitude vs. latitude, colors and grey contours in °C per decade)**. b)** Zonally-averaged temperature trends (latitude versus depth, colors and grey contours in °C per decade) for 1971–2010, with zonally averaged mean temperature over-plotted (black contours in °C). **c)** Globally-averaged temperature anomaly (time versus depth, colors and grey contours in °C) relative to the 1971–2010 mean. **d)** Globally-averaged temperature difference between the ocean surface and 200-m depth (black: annual values, red: 5-year running mean). All plots are constructed from the annual analysis of Levitus et al. (2009).

A potentially important impact of ocean warming is the effect on sea ice, floating glacial ice, and ice sheet dynamics (see Chapter 4). Warm ocean waters have been linked to increased melt of outlet glaciers in both Greenland (Holland et al., 2008; Straneo et al., 2010) and Antarctica (Jacobs et al., 2011; Rignot et al., 2008; Shepherd et al., 2004; Wahlin et al., 2010). Thinning of 20 out of 54 Antarctic ice shelves was attributed to ocean-driven melting, with the most widespread and rapid losses observed in West Antarctica, while atmospheric warming contributed to thinning of ice shelves on the Antarctic Peninsula (Pritchard et al., 2012). In the Arctic Ocean, subsurface pulses of relatively warm water of Atlantic origin can be traced around the Eurasian Basin from 2003–2005 (Dmitrenko et al., 2008), their warmth intensifying further through 2007 (Polyakov et al., 2010b) before decreasing somewhat by 2009 (Polyakov et al., 2012). This warming Atlantic Water has also shoaled, by 75–90 m, in the water column, and model results suggest that it might be affecting melting of sea ice (Polyakov et al., 2010a). Arctic surface waters have warmed, likely from changes in albedo from 1993 to 2007 due to the sea ice melt, which may be driving further reductions in sea ice (Jackson et al., 2010).

3.2.3 Upper Ocean Heat Content

Global integrals of 0–700-m UOHCs (Figure 3.2) have been estimated from ocean temperature measurements (e.g., Domingues et al., 2008; Ishii and Kimoto, 2009; Levitus et al., 2012; Palmer et al., 2007; Smith and Murphy, 2007) usually starting around 1950, although as noted above, historical data coverage is sparse so global integrals are increasingly uncertain for earlier years, especially prior to 1970. There is some convergence towards instrument bias correction since AR4, but other sources of uncertainty include the different assumptions regarding mapping and integrating UOHCs in sparsely sampled regions, differences in quality control of temperature data, and differences among baseline climatologies used for estimating changes in heat content (Lyman et al., 2010). Although there are still apparent interannual variations about the upward trend of global UOHC since 1970, different global estimates have variations at different times and for different periods, suggesting that sub-decadal variability in the time rate of change is still quite uncertain in the historical record.

All of the estimates in Figure 3.2 show that global integrals of UOHCs have increased from at least 1970 to the present. Fitting linear trends to UOHC estimates for the relatively well-sampled 40-year period from 1971–2010 yields a power of 118 [82 to 154] TW (1 TW = 10^{12} W) for Levitus et al. (2012), 82 [67 to 97]

TW for Ishii and Kimoto (2009), 137 [120 to 154] TW for Domingues et al. (2008), 108 [80 to 136] TW for Palmer et al. (2007), and 74 [43 to 105] TW for Smith and Murphy (2007). Uncertainties are calculated as 90% confidence intervals for an ordinary least squares fit, taking into account the reduction in the degrees of freedom implied by the temporal correlation of the residuals. While these rates of energy gain do not all agree within their statistical uncertainties, all are positive, and all are statistically different from zero. Generally the smaller trends are for estimates that assume no anomalies in areas of sparse data, as expected.

[INSERT FIGURE 3.2 HERE]

Figure 3.2: Observation-based estimates of annual global mean upper (0–700 m) ocean heat content in ZJ (1 ZJ = 10^{21} J) updated from (see legend): L12 (Levitus et al., 2012), I09 (Ishii and Kimoto, 2009), D08 (Domingues et al., 2008), P07 (Palmer et al., 2007), and S07 (Smith and Murphy, 2007), Uncertainties for each estimate (except for S07) are shaded, and plotted as published (at the one standard error level, except one standard deviation for L12, with no uncertainties provided for S07). Estimates are shifted to align for 2006–2010, 5 years of overlap well measured by Argo, and then plotted relative to the resulting mean of all curves for 1971, the starting year for trend calculations.

3.2.4 Deep Ocean Temperature and Heat Content

Below 700 m data coverage is too sparse to produce annual global ocean heat content estimates prior to about 2005, after which Argo coverage extends the range to at least 1500 m (von Schuckmann and Le Traon, 2011). Pentadal estimates yield a 700–2000 m global ocean heat content trend from 1957 to 2009 that is about 30% of that for 0–2000 m (Levitus et al., 2012). Global sampling of the ocean below 2000 m is limited to a number of repeat oceanographic transects, many occupied only in the last few decades, and several time-series stations, some of which extend over decades. This sparse sampling in space and time makes assessment of global deep ocean heat content variability less certain than that for the upper ocean, especially at mid-depths, where vertical gradients are still sufficiently large for transient variations (ocean eddies, internal waves, and internal tides) to alias estimates made from sparse data sets. Nevertheless, there is sufficient information to conclude that the warming of the global ocean from circa 1992–2005 is *likely* not distinguishable from zero between 2000 and 3000 m depth, but is greater than zero from 3000 m to the ocean floor (Figure 3.3a; Kouketsu et al., 2011).

[INSERT FIGURE 3.3 HERE]

Figure 3.3: a) Areal mean warming rates versus depth (thick lines) with 95% confidence limits (shading), both global (orange) and for the Southern Ocean south of the Sub-Antarctic Front SAF (purple). **b)** Mean warming rate below 4000 m (colorbar) estimated for deep ocean basins (thin black outlines) and centred on 1992–2005. Stippled basin warming rates are not significantly different from zero at 95% confidence. The mean warming rate for 1000–4000 m south of the SAF (purple line) is also given (purple number) with its 95% confidence interval. Data from Purkey and Johnson (2010).

In the Southern Ocean, much of the water column warmed between 1992 and 2005 (Purkey and Johnson, 2010). The deep warming outside the Southern Ocean is largest near the sea floor (i.e., below 4000 m), which is ventilated by sinking of Antarctic Bottom Water (AABW) around Antarctica (Orsi et al., 1999). The rate of warming is largest in basins that are effectively ventilated by AABW, and attenuates towards the north (Figure 3.3b).

The warming of the global abyssal ocean below 4000 m depth and the Southern Ocean below 1000 m combined amount to a heating rate of 48 [21 to 75] TW, centred on 1992–2005 (Purkey and Johnson, 2010). This 90% uncertainty estimate may be too small, since they assume the usually sparse sampling in each deep ocean basin analysed is representative of the mean trend in that basin. Global scale abyssal warming on relatively short multi-decadal time-scales is possible because of teleconnections established by planetary waves originating within the Southern Ocean, reaching even such remote regions as the North Pacific (Kawano et al., 2010; Masuda et al., 2010).

In the North Atlantic, strong decadal variability in North Atlantic Deep Water (NADW) temperature and salinity (Wang et al., 2010), largely associated with the North Atlantic Oscillation (NAO) (e.g., Sarafanov et al., 2008; Yashayaev, 2007), complicates efforts to determine long-term trends from the relatively short record. In addition, there is longer multi-decadal variability in the North Atlantic Ocean heat content (e.g., Polyakov et al., 2010a).

3.2.5 Conclusion

It is *virtually certain* that the upper ocean has warmed since circa 1970, with the warming strongest near the sea surface. This result is supported by three independent and consistent methods of observation including (i) the subsurface measurements of temperature described here, (ii) sea surface temperature data (Section 2.2.2) from satellites and in situ measurements from surface drifters and ships, and (iii) the record of sea level rise, which is known to include a substantial component due to thermosteric expansion (Section 3.7 and Chapter 13). The greatest remaining uncertainty in the upper ocean temperature evolution is in the magnitude and pattern of warming at high southern latitudes. For the deep ocean, sparse sampling below 2000 m is the greatest obstacle. Strongest warming is found closest to the sea surface (>0.1°C per decade in the upper 75 m), decreasing to about 0.015°C per decade by 700 m. The surface intensification of the warming signal increases the thermal stratification of the upper ocean by about 4% (between 0 and 200 m depth) from 1971–2010. It is *likely* that global ocean warming reaches a minimum at mid-depth (roughly 2500 m) and increases below that. It is *very likely* that waters of Antarctic origin have warmed overall throughout the water column in the Southern Ocean, at a rate of about 0.03°C per decade since circa 1990, and below 4000 m at a global average rate of <0.01°C per decade over the same time period. Decadal variability in formation of North Atlantic Deep Water complicates efforts to determine long-term trends in its temperature.

[START BOX 3.1 HERE]

Box 3.1: Change in Global Energy Inventory

Earth has been in radiative imbalance, with more energy from the sun entering than exiting the top of the atmosphere, since at least circa 1970 (Church et al., 2011). Quantifying this energy gain is useful for understanding the response of the climate system to forcing. Small amounts of this excess energy warm the atmosphere and continents, evaporate water, and melt ice, but the bulk of it warms the oceans (Box 3.1, Figure 1). The ocean dominates the change in energy because of its large mass and high heat capacity compared to the atmosphere. In addition, ice-free oceans have a very low albedo and effectively absorb solar radiation.

[INSERT BOX 3.1, FIGURE 1 HERE]

Box 3.1, Figure 1: Plot of energy change inventory in ZJ (1 ZJ = 10^{21} J) within distinct components of Earth's climate system relative to 1971 and from 1971–2010 unless otherwise indicated. See text for data sources. Ocean warming dominates, with the upper ocean (light blue, above 700 m) contributing more than the deep ocean (dark blue, below 700 m; with below 2000 m starting from 1992); ice melt (light grey; for glaciers and ice caps, Greenland starting from 1992, Antarctica starting from 1992, and Arctic sea ice from 1979–2008); continental (land) warming (orange); and atmospheric warming (purple; starting from 1979) make smaller contributions. The ocean uncertainty also dominates the total uncertainty (dot-dashed lines about the sum of all five components at 90% confidence intervals).

The global atmospheric energy change inventory accounting for specific heating and water evaporation is estimated by combining satellite estimates for temperature anomalies in the lower troposphere (Mears and Wentz, 2009b; but version 3.3) from 70°S to 82.5°N and the lower stratosphere (Mears and Wentz, 2009a; but version 3.3) from 82.5°S to 82.5°N by the ratio of the portions of atmospheric mass they sample (0.87 and 0.13, respectively). These temperature anomalies are converted to energy changes using a total atmospheric mass of 5.14×10^{18} kg, a mean total water vapor mass of 12.7×10^{15} kg (Trenberth and Smith, 2005), a heat capacity of 1 J g^{-1} $°C^{-1}$, a latent heat of vaporization of 2.464 J kg^{-1}, and a fractional increase of integrated water vapor content of 0.075 $°C^{-1}$ (Held and Soden, 2006). Smaller changes in potential and kinetic energy are neglected here. Standard deviations for each year of data are used for uncertainties, and the time-series starts in 1979. The warming trend from a linear fit from 1979 to 2010 amounts to 2 TW (1 TW = 10^{12} W).

The global average rate of continental warming and its uncertainty has been estimated from borehole temperature profiles from 1500–2000 at 50-year intervals (Beltrami et al., 2002). The 1950–2000 estimate of land warming, 6 TW, is extended into the first decade of the 21st century, although that extrapolation is almost certainly an underestimate of the energy absorbed as land surface temperatures for years since 2000 are some of the warmest on record (Section 2.2.1).

All annual ice melt rates (for glaciers and ice-caps, ice sheets, and sea ice from Chapter 4) are converted into energy change using a heat of fusion (334×10^3 J kg^{-1}) and density (920 kg m^{-3}) for freshwater ice. The heat of fusion and density of ice may vary, but only slightly among the different ice types, and warming the ice from sub-freezing temperatures requires much less energy than that to melt it, so these second order effects are neglected here. The linear trend of energy storage from 1971 to 2010 is also 6 TW.

For the oceans an estimate of global upper (0–700 m depth) ocean heat content change using ocean statistics to extrapolate to sparsely sampled regions and estimate uncertainties (Domingues et al., 2008) is used (see Section 3.2), with a linear trend from 1971–2010 of 137 TW. For the ocean from 700–2000 m, annual running pentadal estimates are used from 1970–2009 and annual estimates for 2010–2011 (Levitus et al., 2012). For the ocean from 2000 m–bottom, a uniform rate of energy gain of 35 [6 to 61] TW from warming rates centred on 1992–2005 (Purkey and Johnson, 2010), is applied from 1992–2011, with no warming below 2000 m assumed prior to 1992. The linear trend for heating the ocean below 700 m is 62 TW for 1971–2010.

It is *virtually certain* that Earth has gained substantial energy from 1971–2010 — an estimated first-difference change of 273 [194 to 353] ZJ (1 ZJ = 10^{21} J), with a rate of 213 TW from a linear fit over that time period (Box 3.1, Figure 1). From 1993–2010 the estimated energy gain is from a first difference is 163 [125 to 200] ZJ with a linear rate estimate of 27 TW. Ocean warming dominates the total energy change inventory, accounting for roughly 93% on average from 1971–2010. Melting ice (including Arctic sea ice, ice sheets, and glaciers) accounts for 3% of the total, and warming of the continents 3%. Warming of the atmosphere makes up the remaining 1%. The ocean component of the 1993–2010 rate of energy gain is 257 TW, equivalent to a global mean net air-sea heat flux of 0.71 W m^{-2}, and that for 1971–2010 is 199 TW, implying a mean net air-sea heat flux of 0.55 W m^{-2}.

[END BOX 3.1 HERE]

3.3 Changes in Salinity and the Freshwater Budget

3.3.1 Introduction

The ocean plays a pivotal role in the global water cycle: 86 % of the evaporation and 78 % of the precipitation occurs over the ocean (Schmitt, 2008). The horizontal salinity distribution of the upper ocean largely reflects this exchange of freshwater, with high surface salinity generally found in regions where evaporation exceeds precipitation, and low salinity found in regions of excess precipitation (Figure 3.4a,b). Ocean circulation also affects the regional distribution of surface salinity. The subduction of surface waters transfers the surface salinity signal into the ocean interior, so that subsurface salinity distributions are also linked to patterns of evaporation, precipitation, and continental run-off at the sea surface. At high latitudes, melting and freezing of ice (both sea ice and glacial ice) can also influence salinity.

The water cycle is expected to intensify in a warmer climate, because warm air can contain more moisture. The dominant effect is due to the Clausius–Clapeyron relation: equilibrium water vapour pressure increases by about 7% per degree C (at the current global average temperature of about 14°C). On the other hand, the increase in global precipitation per unit warming has been expected to be weaker than this because of feedbacks and atmospheric dynamics (e.g., Held and Soden, 2006; Wentz et al., 2007) (Section 12.4.3). The water vapour content of the atmosphere has increased since the 1970s, at a rate consistent with the observed warming (Section 2.5, Figure 2.31). However, observations of precipitation and evaporation are sparse and uncertain, particularly over the ocean where most of the exchange of freshwater occurs. The uncertainties in some of the individual terms are so large that it is not yet possible to detect robust trends in the water cycle from these precipitation and evaporation observations (Section 3.4). Ocean salinity, on the other hand, naturally integrates the small difference between these two terms and has the potential to act as a rain gauge (Yu, 2011). Diagnosis and understanding of ocean salinity trends is also important because salinity changes, like temperature changes, affect circulation and stratification, and therefore the ocean's capacity to store heat and carbon as well as to change biological productivity. Also, like temperature changes, salinity changes affect sea level (Steele and Ermold, 2007). Salinity variations contribute more to density changes at low temperatures, hence having a greater impact at high latitudes than in the warm, low latitude oceans.

In AR4, surface and subsurface salinity changes consistent with a warmer climate were highlighted, based on linear trends for the period between 1955 and 1998 in the historical global salinity data set (Boyer et al., 2005) as well as on more regional studies. Additional observations, improvements in the availability and quality of historical data, and new analysis approaches now allow a more complete assessment of changes in salinity.

3.3.2 Global to Basin-Scale Trends

The salinity of near-surface waters is changing on global and basin scales, with increase in the more evaporative regions and decrease in the precipitation-dominant regions in almost all ocean basins. All salinity values quoted in the chapter are expressed on the Practical Salinity Scale 1978 and are unit-less.

3.3.2.1 Sea Surface Salinity

Robust multi-decadal trends in sea surface salinity have been found in studies published since AR4 (Boyer et al., 2007; Durack and Wijffels, 2010; Hosoda et al., 2009; Roemmich and Gilson, 2009), confirming the trends reported in AR4 based mainly on Boyer et al. (2005). The spatial pattern of surface salinity change is similar to the distribution of surface salinity itself: salinity tends to increase in regions of high mean salinity, where evaporation exceeds precipitation, and tends to decrease in regions of low mean salinity, where precipitation dominates (Figure 3.4). For example, the surface salinity maxima formed in the evaporation-dominated subtropical gyres have increased in salinity. The surface salinity minima at subpolar latitudes and the intertropical convergence zones have freshened. Interbasin salinity differences are also enhanced: the relatively salty Atlantic has become more saline on average, while the relatively fresh Pacific has become fresher (Durack and Wijffels, 2010) (see also Figure 3.9). No well-defined trend is found in the subpolar North Atlantic (Hosoda et al., 2009), which is dominated by decadal variability from atmospheric modes like the North Atlantic Oscillation (NAO). Fifty-year salinity trends are statistically significant at the 99% level over 43.8% of the global ocean surface (Durack and Wijffels, 2010).

[INSERT FIGURE 3.4 HERE]

Figure 3.4: a) The 1955–2005 climatological-mean surface salinity (World Ocean Atlas 2009). Contours every 0.5 are plotted in black. **b)** Annual mean Evaporation-Precipitation averaged over the period 1950–2000 (NCEP). Contours every 0.5 m yr^{-1} are plotted in black. **c**) The 50-year (2000 minus1950) surface salinity change (Durack and Wijffels, 2010) and **d**) 30-year (2005 minus 1975) surface salinity change (Hosoda et al., 2009). Contours every 0.1 are plotted in black. Regions where the change is not significant at the 99% confidence level are stippled in grey.

3.3.2.2 Upper Ocean Salinity

Changes in surface salinity are transferred into the ocean interior by subduction and flow along ventilation pathways. Compatible with observed changes in surface salinity, robust multi-decadal trends in subsurface salinity have been detected (Böning et al., 2008; Boyer et al., 2007; Boyer et al., 2005; Durack and Wijffels, 2010; Helm et al., 2010; Steele and Ermold, 2007; Wang et al., 2010). Global zonally-averaged 50-year salinity changes (1950–2000) on pressure surfaces in the upper 2000 m show increases in salinity in the salinity maxima in the upper thermocline of the subtropical gyres, freshening of the low salinity intermediate waters sinking in the Southern Ocean (Subantarctic Mode Water and Antarctic Intermediate Water) and North Pacific (North Pacific Intermediate Water) (Durack and Wijffels, 2010; Helm et al., 2010), freshening of the upper water column north of 40°N in the Pacific and 50°N in the Atlantic/Nordic Seas (Steele and Ermold, 2007), and freshening of the shallow freshwater pool near the equator (see Section 3.5 and Figure 3.9).

Change in subsurface salinity at a given location and depth may reflect water-mass changes driven by changes in surface fluxes or the movement of water-masses (e.g., due to wind-driven changes in ocean circulation). Analysis of property changes in the ocean interior on surfaces of constant pressure and surfaces of constant density allows changes in water mass properties to be distinguished from vertical or lateral displacement of isopycnals (Bindoff and McDougall, 1994). Both processes are found to contribute to changes in subsurface salinity (Durack and Wijffels, 2010). Density layers that are ventilated in precipitation-dominated regions are observed to freshen, while those ventilated in evaporation-dominated regions have increased in salinity, compatible with an enhancement of the mean surface freshwater flux pattern (Helm et al., 2010). In addition, warming of the upper ocean has caused a generally poleward shift of

isopycnals. The observed pattern of change in subsurface salinity is also consistent with subduction and ventilation along isopycnal outcrops migrating through the mean surface salinity field: salinity has increased on layers that have moved to regions of higher mean salinity, and decreased along layers that have moved into regions of lower mean salinity (Durack and Wijffels, 2010). A quantitative assessment of the relative contribution of changes in freshwater fluxes and migration of isopycnal outcrops to the observed change in salinity has not yet been made.

Global ocean freshening at subpolar latitudes and salinification at lower latitudes, with net freshening in the Pacific and salinity increase in the Atlantic, were summarized in AR4 but with a large uncertainty. The estimate of change in globally averaged salinity and freshwater content remains smaller than its uncertainty. For instance, globally averaged SSS change between the 1950s and 2000s is small (+0.0024 ± 0.051) compared to its error estimate (Durack and Wijffels, 2010). Although acceleration of land ice mass loss during the 2000s was observed (Rignot et al., 2008; Velicogna, 2009), the uncertainty due to sparse sampling is large, especially in high-latitude regions.

3.3.3 Regional Changes in Salinity

Regional changes in ocean salinity reinforce the conclusion that regions of net precipitation (precipitation greater than evaporation) have generally become wetter, while regions of net evaporation have become drier. In the high-latitude regions, higher runoff, increased melting of ice, and changes in freshwater transport by ocean currents have *likely* also contributed to observed salinity changes (Bersch et al., 2007; Jacobs and Giulivi, 2010; Polyakov et al., 2008).

3.3.3.1 Pacific and Indian Oceans

In the tropical Pacific, surface salinity has declined over 50 years in the precipitation-dominated western equatorial regions and in the South Pacific Convergence Zone by 0.1 to 0.3 (Cravatte et al., 2009), while surface salinity has increased by up to 0.1 in the evaporation-dominated zones in the southeastern and north-central tropical Pacific (Durack and Wijffels, 2010). The fresh, low density waters in the warm pool of the western equatorial Pacific expanded in area as the surface salinity front migrated eastward by 1500–2500 km over the period 1955–2003 (Cravatte et al., 2009; Delcroix et al., 2007). Similarly, in the Indian Ocean, the net precipitation regions in the Bay of Bengal and the warm pool contiguous with the tropical Pacific warm pool have been freshening by up to 0.1 to 0.2, while the saline Arabian Sea and south Indian Ocean have been getting saltier by up to 0.2 (Durack and Wijffels, 2010).

In the North Pacific, the subtropical thermocline has freshened by 0.1 since the early 1990s, following surface freshening that began around 1984 (Ren and Riser, 2010); the freshening extends down through the intermediate water that is formed in the northwest Pacific (Nakano et al., 2007), continuing the freshening documented by Wong et al. (1999). Warming of the surface water that subducts to supply the intermediate water is one reason for this signal, as the fresh water from the subpolar North Pacific is now entering the subtropical thermocline at lower density. Freshening north of 40°N has contributed to regional sea level rise (Steele and Ermold, 2007).

3.3.3.2 Atlantic Ocean

The net evaporative North Atlantic has become saltier as a whole over the past 50 years (Boyer et al., 2007; Durack and Wijffels, 2010). The largest increase in the upper 700 m occurred in the Gulf Stream region (0.006 per decade between 1955–1959 and 2002–2006) (Wang et al., 2010). Salinity increase is also evident following the circulation pathway of Mediterranean Outflow Water (Figure 3.9; Durack and Wijffels, 2010; Fusco et al., 2008). This increase can be traced back to the western basin of the Mediterranean, where salinity of the deep water increased during the period from 1943 to mid-2000s (Smith et al., 2008; Vargas-Yanez et al., 2010). During the time period between 1955–1959 and 2002–2006, the upper 700 m of the subpolar North Atlantic freshened by up to 0.002 per decade (Wang et al., 2010), while an increase in surface salinity was found between the periods 1960–1989 and 2003–2007 (Hosoda et al., 2009). Decadal and multi-decadal variability in the subpolar gyre and Nordic Seas is vigorous and has been related to various climate modes such as the NAO, the Atlantic multidecadal oscillation (AMO), and even ENSO (Polyakov et al., 2005; Yashayaev and Loder, 2009), obscuring long-term trends. The 1970s–1990s

freshening of the northern North Atlantic and Nordic Seas (Curry and Mauritzen, 2005; Curry et al., 2003; Dickson et al., 2002) reversed to salinification (0–2000 m depth) starting in the late 1990s (Boyer et al., 2007; Holliday et al., 2008), and the propagation of this signal could be followed along the eastern boundary from south of 60°N in the Northeast Atlantic to Fram Strait at 79°N (Holliday et al., 2008). Advection has also played a role in moving higher salinity subtropical waters to the subpolar gyre (Bersch et al., 2007; Hatun et al., 2005; Lozier and Stewart, 2008). The variability of the cross equatorial transport contribution to this budget is highly uncertain. Reversals of North Atlantic surface salinity of similar amplitude and duration to those observed in the last 50 years are apparent in the early 20th century (Reverdin, 2010; Reverdin et al., 2002). The evaporation-dominated subtropical South Atlantic has become saltier by 0.1 to 0.2 during the period of 1950–2008 (Durack and Wijffels, 2010; Hosoda et al., 2009).

3.3.3.3 Arctic Ocean

Sea ice in the Arctic has declined significantly in recent decades (Kwok et al., 2009), which might be expected to freshen the region. However, the lack of historical observations makes it difficult to assess long-term trends in ocean salinity for the Arctic as a whole (Rawlins et al., 2010). Over the 20th century (1920–2003) the central Arctic Ocean became increasingly salty in the upper 150m with a rate of freshwater loss of 239 ± 270 km^3 per decade, while at the Siberian Shelf the river discharge has increased (Shiklomanov and Lammers, 2009) and the shelf became fresher with a rate of 29 ± 50 km^3 per decade (Polyakov et al., 2008). Both trends are modulated by strong multidecadal variability. For instance, the central Arctic Ocean freshened between the periods 1992–1999 and 2006–2008 (Rabe et al., 2011). Upper ocean freshening has also been observed regionally in the southern Canada basin from 1950–1980 to 1990-2000s (Proshutinsky et al., 2009; Yamamoto-Kawai et al., 2009).

Ice production and sustained export of freshwater from the Arctic Ocean in response to winds are suggested as key contributors to the salinification of the upper Arctic Ocean over recent decades (McPhee et al., 2009). The contrasting changes in different regions of the Arctic have been attributed to the effects of Ekman transport, sea ice formation (and melt) as well as a shift in the pathway of Eurasian river runoff (McPhee et al., 2009; Morison et al., 2012; Yamamoto-Kawai et al., 2009).

3.3.3.4 Southern Ocean

Widespread freshening (trend of –0.01 per decade, significant at 95% confidence) of the upper 1000 m of the Southern Ocean was inferred by taking differences between modern data (mostly Argo) and a long-term climatology along mean streamlines (Böning et al., 2008). Both a southward shift of the Antarctic Circumpolar Current and water-mass changes contribute to the observed trends (Meijers et al., 2011).

3.3.4 Evidence for Change of the Global Water Cycle from Salinity

The large scale spatial pattern of the changes in salinity observed at the sea surface supports the hypothesis that the water cycle is intensifying as the planet warms. The striking similarity between the salinity trends and both the mean salinity pattern and the distribution of evaporation–precipitation (Figure 3.4) suggests the global hydrological cycle has been enhanced, as anticipated from thermodynamics and projected by climate models. A similar conclusion was reached in AR4 (Bindoff et al., 2007). From 1950 to 2000, the large-scale pattern of surface salinity has amplified at a rate that is comparable or larger than expected by model simulations and the Clausius–Clapeyron relationship (Durack et al., 2012). Studies published since AR4, based on expanded data sets and new analysis approaches, have substantially increased the level of confidence in the inferred change in the global water cycle (e.g., Durack and Wijffels, 2010; Helm et al., 2010; Hosoda et al., 2009; Roemmich and Gilson, 2009; Stott et al., 2008) (Figure 3.5).

[INSERT FIGURE 3.5 HERE]

Figure 3.5: Zonally integrated freshwater content changes (km^3 per degree of latitude) for the latter half of the 20th century in the upper 500 m over the one-degree zonal belt of the Atlantic, Pacific, Indian, and World Oceans. The time period is from the late-1950s to 2000s (Boyer et al., 2005; blue lines) and 1950–2000 (Durack and Wijffels, 2010; black lines). Calculations are done according to the method of Boyer et al. (2007). Error estimates are 90% confidence intervals.

3.3.5 Conclusion

Robust changes in ocean salinity have been observed throughout much of the ocean, both at the sea surface and in the ocean interior. It is *very likely* that since the 1960s, the mean regional pattern of sea surface salinity has been enhanced: saline surface waters in the evaporation-dominated mid-latitudes have become more saline, while the relatively fresh surface waters in rainfall-dominated tropical and polar regions have become fresher. Similarly, it is *very likely* that the interbasin contrast between saline Atlantic and fresh Pacific surface waters has increased. It is *very likely* that these patterns are caused by an intensification of the water cycle as the lower atmosphere has warmed, reflecting the expected and observed increased water vapour content of the warmer air (Section 2.3).

Changes in salinity have been observed in the ocean interior as well. It is *likely* that the subduction of surface water mass anomalies and the movement of density surfaces have contributed to the observed salinity changes on depth levels. Changes in freshwater flux and the migration of surface density outcrops caused by surface warming (e.g., to regions of lower or higher surface salinity) have *likely* both contributed to the formation of salinity anomalies on density surfaces.

3.4 Changes in Ocean Surface Fluxes

3.4.1 Introduction

Exchanges of heat, water and momentum (wind stress) at the sea surface are important factors for driving the ocean circulation. Changes in air-sea fluxes may result from variations in the driving surface meteorological state variables (air temperature and humidity, wind speed, cloud cover, precipitation, SST) and can impact both water-mass formation rates and ocean circulation. Air-sea fluxes also influence temperature and humidity in the atmosphere and, therefore, the hydrological cycle and atmospheric circulation. Any anthropogenic climate change signal in surface fluxes is expected to be small compared to their natural variability and associated uncertainties. AR4 concluded that, at the global scale, the accuracy of the observations is insufficient to permit a direct assessment of anthropogenic changes in surface fluxes. As described below, while substantial progress has been made since AR4, that conclusion still holds for this assessment.

The net air-sea heat flux is the sum of two turbulent (latent and sensible) and two radiative (shortwave and longwave) components. We adopt a sign convention in which ocean heat gain from the atmosphere is positive. The latent and sensible heat fluxes are computed from the state variables using bulk parameterizations; they primarily depend on the products of wind speed and the vertical near-sea-surface gradients of humidity and temperature respectively. The air-sea freshwater flux is the difference of precipitation (P) and evaporation (E). It is linked to heat flux through the relationship between evaporation and latent heat flux. Thus, when considering potential trends in the global hydrological cycle, consistency between observed heat budget and evaporation changes is required in areas where evaporation is the dominant term in hydrological cycle changes. Ocean surface shortwave and longwave radiative fluxes can be inferred from satellite measurements using radiative transfer models, or computed using empirical formulae, involving astronomical parameters, atmospheric humidity, cloud cover and SST. The wind stress is given by the product of the wind speed squared and the drag coefficient. For detailed discussion of all terms see for example Gulev et al. (2010) and Josey (2011).

3.4.2 Air-Sea Heat Flux

3.4.2.1 Turbulent Heat Fluxes and Evaporation

Latent and sensible heat fluxes show strong regional variations (with annual mean heat loss ranging from close to zero to near –250 W m^{-2}) and have pronounced seasonal cycles. Estimates of these terms have many potential sources of error (e.g., sampling issues, instrument biases, uncertainty in the flux computation algorithms) which are difficult to quantify and strongly spatially variable (Gulev et al., 2007). The overall uncertainty of each term is *likely* in the range 10–20 % for the annual mean global value. In the case of the larger latent heat flux term, this corresponds to an uncertainty of up to 20 W m^{-2} (note the sensible heat flux is an order of magnitude smaller than the latent in the global ocean annual mean). Spurious temporal trends

may also arise as a result of variations in measurement method for the driving meteorological variables, in particular wind speed (Tokinaga and Xie, 2011). In comparison, changes in global mean values of individual heat flux components expected as a result of anthropogenic climate change are at the level of <2 W m^{-2} over the past 50 years (Pierce et al., 2006).

Many new turbulent heat flux datasets have become available since AR4 including products based on atmospheric reanalyses, satellite and in situ observations, and hybrid datasets that combine information from these three different sources. It is not possible to identify a single best product as each has its own strengths and weaknesses; several are highlighted here, for a full discussion see the review of Gulev et al. (2010). The Hamburg Ocean-Atmosphere Parameters and Fluxes from Satellite Data product (Andersson et al., 2011) provides turbulent heat flux (and precipitation) fields developed from observations at microwave and infrared wavelengths. However, in common with other satellite based datasets, it only spans a relatively recent period (in this case 1987–onwards) and is thus of limited utility for identifying changes in these fields. A significant advance in flux dataset development methodology is the Objectively Analysed Air-Sea heat flux (OAFlux) product that covers 1958–2010 and for the first time synthesizes state variables (sea surface temperature, air temperature and humidity, wind speed) from reanalyses and, where available, from satellite observations, prior to flux calculation (Yu and Weller, 2007). By combining these data sources, OAFlux has the potential to avoid severe spatial sampling problems that limit the usefulness of datasets based on ship observations and to provide a new resource for studies of temporal variability. However, the balance of data sources used for OAFlux changed significantly in the mid-1980s, with the advent of satellite data, and the consequences of this change need to be assessed. In an alternative approach, Large and Yeager (2009) modified the NCEP/NCAR reanalysis state variables prior to flux calculation using various adjustment techniques, to produce the Coordinated Ocean-ice Reference Experiments (CORE) turbulent fluxes for 1948–2007 (Griffies et al., 2009). When combined with satellite based radiative flux estimates, CORE provides a globally balanced net heat flux field for forcing ocean models. However, the adjustments employed were based on satellite and in situ based observations spanning only limited periods (e.g., 1999–2004 for the wind speed adjustment) and the CORE product contains several fields that are climatological means prior to 1984. Thus it is not clear to what extent CORE can be reliably used for studies of interdecadal variability.

Analysis of OAFlux suggests that global mean evaporation exhibits variability at interdecadal timescales (Li et al., 2011; Yu, 2007, and Figure 3.6 left panel) although the impact of varying data sources on this variability needs to be determined. The latent heat flux variations (Figure 3.6 middle panel) closely follow those in evaporation (with allowance for the sign definition which results in negative values of latent heat flux corresponding to positive values of evaporation) but do not scale exactly as there is an additional minor dependence on sea surface temperature through the latent heat of evaporation. The overall time series from 1958–2010 provides no evidence for a trend in global mean evaporation.

[INSERT FIGURE 3.6 HERE]

Figure 3.6: Time series of globally averaged annual mean ocean evaporation (E), latent and sensible heat flux from 1958 to 2010 determined from OAFlux. Shaded bands show uncertainty estimates; the time series have been updated to 2010 by Yu following the method described in Yu (2007). The error represents the spread of the input datasets used in the OAFlux analysis and is computed from their standard deviation. The black horizontal bars in the lower panel show the time periods for which NCEP and ERA40 reanalysis output and satellite observations were employed in the OAFlux analysis; they apply to all three panels.

3.4.2.2 Surface Fluxes of Shortwave and Longwave Radiation

The shortwave flux component has strong regional variations with annual mean values up to about 250 W m^{-2} in the Tropics and a pronounced seasonal cycle. The longwave flux is less variable with annual mean losses typically in the range –30 to –70 W m^{-2} depending on location. Estimates of these terms are available from in situ climatologies (that employ empirical formulae requiring ship observer estimates of cloud cover), from atmospheric reanalyses, and, since the 1980s, from satellite observations. As is the case for turbulent fluxes, these sources have many potential sources of error (e.g., uncertainty in the empirical formulae, sampling issues, representation of cloud in the reanalyses, and changing satellite sensors) which are difficult to quantify and strongly spatially dependent. The overall uncertainty of each term is again *likely* in the range of 10–20% for the annual mean at a given location (Gulev et al., 2010). High accuracy in-situ radiometer measurements are available at many sites over land since the 1960s, allowing analysis of decadal variations

in the surface shortwave flux (Wild, 2009; Chapter 2). However, this is not the case over the oceans, where there are very few in-situ measurements. Instead it is necessary to rely on satellite observations, which are less accurate (compared to in-situ determination of radiative fluxes), restrict the period that can be considered to the mid-1980s onwards, but do provide homogeneous sampling.

Estimates based on data over both ocean and land show increases of the globally averaged solar radiation (global brightening) by about 3 W m^{-2} per decade from 1991–1999 (Romanou et al., 2006; Wild et al., 2005) and have been attributed predominantly to aerosol optical depth decreases and cloud changes (Cermak et al., 2010; Mishchenko and Geogdzhayev, 2007). The brief interlude of global brightening in the 1990s has been preceded and followed by periods of decreasing surface insolation (global dimming) by about 2.5 W m^{-2} per decade for 1983–1991 and 5 W m^{-2} per decade for 1999–2004; over the full period 1983–2004 there is no significant trend (Hinkelman et al., 2009). Patterns of regional variability may differ significantly from the global signal (Hinkelman et al., 2009). Analysis of International Satellite Cloud Climatology Project - Fast delivery radiative fluxes for the period 1984–2000 by Romanou et al. (2007) shows a small increase of 1 W m^{-2} per decade in the surface shortwave radiation averaged over the global oceans with larger regional positive trends in the Pacific and North Atlantic tropics and negative trends in the mid-latitudinal North Pacific, Southern Atlantic and southern half of the Indian Ocean. Ship-based and reanalysis estimates of radiative flux variability over the oceans prior to the advent of satellite observations in the 1980s are *unlikely* to be accurate enough to detect global trends of <5 W m^{-2} per decade primarily due to space-time inhomogeneity of sampling in ship-based estimates and uncertainty in the radiative schemes employed in reanalyses.

3.4.2.3 Net Heat Flux and Ocean Heat Storage Constraints

The most reliable source of information for changes in the global mean net heat flux comes from the constraints provided by analyses of changes in ocean heat storage. The estimate of increase in global ocean heat content for 1971–2010 quantified in Box 3.1 corresponds to an increase in mean net heat flux from the atmosphere to the ocean of 0.55 W m^{-2}. In contrast, closure of the global mean net heat flux budget to within 20 W m^{-2} has still not been reliably achieved (e.g., Trenberth et al., 2009). The increase in mean net heat flux is thus small compared to the uncertainties of the global mean and not yet possible to detect from observations. Since AR4, some studies have shown consistency in regional net heat flux variability at sub-basin scale since the 1980s; notably in the Tropical Indian Ocean (Yu et al., 2007) and North Pacific (Kawai et al., 2008). However, detection of a change in surface fluxes responsible for the long-term ocean warming remains beyond the ability of currently available observational surface flux datasets.

3.4.3 Ocean Surface Precipitation and Freshwater Flux

Precipitation observations are available from remote sensing since 1979 and have been used by Smith et al. (2009) to reconstruct precipitation for the period 1900–2008 over 75°S–75°N by means of a Canonical Correlation Analysis (CCA) with SST and Sea Level Pressure (SLP). The CCA makes use of correlation fields between precipitation and SST / SLP that are determined using remote sensing data from the Global Precipitation Climatology Project (GPCP) for 1979–2003. Smith et al. (2012) subsequently revised their analysis method by including the CCA results within an EOF based precipitation reconstruction. Each of the reconstructions shows both centennial and decadal variability in global ocean mean precipitation (Figure 3.7). The trend from 1900 to 2008 is 0.005 mm day^{-1} per decade for Smith et al. (2012) corresponding to an increase approaching 2 mm per month over the 108-year period. For the period of overlap, the reconstructed global ocean mean precipitation time series show consistent variability with GPCP as is to be expected (Figure 3.7). Smith et al. (2012) note that further work is needed to determine the most reliable approach to precipitation reconstruction. In earlier work, focusing on the Tropical Ocean using only GPCP, (Gu et al., 2007) have identified a precipitation trend of 0.06 mm day^{-1} per decade over 1979–2005 for the region 25°S–25°N. However, they conclude that further evaluation of the remotely sensed precipitation datasets and techniques by which they are merged is required before precipitation trends can be firmly established; thus such estimates should be treated with caution.

Trenberth et al. (2011) assess the hydrological cycles in eight current atmospheric reanalyses and their time variability. For the recent period 1989 onwards, they find little consistency of the changes in ocean precipitation in the Modern Era Retrospective and ERA-Interim Reanalyses with the GPCP dataset.

[INSERT FIGURE 3.7 HERE]

Figure 3.7: Long-term reconstruction of ocean precipitation over 75°S–75°N by Smith et al. (2012) (annual values–thin blue line, low-pass filtered data (15-year RM)–bold blue line) and Smith et al. (2009) (low-pass filtered data–dashed grey line). Also shown are GPCP-derived ocean precipitation over the same latitudinal range (annual values–thin magenta line, low-pass filtered data –bold magenta line). Precipitation anomalies were taken relative to the 1979–2008 period.

Schanze et al. (2010) examine inter-annual variability within the OAFlux evaporation and GPCP precipitation datasets. They find that use of satellite data prior to 1987 is limited by discontinuities in the record attributable to variations in data type and such variations also affect atmospheric reanalysis fields. Thus, it is not yet possible to use such datasets to establish whether there are significant multi-decadal trends in mean E-P although regional trends since the 1960s are suggested by the changing salinity field (see Section 3.3.4). Schanze et al. (2010) present a combined OAFlux/GPCP time series of the global ocean annual mean E-P for 1987 to 2006 which varies between 0.6 and 1.2 Sv.

3.4.4 Wind Stress

Wind stress fields are available from reanalyses, satellite-based datasets, and in situ observations. Variability in the ocean wind stress field is expected to largely reflect changes in the surface wind speed discussed in Section 2.6.2. Yang et al. (2007) found a positive trend of Southern Ocean surface zonal wind stress from 1980 to 2001 using the ECMWF Re-analysis (ERA40) averaged over 45–60°S, satellite (SSM/I) winds and island station data. The trend has a strong seasonal dependence with largest values of about 0.02 N m^{-2} per decade in January at 55–60°S. They argue that the strengthening is closely linked with changes in the Southern Annular Mode (SAM), which has continued to show an upward trend since AR4 (see Section 2.6.8). Xue et al. (2010) considered wind stress variability for a broader Southern Ocean region (45–70°S) and longer period (1979–2009) as part of an evaluation of the recent NCEP-CFSR reanalysis. They found a clear tendency for wind stress to increase in the NCEP-NCAR and NCEP-DOE atmospheric reanalyses but not the coupled ocean-atmosphere NCEP-CFSR reanalysis or ERA40 (Figure 3.8). The spread across the reanalyses indicates that convergence of results in the Southern Ocean regarding the strength of the wind stress increase has yet to be achieved. However, when taken in combination with the satellite and island station data analysis they suggest, that Southern Ocean wind stress has strengthened since the early 1980s which is consistent with intensification of circumpolar westerlies noted in AR4.

[INSERT FIGURE 3.8 HERE]

Figure 3.8: Time series of 1-year running mean of zonal mean wind stress over the Southern Ocean (45–70°S) for NCEP-CFSR (red), NCEP R1 (cyan, labelled NCEP-1), NCEP/NCAR R2 (dark blue line, labelled NCEP-DOE) and ERA-40 (green line). Units are N m^{-2} (Xue et al., 2010).

Atmospheric reanalyses have also been used to link wind stress changes to atmospheric teleconnection patterns. In particular, changes in wind stress curl over the North Atlantic from 1950 to early 2000s from NCEP-NCAR and ERA-40 have leading modes that are highly correlated with the NAO and East Atlantic circulation patterns; each of these patterns demonstrates a positive trend over the period from the early 1960s to the late 1990s (Sugimoto and Hanawa, 2010). Wu et al. (2012) find evidence for a poleward shift of the zero wind stress curl line of 2.5° [1.5 to 3.5°] over the past century in the North Atlantic and 3.0° [1.6 to 4.4°] in the North Pacific from an analysis of 20CRv2. They note that this trend may be related to enhanced warming of the subtropical western boundary currents in these basins. Häkkinen et al. (2011), also using 20CRv2, identify a relationship between atmospheric blocking and North Atlantic ocean surface temperature mediated by wind stress curl and air-sea heat exchange. The results of these and other studies with 20CRv2 must be treated with caution as they are based on this single reanalysis product which is the only one to span a timescale longer than a century (other available reanalyses cover shorter periods, the longest is NCEP-NCAR which commences in 1948).

In the period prior to the NCEP-NCAR and ERA-40 reanalyses, attempts have been made to reconstruct the wind stress field in the Tropics by making use of the relationship between wind stress and SST/SLP in combination with historic datasets of these fields. Using this approach, (Deng and Tang, 2009) reconstructed time series of the wind stress over the Equatorial Pacific for 1875–1947 and found significant interannual and multidecadal variability over this period. Vecchi et al. (2006), also using SLP, found a reduction of 7%

in zonal mean wind stress across the Equatorial Pacific for the longer period 1854-2005 and related it to a weakening of the tropical Walker circulation.

3.4.5 Changes in Surface Waves

Surface wind waves are generated by direct wind forcing and are partitioned into two components, namely wind sea (wind-forced waves propagating slower than surface wind) and swell (resulting from the wind sea development and propagating typically faster than surface wind). Significant wave height (SWH) represents the measure of the wind wave field consisting of wind sea and swell and is frequently attributed to the highest one-third of wave heights. Local wind changes influence wind sea properties, while changes in remote storms affect swell. Wind sea integrates characteristics of atmospheric dynamics over different scales and could serve as an indicator of climate variability and change. Variability patterns of wind sea and surface wind may not necessarily be consistent since wind sea integrates wind properties over a larger domain. Global and regional time series of wind sea characteristics are available from buoy data, Voluntary Observing Ship (VOS) reports, satellite measurements, and model wave hindcasts. No source is superior, as all have their strengths and weaknesses.

AR4 reported statistically significant positive SWH trends during 1900–2002 in the North Pacific (up to 8 cm per decade) and stronger trends (up to 14 cm per decade) from 1950 to 2002 for most of the mid-latitudinal North Atlantic and North Pacific, with insignificant trends, or small negative trends, in most other regions (Trenberth et al., 2007). Since AR4, further studies have provided confirmation of previously reported trends with more detailed quantification and regionalization.

At the centennial scale, hindcasts based on 20CRv2 (Wang et al., 2012) for 1871–2008 show an increase in the annual maximum SWH over the mid-latitude North Atlantic with the largest tendency of more than 10 cm/decade in the Central Northern North Atlantic. For the period 1958-2001, the 20CRv2 based hindcasts have a smaller tendency in mean SWH than one based on ERA-40 (Wang et al., 2012; Wang et al., 2009). Starting from the 1950s, forced model experiments are in qualitative agreement with observational data, indicating trends in SWH varying from 8 cm per decade to 20 cm per decade in winter months in the North Atlantic with smaller magnitudes in the North Pacific (Gulev and Grigorieva, 2006; Sterl and Caires, 2005; Wang et al., 2012; Wang and Swail, 2006; Wang et al., 2009). An ERA-40-WAM model hindcast covering 1958–2002 (Semedo et al., 2011) also shows an upward trend in both wind sea and swell heights in the North Atlantic and the North Pacific with the changes in SWH (1.18% per decade in the North East Pacific and nearly 1% per decade in the North East Atlantic) mainly related to the increase in swell heights. There is also evidence of increasing peak wave period during 1953–2009 in the Northeast Atlantic of up to 0.1 s per decade (Dodet et al., 2010), supported by the hindcast of Wang et al. (2009) for the same period. Positive trends in extreme waves have been reported in numerous locations since the late 1970s, including the North American Atlantic coast (Komar and Allan, 2008; Ruggiero et al., 2010), the North American Pacific coast (Menendez et al., 2008), the western tropical Pacific (Sasaki et al., 2005) and south of Tasmania (Hemer, 2010).

Analysis of reliable long-term trends in SWH in the Southern Hemisphere remains a challenge due to limited in-situ data and temporal inhomogeneity in the data used for reanalysis products. Studies comparing altimeter-derived SWH with data from buoys and output from models indicate that while there are some areas with statistically significant increases in wave height, they occur in a narrower area than the models predict, or with smaller trends (Hemer, 2010; Hemer et al., 2010). Positive trends in the data occur mainly south of 45°S (Hemer et al., 2010). In the South Atlantic Ocean, in the area of the South American shelf between 30°S and 40°S, Dragani et al. (2010) reported a 7% increase in SWH during the 1990s and early 2000s, supported by TOPEX altimetry, in-situ data and a SWH hindcast model forced by NCEP winds.

Young et al. (2011) compiled global maps of mean and extreme surface wind speed and mean SWH trends for 1985–2008 using altimeter measurements. For mean SWH they report statistically significant positive linear trends of up to 0.25–0.5% per year in the Southern Ocean (with strongest changes between 80°E–160°W) and negative trends in many Northern Hemisphere ocean regions. The Northern Hemisphere SWH trends are of opposite sign to, and thus inconsistent with, those in wind speed — the latter being primarily positive. Nevertheless, for the 90th and, especially, 99th SWH percentiles, strong positive trends up to 30cm per decade were identified in the Southern Ocean, North Atlantic, and North Pacific. The trends are

consistent with extreme wind speed tendencies found by Young et al. (2011), however, these have been questioned by Wentz and Ricciardulli (2011). As the length of the dataset is short, it is not possible to determine whether the results reflect long-term SWH and wind speed trends, or are part of a multidecadal oscillation.

3.4.6 Conclusions

The global mean net heat flux signal expected from observed ocean heat content changes is extremely small (about 0.5 W m^{-2}) and beyond the detection ability of currently available observational surface flux datasets. The accuracy of reanalysis and satellite observation based freshwater flux products prior to the mid-1980s is limited by changing data sources. Thus, it is not yet possible to establish whether there are significant multi-decadal trends in regional or global mean E-P although regional trends since the 1960s are suggested by the changing salinity field (see Section 3.3.4).

There is increasing evidence for a strengthening of the wind stress field in the Southern Ocean since the early 1980s from atmospheric reanalyses, satellite observations and island station data. Information on significant wave height (SWH) trends is severely limited by available data. It is *likely* that mean SWH has been increasing since the 1950s over much of the mid-latitude North Atlantic and North Pacific with typical winter season trends of 8 to 20 cm $decade^{-1}$. Over much of the Southern Ocean since the mid 1980s mean SWH *likely* increases by up to 2.5–5% $decade^{-1}$ with strongest changes between 80°E–160°W.

3.5 Changes in Water-Mass Properties and Ventilation

3.5.1 Introduction

To a large degree, water-mass properties are set at the sea surface through interaction between the ocean and the overlying atmosphere (and ice, in polar regions). The water characteristics resulting from these interactions (e.g., temperature, salinity, and concentrations of dissolved gases and nutrients) are transferred into the ocean interior through convection and subduction (ventilation). They are slowly modified by mixing and, for some substances, influenced by biogeochemical sources and sinks. The formation and subduction of water masses largely determine the ocean's capacity to store heat, freshwater, carbon, oxygen, and other properties relevant to climate. Water mass analysis, therefore, provides a useful tool to assess modes and rates of ocean climate change. In this section, evidence for changes in the major water masses of the world ocean is summarized.

The changes evident in zonally averaged temperature, salinity, and density (Figure 3.9) reflect changes in water-mass properties and ventilation as well as changes in circulation that result in vertical or horizontal migration of density layers. The tendency for warming of the upper ocean and a decrease (increase) of salinity in high (subtropical) latitudes discussed in Section 3.2 and 3.3 are clearly evident in the zonally averaged fields. The density of the surface layers has generally declined, increasing the upper ocean stratification. Warming surface waters can hold less dissolved oxygen, while increasing stratification can change the rate of ventilation on density surfaces that were formerly vigorously ventilated, consistent with the observed tendency for declining oxygen in much of the upper ocean (Section 3.8).

3.5.2 North Atlantic Deep Water (NADW)

Labrador Sea Water (LSW) is formed by convection in the western subpolar North Atlantic and exhibits strong multi-decadal variability in temperature and salinity (e.g., Yashayaev and Loder, 2009). AR4 assessed this variability starting from the 1950s, but did not report on quantitative estimates of LSW formation rates. The LSW temperature and salinity increase since the mid 1990s (Yashayaev and Loder, 2009) was accompanied by ventilation of only the lighter varieties of LSW (Kieke et al., 2007; Rhein et al., 2011), while for the time period 1970–1997, formation of dense LSW dominated (LeBel et al., 2008). The total LSW formation rate decreased from about 7.6–8.9 Sv in 1997–1999 (Kieke et al., 2006) to roughly 0.5 Sv in 2003–2005 (Rhein et al., 2011), mostly due to changes in the local buoyancy fluxes related to the state of the NAO (Yashayaev and Loder, 2009). There is evidence that formation of the denser LSW occurred in 2008 (Våge et al., 2009), but not in the following years (Rhein et al., 2011; Yashayaev and Loder, 2009). The shift of LSW properties induced by the change in the ventilation in the mid 1990s has also been observed further

south in the Deep Western Boundary Current (Pena-Molino et al., 2011). In Figure 3.9 it is the strong, freshening signal from the 1960s to the 1990s that dominates the trend.

The deeper part of the NADW consists of dense waters overflowing the sills between Greenland and Scotland. Observations of the dense overflows are dominated by short-term variability and there is no evidence of a long-term change in transport (Jochumsen et al., 2012). Thus there is no evidence that the ventilation rates of these water masses have changed. However, there have been large changes in the temperature and salinity of these water masses, as noted in AR4. Assuming no change in transport, Eldevik et al. (2009) found that the variability in the overflow water masses could be traced back to their sources in the Nordic Seas. The freshening observed since the mid-1960s in both overflows, highlighted in AR4, stopped in the mid-1990s (Dickson et al., 2008). The salinity of the Faroe Bank overflow, especially in its warmer reaches, increased substantially since 1995, implying a density increase on the order of 0.01 kgm^{-3} (Hansen and Osterhus, 2007). The other main overflow, through Denmark Strait, shows large interannual variability in temperature, salinity for the time period 1996–2011, but no trends (Jochumsen et al., 2012).

As the overflows descend into the North Atlantic they entrain substantial amounts of ambient subpolar waters. Temperature and salinity variability in the overflow water masses south of the overflow region therefore display a strong, delayed signature of the (NAO-dominated) upper, subpolar waters (Mauritzen et al., 2012), while the temperature and salinity variability of the overflows themselves have been of less importance.

3.5.3 North Pacific Intermediate Water (NPIW) and Subtropical Mode Water (STMW)

As stated in AR4, North Pacific Intermediate Water (NPIW) has steadily warmed since the 1950s . A recent study (Nakanowatari et al., 2007) reported warming by roughly 0.5°C from 1955 to 2004 in the northwestern North Pacific (Figure 3.9). The warming was accompanied by a significant oxygen reduction, indicating weaker ventilation. The trends are strongest in the Sea of Okhotsk, the formation area of NPIW. The changes in NPIW properties have been tentatively linked to increased air temperature and decreased sea-ice extent in winter. In contrast, decadal variability of the ventilation of the North Pacific Subtropical Mode Water (STMW) is mainly influenced by circulation variability and not so much by air-sea flux changes (Qiu and Chen, 2006).

3.5.4 Southern Ocean

3.5.4.1 Antarctic Intermediate Water (AAIW)

AAIW has freshened since the 1960s, as reported in AR4, and the change is visible in the 50-year trends in all basins of the Southern Hemisphere when plotted against isobars (Figure 3.10). Isopycnals above the AAIW salinity minimum became cooler and fresher, while the isopycnals below warmed and became more saline (Böning et al., 2008; Durack and Wijffels, 2010; Helm et al., 2010; McCarthy et al., 2011). The freshening above the AAIW core in the Southern Ocean has been interpreted as being caused by an intensification of the hydrological cycle (Helm et al., 2010), but poleward migration of isopycnal outcrops with surface warming is also *likely* to contribute to the observed salinity changes (Durack and Wijffels, 2010). Other mechanisms may contribute to changes in particular regions. For instance, AAIW salinity changes in the South Atlantic have been linked with variability in the Agulhas leakage related to SAM (McCarthy et al., 2011). Observed changes of AAIW properties in the Drake Passage between 1969 and 2005 were traced to changing Winter Water (WW) properties, ultimately linked to ENSO-related changes in meridional winds, winter-time buoyancy fluxes and sea ice melt west of the Antarctic Peninsula (Garabato et al., 2009).

The salinity minimum core of the AAIW shoaled (30–50 dbar per decade), warmed (0.05°C–0.15°C per decade) and became less dense (up to 0.03 kg m^{-3} per decade) since the mid 1970s, with the strongest trends observed near the formation regions in the southeast Pacific and Atlantic (Schmidtko and Johnson, 2012). Salinity trends in the AAIW core are small and vary regionally, with temperature changes dominating the density trend (Schmidtko and Johnson, 2012). Whether these changes in properties also affected the formation rates of AAIW cannot be assessed from the available observations.

3.5.4.2 Antarctic Bottom Water (AABW)

The AABW has warmed since the 1980s, most noticeably near Antarctica (Aoki et al., 2005; Johnson et al., 2008b; Kouketsu et al., 2011; Purkey and Johnson, 2010; Rintoul, 2007), but with warming detectable into the North Pacific and even the North Atlantic Oceans (Johnson et al., 2008a; Kawano et al., 2010). The global warming of AABW between the 1980s and 2000 contributed about 10% to ocean heat uptake during this period (see Section 3.2 and Purkey and Johnson, 2010). In parallel, a reduction of the AABW volume was observed, equivalent to a reduction of the global formation of AABW of about 8.2 [5.6 to 10.8] Sv (Purkey and Johnson, 2012).

The decrease in volume of dense AABW is accompanied by the freshening of AABW sources in the Indian and Pacific sectors of the Southern Ocean. The strongest signal (0.03 per decade, between 1958 and 2008) is observed in the Ross Sea and has been linked to inflow of glacial melt water from the Amundsen and Bellingshausen Seas (Jacobs and Giulivi, 2010; Rignot et al., 2008; Shepherd et al., 2004). In the Weddell Sea (the primary source of AABW in the Atlantic), a contraction of the bottom water mass was observed between 1984 and 2008 at the Prime Meridian, accompanied by warming of about 0.015°C, and by salinity variability on a multi-annual time scale. These changes could be explained by variability in the wind-driven circulation of the Weddell Sea (Fahrbach et al., 2011). Aging of the AABW in the Weddell Sea, inferred from transient tracer observations between 1984 and 2011, has been linked to mixing with the aging ambient deep water mass rather than to a reduction in the formation of dense water (Huhn et al., 2012).

[INSERT FIGURE 3.9 HERE]

Figure 3.9: Upper 2000 m zonally averaged mean trend distribution, 1950–2000 (colours with white contours) of potential temperature (column 1), neutral density (column 2), and salinity (column 3), for the Atlantic Ocean (ATL) in row 1, Indian Ocean (IND), row 2, Pacific Ocean (PAC), row 3, and global ocean (GLO) in row 4. The mean fields are shown as black lines. Regions where the resolved linear trend is not significant at the 90% confidence level are stippled in gray.

3.5.5 Conclusions

AR4 discussed regional and basin-wide changes in water mass properties. The conclusion in AR4–that observed changes in upper ocean water masses reflect the combination of long-term trends and interannual-to-decadal variability related to climate modes like ENSO, NAO and SAM–is supported by more recent studies. The source waters of the North Atlantic Deep Water exhibit strong variability in temperature and salinity on interannual to multidecadal time-scales, with little evidence of long-term trends; in particular, the freshening trend of the dense water overflows since the mid-1960s, noted in AR4, reversed in sign in the mid-1990s. It is *very likely* that changes in the formation of Labrador Sea Water are dominated by the impact of the NAO on the air-sea exchange of buoyancy. North Pacific Intermediate Water likely warmed and became lower in oxygen between 1955 and 2004, implying a reduction in ventilation. Antarctic Intermediate Water has *likely* freshened since the 1960s, reflecting changes in the hydrological cycle and the poleward migration of isopycnals. It is *likely* that the abyssal layer ventilated by Antarctic Bottom Water (AABW) warmed over much of the globe since the 1980s and the volume of AABW has reduced.

3.6 Changes in Ocean Circulation

3.6.1 Observing Ocean Circulation Variability

The present-day ocean observing system includes global observations of velocity made at the sea surface by the Global Drifter Program (Dohan et al., 2010), and at 1000-m depth by the Argo Program (Freeland et al., 2010). In addition, Argo observes the geostrophic shear between 2000 m and the sea surface. These two recently implemented observing systems, if sustained, will continue to document the large-spatial scale, long-timescale variability of circulation in the upper ocean.

Historical measurements of ocean circulation are much sparser, so estimates of decadal and longer changes in circulation are very limited. Since 1992, high-precision satellite altimetry has measured the time variations in sea surface height (SSH), whose horizontal gradients are proportional to the surface geostrophic velocity. In addition, mostly during 1991–1997, a single global top-to-bottom hydrographic survey was carried out by the World Ocean Circulation Experiment (WOCE), measuring geostrophic shear as well as velocity from

mid-depth floats and from lowered acoustic Doppler current profilers. A subset of WOCE and pre-WOCE transects is being repeated at 5–10 year intervals (Hood et al., 2010).

Foci of ocean circulation studies in relation to climate include variability in the wind-driven gyres (Section 3.6.2) and changes in the meridional overturning circulations (MOCs, Section 3.6.3 and 3.6.4) influenced by buoyancy loss and water-mass formation. The MOCs are responsible for much of the ocean's capacity to carry excess heat from the tropics to middle latitudes, and also are important in the ocean's sequestration of carbon. The connections between ocean basins (Section 3.6.5) have also been subject to study because of the significance of inter-basin exchanges in wind-driven and thermohaline variability, and also because these can be logistically advantageous regions for measurement ("chokepoints"). In the following, the best-studied and most significant aspects of circulation variability and change are assessed including wind-driven circulation in the Pacific, the Atlantic and Antarctic MOCs, and selected interbasin exchanges.

An assessment is now possible of the recent mean and the changes in global geostrophic circulation over the previous decade (Figure 3.10, and discussion in Section 3.6.2). In general, changes in the slope of SSH across ocean basins indicate changes in the major gyres and the interior component of MOCs (western boundary-current components may also be important but are not resolved in these observations). Changes occurring in high gradient regions such as the Antarctic Circumpolar Current (ACC) indicate shifts in the location of those currents.

[INSERT FIGURE 3.10 HERE]

Figure 3.10: The mean SSH (black contours, 10 cm CI) for the Argo era is the sum of the geostrophic pressure field at 1000 m based on Argo trajectory data (Katsumata and Yoshinari, 2010) plus the relative pressure field (0/1000 dbar steric height) based on Argo profile data from Roemmich and Gilson (2009). The SSH trend (cm per decade, color shading) for the period 1993–2011 is based on the AVISO altimetry "reference" product (Ducet et al., 2000). Spatial gradients in the SSH trend are proportional to changes in surface geostrophic velocity.

3.6.2 Wind-Driven Circulation Variability in the Pacific Ocean

The upper Pacific Ocean is less influenced than the Atlantic by the deep MOC (the North Pacific has no deep water formation), and variability in the horizontal gyre circulations of the Pacific is mostly wind-driven. Consistent changes in circulation throughout the Pacific in the past two decades are seen with good agreement among satellite ocean data, in-situ ocean measurements, and wind stress forcing.

The subarctic gyre in the North Pacific poleward of about 40°N consists of the Alaska Gyre to the east and the Western Subarctic Gyre (WSG) to the west. Over the past two decades, the cyclonic Alaska Gyre has strengthened while shrinking in size. The shrinking is due to strengthening and northward expansion of the North Pacific Current (NPC, the high gradient region centred about 40°N in Figure 3.10) and has been described using the satellite altimeter, XBT/hydrography, and, more recently, Argo profiling float data (Cummins and Freeland, 2007; Douglass et al., 2006). A similar trend is detected in the WSG, with the northern WSG in the Bering Sea strengthened while the southern WSG south of the Aleutian Islands has weakened. These decadal changes are attributable to strengthening and northward expansion of the Pacific High and Aleutian Low atmospheric pressure systems over the subarctic North Pacific Ocean (Carton et al., 2005).

Accompanying the NPC's northward expansion, the subtropical gyre in the North Pacific also expanded along its southern boundary over the past two decades. The North Equatorial Current (NEC) shifted southward along the 137°E meridian (Qiu and Chen, 2012, also note the SSH increase east of the Philippines in Figure 3.10 indicating the southward shift). The NEC's bifurcation latitude along the Philippine coast migrated southward from a mean latitude of 13°N in the early 1990s to 11°N in the late 2000s (Qiu and Chen, 2010). These changes are due to a strengthening of the Walker circulation generating a positive wind stress curl anomaly (Mitas and Clement, 2005; Tanaka et al., 2004). This regional wind stress curl anomaly is also responsible for the enhanced regional sea level rise, >10 mm yr^{-1}, in the western tropical North Pacific Ocean (Timmermann et al., 2010, Figure 3.10). The 20-year timescale expansion of the North Pacific subtropical gyre has high confidence due to the good agreement seen in satellite altimetry, subsurface ocean data, and wind stress changes.

Variability in the mid-latitude South Pacific over the past two decades is characterized by a broad increase in SSH in the 35°S–50°S band and a lesser increase south of 50°S along the path of the ACC (Figure 3.10). These dipolar SSH fluctuations are induced by the intensification in the Southern Hemisphere westerlies (i.e., the SAM, see also Section 3.5.4), generating positive and negative wind stress curl anomalies north and south of 50°S. In response, the southern limb of the South Pacific subtropical gyre has intensified in the past two decades (Cai, 2006; Qiu and Chen, 2006; Roemmich et al., 2007) along with a southward expansion of the East Australian Current (EAC) into the Tasman Sea (Hill et al., 2008). The intensification in the South Pacific gyre extends to a greater depth (>1800 m) than that in the North Pacific gyre (Roemmich and Gilson, 2009). As in the north, the 20-year changes in the South Pacific are seen with high confidence as they occur consistently in multiple lines of medium and high quality data.

The strengthening of southern hemisphere westerlies is a multi-decadal signal (as seen in decreasing trends in high southern latitude sea level pressure, see Box 2.2, Figure 1), and the multi-decadal warming in the Southern Ocean (e.g., Figure 3.1) is consistent with a poleward displacement of the ACC (Gille, 2008) and the southern limb of the subtropical gyres, by about 1° of latitude in 40 years. The warming and corresponding sea level rise signals are not confined to the South Pacific, but are seen globally in zonal mean fields (e.g., at 40°S in Figure 3.10). Alory et al. (2007) describe the broad warming consistent with a southward shift of the ACC in the South Indian Ocean. In the Atlantic, a southward trend in the location of the Brazil-Malvinas confluence (at around 39°S) is described from surface drifters and altimetry by Lumpkin and Garzoli (2011), and in the location of the Brazil Current separation point from sea surface temperature and altimetry by Goni et al. (2011). Enhanced surface warming and poleward displacement, globally, of the western boundary currents is described by Wu et al. (2012).

3.6.3 The Atlantic Meridional Overturning Circulation (AMOC)

The AMOC is a time-varying circulation in the vertical-meridional plane, whose magnitude can be calculated from the zonal integral of the meridional velocity in an east–west section across an ocean basin The AMOC is primarily a two-layer system, with an upper limb moving northward between the surface and approximately 1200 m depth and a mass-balancing lower limb return flow between approximately 1200 m and 5000 m.

Observations of the AMOC are directed toward detecting possible long-term changes in its amplitude, its northward energy transport, and in the ocean's capacity to absorb excess heat and greenhouse gases, as well as characterizing short-term variability and its relationship to changes in forcing. The overturning circulation is a global-scale phenomenon, with a bottom limb of AABW spreading northward below the AMOC. (Section 3.6.4).

[INSERT FIGURE 3.11 HERE]

Figure 3.11: a) Volume transport of the Florida Current from dropsonde measurements (symbols) and cable voltages (continuous line), extending the time-series shown in Meinen et al. (2010) **b)** AMOC transport estimates in Sverdrups (Sv; where 1 Sv = 10^6 m^3 s^{-1}). 1. RAPID/MOCHA (Rapid Climate Change programme/Meridional Ocean Circulation and Heatflux Array) at 26.5°N (red): The array monitors the top-to-bottom Atlantic wide circulation, ensuring a closed mass balance across the section, and hence a direct measure of the upper and lower limbs of the AMOC. 2. 41°N (black): An index of maximum AMOC strength from Argo float measurements in the upper 2000 m only, combined with satellite altimeter data. The lower limb is not measured. 3. MOVE at 16°N (blue): Transport of North Atlantic Deep Water in the lower limb of the AMOC between 1100m and 4800m depth between the Caribbean and the mid-Atlantic Ridge. This transport is thought to be representative of maximum MOC variability based on model validation experiments. The temporal resolution of the three timeseries is ten days for 16°N and 26°N and one month for 41°N. In this figure the data have been three month low-pass filtered. The means and standard deviations for the common period of 2 April 2004 to 1 April 2010 are 17.5 ± 3.8 Sv, 13.7 ± 3.3 Sv and –16.8 ± 4.1 Sv for 26.5°N, 41°N and 16°N respectively. Means over this period are indicated by the horizontal line on each timeseries.

Presently, changes in the AMOC and meridional heat flux are being estimated on the basis of direct observations of the full MOC at 26.5°N by the RAPID/MOCHA array (Cunningham et al., 2007; Johns et al., 2011; Kanzow et al., 2007) or of observations that target one component of the AMOC (e.g., a specific current or ocean layer, e.g., Kanzow et al., 2008; Meinen et al., 2010; Toole et al., 2011; Willis, 2010). Other estimates of the temporal evolution of the AMOC are indirect, from measurements of forcing fields such as air-sea fluxes (e.g., Grist et al., 2009; Josey et al., 2009; Marsh, 2000; Speer, 1997), or from properties that

may be related to AMOC changes, such as abyssal temperature or salinity (e.g., Johnson et al., 2008a), changes in water-mass formation rates (e.g., Kieke et al., 2007; Myers and Donnelly, 2008), latitude of the Gulf Stream after separation (Joyce and Zhang, 2010), or coastal sea level (Bingham and Hughes, 2009).

Continuous time series of components of the AMOC, longer than those of the complete system at 26.5°N, have been obtained using moored instrumentation. These include the inflow into the Arctic through Fram Strait (since 1997, Schauer and Beszczynska-Möller, 2009) and through the Barents Sea (since 1997, Ingvaldsen et al., 2004; Mauritzen et al., 2011), dense inflows across sills between Greenland and Scotland (since 1999 and 1995 respectively, Jochumsen et al., 2012; Olsen et al., 2008), and North Atlantic Deep Water carried southward within the Deep Western Boundary Current - at 53°N (since 1997, Fischer et al., 2010), at 39°N (Line W, since 2004, Toole et al., 2011), and at 16°N since 2000 (Kanzow et al., 2009). The longest time-series of observations of ocean transport in the world (dropsonde and cable voltage measurements in the Florida Straits), extend from the mid-1960s to the present (Meinen et al., 2010), with small decadal variability of about 1 Sv and no evidence of a multi-decadal trend (Figure 3.11a).

The RAPID/MOCHA array at 26.5°N show a mean AMOC magnitude (± annual mean error) of 18 ± 1.3 Sv between April 2004 and April 2009, with 10-day values ranging from 3–32 Sv. Earlier estimates of AMOC strength from 5 shipboard expeditions over 47 years (Bryden et al., 2005) were in the range of variability seen by the RAPID/MOCHA array (Kanzow et al., 2010). For the 1-year period 1 April 2009 to 31 March 2010, the AMOC mean strength was 12.8 Sv, a 5.7 Sv reduction relative to the previous 5 years (McCarthy et al., 2012). This change was manifest in a strengthening of southward interior flow in the upper 1000 m and a weakening of the southward flow in deep layers. While the AMOC weakening in 2009/2010 was relatively large, it subsequently rebounded and the time-series (Figure 3.11b) is too short to detect a trend in the presence of large interannual variations.

To estimate AMOC strength and variability at 41°N, Willis (2010) combines velocities from Argo drift trajectories, Argo temperature and salinity profiles and satellite altimeter data (Figure 3.11b). Here the AMOC magnitude is 15.5 Sv ± 2.2 from 2002–2009 (Figure 3.11b). This study suggests an increase in the AMOC strength of about 2.6 Sv from 1993–2010, though with low confidence because it is based on SSH alone in the pre-Argo interval of 1993–2001.

At 16°N, geostrophic array-based observations of the southward transport of North Atlantic Deep Water (NADW) in the depth range 1100 to 4700 m have been made continuously since 2000 (Kanzow et al., 2008). These measurements of the southward flow of NADW in the western basin may be representative of overall AMOC transport and variability, assuming a constant reference level for the geostrophic calculations and negligible flow east of the Mid-Atlantic Ridge. For the period 2000 to mid-2009, a downward trend was found (at 85% confidence) by Send et al. (2011); for the updated transport time series shown in Figure 3.11b, including mid-2009 through 2010, there is no apparent trend.

The measured or inferred AMOC estimates at 16°N, 26.5°N, and 41°N have time series of length nine, eight, and seven years respectively (Figure 3.11b). All show a substantial variability of ~3–5 Sv for three month low-pass time series, with a peak-to-peak interannual variability of 5 Sv. The shortness of these time series, and the relatively large interannual variability emerging in them suggests that trend estimates be treated cautiously, and no trends are seen at 95% confidence in any of the time series.

Indirect estimates of the annual average AMOC strength and variability can be made (Grist et al., 2009; Josey et al., 2009) from diapycnal transports driven by air-sea fluxes (NCEP-NCAR reanalysis fields from 1960 to 2007) or by inverse techniques (Lumpkin and Speer, 2007). Decadal fluctuations of up to 2 Sv are seen, but no trend. The decadal variability is generally in phase from 30–80°N, except in the 1990s when anomalies north and south of 60°N are out of phase. Consistent with Grist et al. (2009), the sea level index of the strength of the AMOC, based on several coherent western boundary tide gauge records between 39°N and 43°N at the American coast (Bingham and Hughes, 2009) shows no long-term trend from 1960 to 2007. Similarly, none of the direct, continuous transport estimates of single components of the AMOC exhibit long-term trends at 95% significance. These include the Florida Current (going back to 1982; Meinen et al., 2010), the overflows entering the Atlantic across Greenland-Scotland Ridge (going back to 1995; Olsen et al., 2008) and the DWBC at the exit of the Labrador Sea (going back to 1997; Fischer et al., 2010).

Measurements of the AMOC and of circulation elements contributing to it, at various latitudes and covering different time periods, agree that the range of inter-annual variability is 5 Sv (Figure 3.11b). These estimates do not have trends, in either the subtropical or the subpolar gyre. However, the observational record of AMOC variability is short, and there is insufficient evidence to support a finding of meridionally coherent change in the transport of the AMOC.

3.6.4 The Antarctic Meridional Overturning Circulation

Below the AMOC, AABW sinks around Antarctica and spreads northward ventilating the bottom-most portions of much of the ocean (Orsi et al., 1999). Observed widespread warming of AABW in recent decades (Section 3.5.4) implies a concomitant reduction in its northward spread. Reductions of 1–4 Sv in northward transports of AABW across 24°N have been estimated by geostrophic calculations using repeat oceanographic section data between 1981 and 2004 in the North Atlantic Ocean (Johnson et al., 2008a) and between 1985 and 2005 in the North Pacific (Kouketsu et al., 2009). A global full-depth ocean data assimilation study shows a reduction of northward AABW flow across 35°S of ~2 Sv in the South Pacific starting around 1985 (Kouketsu et al., 2011). This reduction is consistent with the contraction in volume of AABW (Purkey and Johnson, 2012) discussed in Section 3.5.4.

3.6.5 Water Exchange Between Ocean Basins

3.6.5.1 The Indonesian Throughflow (ITF)

The transport of water from the Pacific to the Indian Ocean via the Indonesian archipelago is the only low-latitude exchange between oceans, and is significant because it is a fluctuating sink/source for very warm tropical water in the two oceans. ITF transport has been estimated from hydrographic and XBT transects between Australia and Indonesia, and as a synthesis of these together with satellite altimetry, wind stress, and other data (Wunsch, 2010), and from moorings in the principal Indonesian passages. The most comprehensive observations were obtained in 2004–2006 in three main passages by the INSTANT mooring array (Sprintall et al., 2009), and show a transport of 15.0 (±4) Sv. On a longer timescale, Wainwright et al. (2008) analyzed data along the IX1 Australia-Indonesia XBT transect and found a change in the slope of the thermocline for data before and after 1976, indicating a decrease in geostrophic transport by 23%, consistent with a weakening of the trade winds (e.g., Vecchi et al., 2006). Other transport estimates based on the IX1 transect show correlation with ENSO variability (Potemra and Schneider, 2007) and no significant trend for the period since 1984 having continuous sampling along IX1 (Sprintall et al., 2002). Overall, the limited evidence provides low confidence that a trend in ITF transport has been observed or can be excluded.

3.6.5.2 The Antarctic Circumpolar Current (ACC)

Westerly winds in the Southern Ocean have increased since the 1970's, associated with a positive trend in the SAM (Marshall, 2003). While a few observational studies have found evidence for correlation between SAM and ACC transport on subseasonal to interannual scales (e.g., Hughes et al., 2003; Meredith et al., 2004), there is no significant observational evidence of an increase in ACC transport associated with the multi-decadal trend in wind forcing over the Southern Ocean. Repeat hydrographic sections in Drake Passage (e.g., Cunningham et al., 2003; Gladyshev et al., 2008; Koshlyakov et al., 2007; Koshlyakov et al., 2011), south of Africa (Swart et al., 2008) and south of Australia (Rintoul et al., 2002) reveal moderate variability but no significant trends in these short and discontinuous records. A comparison of recent Argo data and a long-term climatology showed that the slope of density surfaces (hence baroclinic transport) associated with the ACC had not changed in recent decades (Böning et al., 2008). Models that resolve eddies also suggest the ACC transport is relatively insensitive to trends in wind forcing, consistent with the ACC being in an "eddy-saturated" state where increases in wind forcing are largely compensated by changes in the eddy field (Farneti et al., 2010; Hallberg and Gnanadesikan, 2006; Spence et al., 2010). While there is limited evidence for (or against) multi-decadal changes in transport of the ACC, observations of changes in temperature, salinity and sea surface height indicate the current system has shifted polewards along with a poleward shift in the westerly winds in recent decades (Böning et al., 2008; Gille, 2008; Kazmin, 2012; Sokolov and Rintoul, 2009).

3.6.5.3 North Atlantic / Nordic Seas Exchange

There is no observational evidence of changes during the past two decades in the flow across the Greenland-Scotland Ridge, which connects the North Atlantic with the Norwegian and Greenland Seas. Direct current measurements since the mid-1990s have not shown any significant trends in volume transport for any of the three inflow branches (Hansen et al., 2010; Jónsson and Valdimarsson, 2012; Mauritzen et al., 2011; Østerhus et al., 2005).

The two primary pathways for the deep southward overflows across the Greenland-Scotland Ridge are the Denmark Strait and Faroe Bank Channel. Moored measurements of the Denmark Strait overflow demonstrate significant interannual transport variations (Jochumsen et al., 2012; Macrander et al., 2005), but the time-series is not long enough to detect a multi-decadal trend. Similarly, a ten-year time-series of moored measurements in the Faroe Bank channel (Olsen et al., 2008) does not show a trend in transport.

3.6.6 Conclusion

In summary, recent observations have strengthened evidence for variability in major ocean circulation systems on time scales from years to decades. It is *very likely* that the subtropical gyres in the North Pacific and South Pacific have expanded and strengthened since 1993, but it is *about as likely as not* that this reflects a decadal oscillation linked to changes in wind forcing, including changes in winds associated with the modes of climate variability. There is no evidence for a long-term trend in the AMOC or any component of the AMOC, although there are large interannual fluctuations. Nor is there evidence of a trend in the transports of the ITF, the ACC, or between the Atlantic and Nordic Seas. Given the short duration of direct measurements of ocean circulation, we have *very low confidence* that multi-decadal trends can be separated from decadal variability.

3.7 Sea Level Change, Including Extremes

3.7.1 Introduction and Overview of Sea Level Measurements

Sea level will vary as the ocean warms or cools, as water is transferred between the ocean and continents, and as water is redistributed within the ocean due to changes in the tides and ocean and atmospheric circulation. Time scales range from days to centuries, spatial scales from <1 km to global, and height from a few mm to a meter or more (due to tides). Thus, sea level integrates multiple climatic and dynamical signals, and, perhaps more importantly, measurements of sea level are our longest-running ocean observation system. This chapter assesses interannual and longer variations in sea level from the instrumented period (late 18th Century to the present). Chapter 4 assesses contributions of ice mass to sea level, Chapter 5 assesses reconstructions of sea level from the geological record, and Chapter 13 synthesizes results and assesses projections of sea level change.

There are intermittent records of sea level at Amsterdam from 1700 and at three more sites in Northern Europe starting after 1770. By the late 1800s, more tide gauges were being operated in Northern Europe, along with three more on the North American East Coast and two on the North American West Coast. The first measurements of sea level from the Southern Hemisphere began after 1880, all in Australia and New Zealand. There were no tide gauges on islands within the Pacific, Indian, or Atlantic Oceans (except at Hawaii) until the 1950s, and the majority were not placed until the 1980s. Tide gauge records measure the combined effect of ocean volume change and vertical land motion (VLM). For detecting climate change variability in tide gauge sea level records, one is interested in measuring the ocean volume change, so the VLM signal must be removed. One component that can be accounted for to a certain extent is the VLM associated with glacial isostatic adjustment (GIA) (Peltier, 2001). In some areas, however, VLM from tectonic activity, ground-water mining or hydrocarbon extraction is greater than GIA; these effects can be reduced by selecting gauges with no known tectonic or subsidence issues (e.g., Holgate, 2007) or by selecting gauges where GIA models tend to have small differences, suggesting low uncertainty (Spada and Galassi, 2012). More recently, global positioning system (GPS) receivers have been installed at tide gauge sites to measure VLM as directly as possible (e.g., Wöppelmann et al., 2009). However, these measurements of VLM are only available since the late 1990s at the earliest, and either have to be extrapolated into the past to apply to older records, or used to identify sites without extensive VLM.

Satellite radar altimeters in the 1970s and 1980s made the first nearly global observations of sea level, but these early measurements were highly uncertain and of short duration. The first precise record began with the launch of TOPEX/Poseidon (T/P) in 1992. This satellite and its successors (Jason-1, Jason-2) have allowed for continuous measurements of sea level variability at 10-day intervals between ±65° latitude. Additional altimeters in different orbits (ERS-1, ERS-2, Envisat, Geosat Follow-on) have allowed for measurements up to ±82° latitude and at different temporal sampling (3-days to 35-days), although these measurements are not as accurate as those from the T/P and Jason satellites. Unlike tide gauges, altimetry measures sea level relative to a fixed geodetic reference (classically a reference ellipsoid that coincides with the mean shape of the Earth, defined within a globally realized terrestrial reference frame) and thus will not be affected by VLM, although a small correction which depends on the area covered by the satellite (~0.3 mm yr^{-1}) must be added to account for the change in location of the ocean bottom relative to the reference frame of the satellite due to GIA (Peltier, 2001).

Tide gauges and satellite altimetry measure the combined effect of ocean warming and mass changes on ocean volume. Although variations in the density related to upper-ocean salinity changes will cause regional changes in sea level, when globally averaged their effect on sea level rise is an order of magnitude or more smaller than thermal effects (Lowe and Gregory, 2006). The thermal contribution to sea level can be calculated from in situ temperature measurements (Section 3.2). It has only been possible to directly measure the mass component of sea level since the launch of the Gravity Recovery and Climate Experiment (GRACE) in 2002 (Chambers et al., 2004). Before that, estimates were based either on estimates of glacier and ice sheet melting (trends only) or using residuals between sea level measured by altimetry or tide gauges and estimates of the thermosteric component (e.g., Domingues et al., 2008; Willis et al., 2004), which allowed for the estimation of seasonal and interannual variations as well. GIA also causes a gravitational signal in GRACE data that must be removed in order to determine present-day mass changes; this correction is of the same order of magnitude as the expected trend and is still uncertain at the 30% level (Chambers et al., 2010).

3.7.2 Trends in Global Mean Sea Level and Components

Tide gauges with the longest continuous records of sea level show increasing sea level over the 20th Century (Figure 3.12; Mitchum et al., 2010; Woodworth et al., 2009). There are, however, significant interannual and decadal-scale fluctuations about the average rate of sea level rise in all records. Multiple methods have been used to compute the mean rate of 20th Century global mean sea level (GMSL) rise from the available tide gauge data: computing average rates from only very long, nearly continuous records (Douglas, 2001; Holgate, 2007); using more numerous but shorter records and filters to separate nonlinear trends from decadal-scale quasi-periodic variability (Jevrejeva et al., 2006; Jevrejeva et al., 2008); neural network methods (Wenzel and Schroeter, 2010); computing regional sea level for specific basins then averaging based on the ocean area covered (Jevrejeva et al., 2006; Jevrejeva et al., 2008; Merrifield et al., 2009); or projecting tide gauge records onto empirical orthogonal functions (EOFs) computed from modern altimetry (Church and White, 2011; Church et al., 2004; Ray and Douglas, 2011) or EOFs from ocean models (Llovel et al., 2009; Meyssignac et al., 2012). The time-series from different approaches show very similar long-term trends, but noticeably different interannual and decadal-scale variability (Figure 3.13a). Only the time-series from Church and White (2011) extends to 2010, so it is used in the assessment of rates of sea level rise. The rate from 1901 to 2010 is 1.7 [1.5 to 1.9] mm yr^{-1} (90% confidence; Table 3.1), which is unchanged from the value in AR4. Rates computed from the different time series over the longest common interval (1900–2003) agree with this estimate within the uncertainty.

[INSERT FIGURE 3.12 HERE]

Figure 3.12: 3-year running mean sea level from long tide gauge records representing each ocean basin from the Permanent Service for Mean Sea Level (PSMSL), corrected for Glacial Isostatic Adjustment (GIA) (Peltier, 2004), after Woodworth et al. (2009).

Since AR4, significant progress has been made in quantifying the uncertainty in GMSL associated with unknown VLM, or uncertainty in GIA models. While rates of GMSL rise computed with and without VLM from GPS do differ, the differences are smaller than the estimated uncertainties (Merrifield et al., 2009; Wöppelmann et al., 2009). Studies have also examine the effect of using different GIA models to correct tide

gauge measurements and show the differences are less than 0.2 mm yr^{-1} (one standard error), and that the rate of GMSL rise computed from uncorrected tide gauges with that computed from corrected gauges differs by only 0.4 mm yr^{-1} (Spada and Galassi, 2012), which is again within the uncertainty estimates. This gives increased confidence that the 20th Century rate of GMSL rise is not biased high due to under-corrected VLM at the gauges.

Satellite altimetry can better resolve interannual fluctuations in GMSL (Figure 3.13b), and it is clear that deviations from the long-term trend can exist for periods of several years, especially during El Niño (e.g., 1997–1998) and La Niña (e.g., 2011) events (Boening et al., 2012; Cazenave et al., 2012; Nerem et al., 1999). The rate of GMSL rise since 1993 is 3.2 [2.8 to 3.6] mm yr^{-1} based on the average of altimeter time series published by multiple groups (Ablain et al., 2009; Beckley et al., 2010; Church and White, 2011; Leuliette and Scharroo, 2010; Nerem et al., 2010, Figure 3.13). As noted in AR4, this continues to be a statistically higher rate than that for the 20th-Century (Table 3.1). There is high confidence that this change is real and not an artefact of the different sampling or change in instrumentation, as the trend estimated over the same period from either the tide gauge records or the altimetry is consistent. The higher rate is *likely* the result of a multi-decadal oscillation rather than an acceleration (Section 3.7.4). The 6-year rate of GMSL rise since 2005 is lower than the longer, 18-year rate (Figure 3.13b; Table 3.1), but this *likely* reflects an interannual fluctuation, possibly due to a decrease in insolation during the last solar cycle (Hansen et al., 2011). The lower rate since 2005 is not unusual, being consistent with earlier interannual fluctuations in the record (e.g., 1993–1997).

Since AR4, estimates of both the thermosteric component and mass component of GMSL rise have improved, although for the latter it is only possible since the start of the GRACE measurements in 2002. After correcting for biases in older XBT data (Section 3.2), the rate of thermosteric sea level rise in the upper 700 m since 1971 is 50% higher than estimates used for AR4 (Domingues et al., 2008; Wijffels et al., 2008). Because of much sparser upper ocean measurements before 1971, we only estimate the trend since then (Section 3.2). The warming of the upper 700 m from 1971 to 2010 caused an estimated mean thermosteric rate of rise of 0.6 [0.4 to 0.8] mm yr^{-1} (90% confidence), which is 30% of the observed rate of GMSL rise for the same period (Table 3.1; Figure 3.13c). Although still a short record, more numerous, better distributed, and higher quality CTD measurements from the Argo program are now being used to estimate the steric component for the upper 700 m as well as for the upper 2000 m. Published trends for the upper 700 m from Argo have been computed over periods from as short as 3 years and as long as 6 years, with trends ranging from 0 to 0.9 mm yr^{-1} (Cazenave et al., 2009; Leuliette and Miller, 2009; Leuliette and Willis, 2011; Llovel et al., 2011; von Schuckmann and Le Traon, 2011; Willis et al., 2008; Willis et al., 2010). However, these data have been shown to be best suited for global analyses after 2005 due to a combination of interannual variability and large biases when using data before 2005 due to sparser sampling (Leuliette and Miller, 2009; von Schuckmann and Le Traon, 2011). The most recent estimate from 2005 to 2010 for the upper 700 m is 0.6 [0.4 to 0.8] mm yr^{-1} (Leuliette and Willis, 2011; Table 3.1).

Observations of the contribution to sea level rise from warming below 700 m are still highly uncertain due to limited historical data, especially in the Southern Ocean (Section 3.2). Before Argo, they are based on 5-year averages to 2000-m depth (Levitus et al., 2012). From 1971 to 2010, the estimated trend for the contribution between 700 m and 2000 m is 0.1 [0 to 0.2] mm yr^{-1} (90% confidence; Table 3.1; Levitus et al., 2012). This rate is unchanged during the period (2005–2010) when we have more global observations of this depth range with Argo (Table 3.1; von Schuckmann and Le Traon, 2011). To measure the contribution of warming below 2000 m, much sparser but very accurate CTD casts along repeat hydrographic sections are utilized (Kouketsu et al., 2011; Purkey and Johnson, 2010). The studies have found a significant warming trend between 1000 and 4000 m within and south of the Sub-Antarctic Front (Figure 3.3). The estimated total contribution of warming below 2000 m to global mean sea level rise between circa 1992 and 2005 is 0.11 [0.01 to 0.21] mm yr^{-1} (95% confidence as reported by authors; Purkey and Johnson, 2010). The influence of salinity changes below 3000m depth on global sea level were negative in the 1990s to 2000 and of the order of –10% of the warming signal (Kouketsu et al., 2011).

Ocean mass from the GRACE mission was not assessed in AR4, as the record was too short and there was still considerable uncertainty in the measurements and corrections required. Considerable progress has been made since AR4, and all recently published trends in ocean mass measured by GRACE show increasing mass since 2002 at a rate between 1 and 2 mm yr^{-1} (Cazenave et al., 2009; Chambers et al., 2010; Leuliette

and Miller, 2009; Leuliette and Willis, 2011; Llovel et al., 2010; Willis et al., 2008; Willis et al., 2010). Differences are due to the time periods used to compute trends, as there are significant interannual variations in the mass component of GMSL (Chambers et al., 2010; Llovel et al., 2010; Willis et al., 2008), but are also due to a substantial difference in GIA corrections applied, of order 1 mm yr^{-1}. Recent evaluations of the GIA correction have found explanations for the large difference (Chambers et al., 2010; Peltier et al., 2012). The trend in the measured mass component of sea level (between ±65° latitude) from 2005 to 2010 is 1.2 [0.8 to 1.6] mm yr^{-1} (90% confidence level; Table 3.1; updated from Leuliette and Willis, 2011). Adding the 2005–2010 rates of thermosteric sea level rise from Argo to 2000 m depth ([0.7 to 1.3] mm yr^{-1}) with that from ocean mass ([0.8 to 1.6] mm yr^{-1}) gives a rate of GMSL rise ([1.5 to 2.9] mm yr^{-1}) that is consistent with the rate measured by altimetry ([1.7 to 2.9] mm yr^{-1}) within the uncertainty, which gives high confidence that the current ocean observing system is capable of resolving the long-term rate of sea level rise and its components, assuming continued measurements. Moreover, the data are also consistent at monthly-scales (Figure 3.13d).

[INSERT FIGURE 3.13 HERE]

Figure 3.13: Global mean sea level from the different measuring systems as they have evolved in time. **a)** Yearly average GMSL reconstructed from tide gauges (1900–2010) by three different approaches (Church and White, 2011; Jevrejeva et al., 2012; Ray and Douglas, 2011), **b)** GMSL (1993–2010) from tide gauges, along with measurement from altimetry (Nerem et al., 2010) with seasonal variations removed and smoothed with a 60-day running mean **c)** GMSL (1970–2010) from tide gauges along with the thermosteric component, (3-year running mean) estimated from in situ temperature profiles (updated from Domingues et al., 2008), **d)** the GMSL (nonseasonal) from altimetry and that computed from the mass component (GRACE) and steric component (Argo) from 2005–2010 (Leuliette and Willis, 2011), all with a 3-month running mean filter. All uncertainty bars are one standard error as reported by the authors. The thermosteric component is just a portion of total sea level, and is not expected to agree individually with total sea level. The time-series are plotted relative to 5-year mean values that start at **a)** 1900, **b)** 1970, **c)** 1993, and **d)** 2005.

3.7.3 Regional Patterns of Sea Level Change

Global patterns of sea level change are known to high precision only since 1993, based on satellite altimetry (Figure 3.10). These data have shown a persistent pattern of change since the early 1990s in the Pacific, with rise rates in the Warm Pool of the western Pacific up to three times larger than those for GMSL, while rates over much of the eastern Pacific are near zero or negative (Beckley et al., 2010). The increasing sea level in the Warm Pool started shortly before the launch of TOPEX/Poseidon (Merrifield, 2011), and is caused by an intensification of the trade winds (Merrifield and Maltrud, 2011) that may be related to the PDO (Merrifield et al., 2012; Zhang and Church, 2012). The lower rate of GMSL rise along the western coast of the United States has also been attributed to changes in the wind stress curl over the North Pacific associated with the PDO (Bromirski et al., 2011). While global maps can be created using EOF analysis (e.g., Church et al., 2004; Llovel et al., 2009), the patterns are still highly uncertain, as the method assumes that the EOFs since 1993 are capable of representing the patterns in previous decades, and results may be biased in the middle of the ocean where there are no tide gauges to constrain the estimate (Ray and Douglas, 2011). Several studies have examined the individual long tide gauge records in the North Atlantic and have found coherent decadal-scale variations along both the U.S. east coast (Hong et al., 2000; Miller and Douglas, 2007; Sturges and Hong, 1995)and the European coast (Calafat et al., 2012; Sturges and Douglas, 2011; Woodworth et al., 2010), all caused by a variety of mechanisms related to natural climate variability. It is difficult to map such patterns globally before 1993 using tide gauge data directly, except on the very broadest scales (i.e., by averaging regional gauges).

There is still considerable uncertainty on how long such large-scale patterns of regional sea level change can persist, especially in the Pacific where the majority of tide gauge records are less than 40-years long. Based on the analysis of the long-records discussed in the previous paragraph, it is *likely* that regional rates of sea level rise can be significantly higher or lower than the GMSL rate for periods of a decade or more. Reconstructions of mean sea level over basin-scales and larger suggest significant variations with periods between 50 and 75 years (Jevrejeva et al., 2008; Wenzel and Schroeter, 2010), which have also been observed in individual records in the Atlantic, Indian, and Pacific Oceans (including the available gauges in the Southern Ocean) (Chambers et al., 2012).

The previous analysis of regional sea level trends has focused on effects that appear to be related to regional ocean volume change, and not those due to VLM. As discussed in Section 3.7.1, VLM can dramatically

affect local sea level change. Some extreme examples of this are Neah Bay, Alaska, where the VLM is +3.8 mm yr^{-1} (uplift from tectonic activity); Galveston, Texas, where the VLM is –5.9 mm yr^{-1} (subsidence from groundwater mining); and Nedre Gavle, Sweden where the VLM is +7.1 mm yr^{-1} (uplift from GIA), all computed from nearby GPS receivers (Wöppelmann et al., 2009). These areas will all have long-term rates of sea level rise that are significantly higher or lower than those due to ocean volume change alone, but as these rates are not related to climate change, they are outside the scope of this assessment.

3.7.4 Observations of Accelerations in GMSL

AR4 concluded that there was "high confidence that the rate of global sea level rise increased from the 19th to the 20th Century" but could not be certain as to whether the higher rate since 1993 was reflective of decadal variability or a further increase in the longer-term trend. Since AR4, there has been considerable effort to quantify the level of decadal and multi-decadal variability in GMSL and to detect acceleration in GMSL and mean sea level at individual tide gauges. It has been clear for some time that there was a significant increase in the rate of sea level rise in the four oldest records from Northern Europe starting in the early- to mid-19th Century (Ekman, 1988; Mitchum et al., 2010; Woodworth, 1990, 1999). Estimates of the change in the rate have been computed, either by comparing trends over 100-year intervals for the Amsterdam site (Ekman, 1988; Woodworth, 1990), or by fitting a quadratic term to all the long records starting before 1850 (Woodworth, 1990, 1999). The results are consistent and indicate a significant acceleration that started in the early- to mid- 19th Century (Woodworth, 1990, 1999), although some have argued it may have started in the late 1700s (Jevrejeva et al., 2008). The increase in the rate of sea level rise at Amsterdam (the longest record) is 1.0 [0.7 to 1.3] mm yr^{-1} (1 standard error, as calculated by Woodworth, 1990), based on differencing 100-year trends from 1874–1884 and 1885–1985. Although sites in other ocean basins do show an increased trend after 1860 (e.g., Figure 3.12), it is impossible to detect the change that occurred in Northern Europe in the early- to mid-1800s in other parts of the ocean using tide gauge data alone, as there are no observations.

Numerous studies have attempted to quantify if the acceleration has continued in the 20th Century. Studies have attempted to detect an acceleration in the rate of sea level rise by fitting a quadratic to data at individual tide gauges (Houston and Dean, 2011; Watson, 2011; Woodworth et al., 2011; Woodworth et al., 2009) as well as to reconstructed time-series of GMSL (Church and White, 2006; Church and White, 2011; Jevrejeva et al., 2008), or by examining differences in long-term rates computed at different tide gauges (Sallengar et al., 2012). Results are very dependent on the time-period and locations used. Woodworth et al. (2011) find significant acceleration terms at the sites that extend back before 1860 (all in the Northern Hemisphere). Other authors have used more numerous but significantly shorter records (all starting after 1920) and have found either insignificant change or small deceleration terms (Houston and Dean, 2011; Watson, 2011), or highly significant regional acceleration since 1950 (Sallengar et al., 2012). This discrepancy is related to three inflections in the 20th Century data (Holgate, 2007; Mitchum et al., 2010; Woodworth et al., 2011; Woodworth et al., 2009). They are marked by an increasing trend starting in 1920-1940 and a downward trend (i.e., leveling of sea level) starting around 1960, and an increasing trend in the late 1980s. This pattern can be seen in New York, Mumbai, and Fremantle records, for instance (Figure 3.12). Fitting a quadratic terms to tide gauge data after 1920 results in a negative acceleration due to the levelling of sea level after 1960 (Rahmstorf and Vermeer, 2011). Using data before 1900, however, the acceleration term computed from both individual tide gauge records and GMSL reconstructions is significantly positive (Church and White, 2011; Jevrejeva et al., 2008; Rahmstorf and Vermeer, 2011; Woodworth et al., 2011). Church and White (2006) report that the estimated acceleration term in GMSL (twice the quadratic parameter) is 0.009 [0.006 to 0.012] mm yr^{-2} (1 standard deviation) from 1880 to 2009, which is consistent with the other published estimates (e.g., Jevrejeva et al., 2008; Woodworth et al., 2009) that use observations before 1920.

[INSERT FIGURE 3.14 HERE]

Figure 3.14: 18-year trends of GMSL rise estimated at 1-year intervals. The time is the start date of the 18-year period, and the shading represents the 90% confidence. The estimate from satellite altimetry is also given, with the 90% confidence given as an error bar.

It is possible that the inflections in 1920, 1960, and 1990 are caused by a multi-decadal climate oscillation with a strong peak between 50 and 60 years (e.g., Holgate, 2007; Jevrejeva et al., 2008). This is seen in all reconstructions (Figure 3.14; Church and White, 2011; Jevrejeva et al., 2008; Merrifield et al., 2009; Ray

and Douglas, 2011) as well as in tide gauge records around the world that extend back to 1900 (Chambers et al., 2012). Although the calculations of 18-year rates of GMSL rise based on the different reconstruction methods disagree by as much as 2 mm yr^{-1} before 1950, all do indicate 18-year trends that were significantly higher than the 20th Century average between 1930 to 1950, with rates comparable to the those measured in the recent period with satellite altimetry. Multi-decadal fluctuations with periods around 60 years appear in many climate indices (Section 2.6.8), including the AMO and PDO. Whether these quasi 60-year oscillations represent a real global variation or are related to sampling regional oscillations at the tide gauge locations is still unknown, but this should be accounted for when computing acceleration terms, especially over a portion of the cycle. When a 60-year oscillation is modeled along with an acceleration term, the estimated acceleration in GMSL since 1900 ranges from: 0.000 [–0.002 to 0.002] mm yr^{-2} (90% confidence) in the Ray and Douglas (2011) record, 0.013 [0.007 to 0.019] mm yr^{-2} in the Jevrejeva et al. (2008) record, and 0.012 [0.009 to 0.015] mm yr^{-2} (90% confidence) in the Church and White (2011) record. Thus, while there is more disagreement on the value of a 20th Century acceleration in GMSL when accounting for possible multi-decadal fluctuations, two out of three records still indicate a significant positive value. The much higher trend in GMSL calculated since 1993, however, *likely* reflects, in part, a multidecadal oscillation.

3.7.5 Changes in Extreme Sea Level

Aside from non-climatic events like tsunamis, extremes in sea level (i.e., coastal flooding, high water events, etc.) occur mainly due to tropical and extra-tropical storms. Changes in storminess are treated in Chapter 2, as well as SREX Chapter 3. However, as mean sea level rises, the frequency of high-water events relative to a fixed benchmark will also increase. We consider evidence of changes in extreme sea level independent of changes in storminess but related to changes in mean sea level. Since extreme sea level events are often perceived as a regional problem, global analyses of the changes in extremes are limited, and most reports are based on analysis of regional data (see Lowe et al., 2010 for a review). Methods used to derive changes in extremes rely either on the analysis of local tide gauge data, or on multi-decadal hindcasts of a dynamical model (WASA-Group, 1998). Most analyses have focused on specific regions and find that extremes have been increasing, using various statistical measures such as annual maximum surge, annual maximum surge-at-high-water, or changes in 99th percentile events (e.g., Church et al., 2006; D'Onofrio et al., 2008; Haigh et al., 2010; Letetrel et al., 2010; Marcos et al., 2009; Tsimplis and Shaw, 2010; Vilibic and Sepic, 2010). A global analysis of tide gauge records has been performed for data from the 1970s onwards when the 'global' data set has been reasonably copious, although a smaller subset of gauges were used to examine changes over the 20th Century (Menendez and Woodworth, 2010; Woodworth and Blackman, 2004; Woodworth et al., 2011).

AR4 concluded that the majority of extreme sea level trends are related to increasing mean sea level. The more recent studies published since AR4 continue to support this conclusion. The global studies (Menendez and Woodworth, 2010; Woodworth et al., 2011) find that while extreme sea levels have increased in amplitude and frequency at most locations around the world, this is largely as a result of the long-term change in mean sea level, although higher regional extremes are also related to interannual sea level changes associated with climate variations like ENSO and NAO (e.g., Abeysirigunawardena and Walker, 2008; Haigh et al., 2010; Menendez and Woodworth, 2010).

3.7.6 Conclusions

It is *virtually certain* that globally averaged sea level has risen at a mean rate between 1.4 and 2.0 mm yr^{-1} over the 20th Century and between 2.7 and 3.7 mm yr^{-1} since 1993 (both ranges 99% confidence). This assessment is based on high agreement among multiple studies using different methods, and from independent observing systems (tide gauges and altimetry) since 1993. It is *likely* that a rate comparable to that since 1993 occurred between 1930 and 1950, possibly due to a multi-decadal climate oscillation, as individual tide gauges around the world and all reconstructions of GMSL show increased rates of sea level rise during this period. Although local vertical land motion can cause even larger rates of sea level rise (or fall) relative to the coastline, it is *very likely* that this does not affect the estimates of the global average rate, based on multiple estimations of the average with and without VLM corrections.

It is *virtually certain* that interannual and decadal changes in the large-scale winds and ocean circulation can cause significantly higher or lower rates over shorter periods at individual locations, as this has been

observed in tide gauge records around the world. Warming of the upper 700 m of the ocean has *very likely* contributed an average of 0.6 [0.4 to 0.8] mm yr^{-1} of sea level change since 1971. Warming between 700 m and 2000 m has *likely* been contributing an additional 0.1 mm yr^{-1} [0 to 0.2] of sea level rise since 1971, and warming below 2000 m has been contributing another 0.11 [0.01 to 0.21] mm yr^{-1} of sea level rise since the early 1990s.

It is *virtually certain* that the ocean mass has increased at a rate between [0.8 to 1.6] mm yr^{-1} since 2005, based on high agreement between GRACE estimates over the same 6-year period and from the closure of the sea level balance equation based on multiple independent observations (altimetry, GRACE, Argo). It is *very likely* that the rate of mean sea level rise along Northern European coastlines has accelerated since the early 1800s and that this has continued into the 20th Century, as the signal has been observed in multiple long tide gauge records and by different groups using different analysis techniques. It is *likely* that sea level rise throughout the Northern Hemisphere has also accelerated since 1850, as this is also observed in a smaller number of gauges along the coast of North America. Two of the three time series based on reconstructing GMSL from tide gauge data back to 1900 or earlier indicate a non-zero acceleration, while one does not. The range is 0.0 to 0.019 mm yr^{-2}, so it is *likely* that GMSL has accelerated since 1900. Finally, it is l*ikely* that extreme sea levels have increased since 1970, and this is mainly attributable to rising mean sea level.

Table 3.1: Estimated trends in GMSL and components over different periods from representative time-series. Trends and uncertainty have been estimated from a time-series provided by the authors using ordinary least squares with the uncertainty representing the 90% confidence interval. The model fit for yearly averaged time-series was a bias + trend; the model fit for monthly and 10-day averaged data was a bias + trend + seasonal sinusoids. Uncertainty accounts for correlations in the residuals.

Quantity	Period	Trend (mm yr^{-1})	Source	Resolution
GMSL	1901–2010	1.7 [1.5 to 1.9]	Tide Gauge Reconstruction (Church and White, 2011)	Yearly
	1901–1990	1.5 [1.3 to 1.7]	Tide Gauge Reconstruction (Church and White, 2011)	Yearly
	1971–2010	2.0 [1.7 to 2.3]	Tide Gauge Reconstruction (Church and White, 2011)	Yearly
	1993–2010	2.8 [2.3 to 3.3]	Tide Gauge Reconstruction (Church and White, 2011)	Yearly
	1993–2010	3.2 [2.8 to 3.6][a]	Altimetry (Nerem et al., 2010) time-series	10-day
	2005–2010	2.3 [1.7 to 2.9][a]	Altimetry (Nerem et al., 2010)	10-day
Thermosteric Component (upper 700 m)	1971–2010	0.6 [0.4 to 0.8]	XBT Reconstruction (updated from Domingues et al., 2008)	3-year running means
	1993–2010	0.7 [0.4 to 1.0]	XBT Reconstruction (updated from Domingues et al., 2008)	3-year running means
	2005–2010	0.6 [0.4 to 0.8]	Argo (von Schuckmann and Le Traon, 2011)	Monthly
Thermosteric Component (700–2000 m)	1971–2010	0.1 [0 to 0.2]	Objective mapping of historical temperature data (Levitus et al., 2012)	5-year averages
	1993–2010	0.2 [0.1 to 0.3]	Objective mapping of historical temperature data (Levitus et al., 2012)	5-year averages
	2005–2010	0.2 [0 to 0.4]	Argo (von Schuckmann and Le Traon, 2011)	Monthly
Thermosteric Component (below 2000 m)	1992–2005	0.11 [0.01 to 0.21][b]	Deep hydrographic sections (Purkey and Johnson, 2010)	Trend only
Thermosteric Component (whole depth)	1971–2010	0.8 [0.5 to 1.1]	Combination of estimates from 0–700 m, 700–2000 m, and below 2000 m[c]	Trend Only
	1993–2010	1.0 [0.7 to 1.3]	Combination of estimates from 0–700 m, 700–2000 m, and below 2000 m[c]	Trend Only
	2005–2010	0.9 [0.6 to 1.2]	Combination of estimates from 0–700 m,	Trend Only

			700–2000 m, and below 2000 m[c]	
Ocean Mass Component	2005–2010	1.2 [0.8 to 1.6][d]	GRACE (updated from Leuliette and Willis, 2011)	Monthly

Notes:
(a) Uncertainty estimated from fit to Nerem et al. (2010) time series and includes potential systematic error due to drift of altimeter, estimated to be ±0.4 mm yr^{-1} (Beckley et al., 2010; Nerem et al., 2010), applied as the root-sum-square (RSS) with the least squares error estimate.
(b) Trend value taken from Purkey and Johnson (2010), Table 1. Uncertainty represents the 95% confidence interval.
(c) Assumes no trend below 2000 m before 1 January 1992, then value from Purkey and Johnson (2010) afterwards. Uncertainty for 0–700 m, 700–2000 m, and below 2000 m is assumed to be uncorrelated, and uncertainty is calculated as RSS of the uncertainty for each layer.
(d) Uncertainty estimated from fit to time series and includes potential systematic error due to GIA correction, estimated to be ±0.3 mm yr^{-1} (Chambers et al., 2010), applied as the RSS with the least squares error estimate.

3.8 Ocean Biogeochemical Changes, Including Anthropogenic Ocean Acidification

In this section, observations of the air-sea flux of carbon dioxide and of the evolving inventory of C_{ant} are summarised, followed by a summary of observed changes in oxygen content, which are related to changing ventilation, and a summary of nutrient changes.

3.8.1 Ocean Carbon

The reservoir of inorganic carbon in the ocean is roughly 50 times that of the atmosphere (Sabine et al., 2004). Thus, even small changes in the ocean reservoir may have a significant impact on the atmospheric concentration of CO_2. The fraction of total dissolved inorganic carbon (C_T) in the ocean due to increased atmospheric CO_2 concentrations (i.e., the anthropogenic CO_2, C_{ant}) cannot be measured directly but various techniques exist to infer C_{ant} from observations of interior ocean properties.

3.8.1.1 Long-Term Trends and Variability in the Ocean Uptake of Carbon from Observations

Currently, an amount of CO_2 equivalent to approximately 25% of the total CO_2 released to the atmosphere by burning of fossil fuels and land-use change enters the ocean across the air-sea interface (Le Quéré et al., 2010; Mikaloff-Fletcher et al., 2006). The air-sea flux of CO_2 can be computed from the observed difference in the partial pressure of CO_2 across the air-water interface ($\Delta pCO_2 = pCO_{2sw} - pCO_{2air}$), the solubility of CO_2 in seawater, and the gas transfer velocity (Wanninkhof et al., 2009). In general, the ΔpCO_2 remains roughly unchanged, that is surface ocean pCO_2 values have kept pace with the atmospheric CO_2 increase (Bates, 2012; Ishii et al., 2009; Keeling et al., 2004; McKinley et al., 2011; Midorikawa et al., 2005; Schuster and Watson, 2007b; Takahashi et al., 2006; Takahashi et al., 2009; Yoshikawa-Inoue and Ishii, 2005). However, the limited geographic and temporal coverage of the ΔpCO_2 measurement as well as uncertainties in wind forcing and transfer velocity parameterizations mean that significant uncertainties exist in global and regional fluxes calculated from ΔpCO_2 . In addition, the air-sea flux varies with climate forcing on a range of time-scales, as discussed below. As a consequence, regional estimates of decadal trends in fluxes are uncertain (± 50%), and no robust global trends in CO_2 fluxes based on ΔpCO_2 alone have been detected.

Quantitative information on trends of surface ocean pCO_2 and CO_2 uptake are available for specific regions. While local variations of ΔpCO_2 with time have little effect on the atmospheric CO_2 growth rate in the short term, they provide important information on the dynamics of the ocean carbon cycle and the potential for longer-term climate feedbacks. El Niño and La Niña can drive large changes in the efflux of CO_2 in the Pacific. For example, differences in ΔpCO_2 can exceed 100 µatm in the eastern and central equatorial Pacific between El Niño and La Niña (Feely et al., 2006). The efflux of CO_2 from the equatorial Pacific increased since 1998–2000 due a change in circulation associated with the Pacific Decadal Oscillation (PDO) and increasing winds (Feely et al., 2006). CO_2 uptake in the North Atlantic decreased by 0.24 Pg C yr^{-1} between 1994 and 2003 (Schuster and Watson, 2007a) and has partially recovered since then (Watson et al., 2009). Uptake of CO_2 in the Subtropical Mode Water (STMW) of the North Atlantic was enhanced during the 1990s, during a predominantly positive phase of the NAO, and much reduced in the 2000s when the NAO phase was neutral or negative Bates (2012). Flux anomalies in the North Atlantic have been linked to multiple climate indices, often with appreciable time lags, rather than a simple correlation with the NAO (Bates, 2007). Observations of pCO_2 from the Indian sector of the Southern Ocean were interpreted as

evidence for reduced CO_2 uptake as a result of increased winds, increased upwelling, and outgassing of natural CO_2 (Metzl, 2009).

3.8.1.2 Variations in C_{ant} Inventories with Time over the Past Four Decades

Ocean uptake and storage can also be assessed by considering changes in the inventory of anthropogenic carbon. Two independent data-based methods to calculate anthropogenic carbon inventories exist: the ΔC* method (Sabine et al., 2004), and the transit time distribution (TTD) method (Waugh et al., 2006). The Green's function approach (Khatiwala et al., 2009) is related to the latter. These approaches use tracer information and assume steady state ocean circulation, which tends to underestimate natural variability and changes in ocean productivity and biogeochemistry (Chavez et al., 2011). Errors introduced due to neglecting changes in circulation are likely much smaller than the inherent uncertainty of the methods.

The anthropogenic carbon inventory inferred from these methods for the year 1994 agree with each other within their uncertainties and range between 107 ± 14 PgC and 118 ± 19 PgC (Khatiwala et al., 2009; Sabine et al., 2004; Waugh et al., 2006). A recent compilation of inventories of C_{ant} from these methods combined with some model results suggests a "best" estimate of the global ocean inventory of anthropogenic carbon from 1750 to 2011 of 155 PgC with an uncertainty of ±20% (Khatiwala et al., 2012; Figure 3.15). While the estimates of total inventory agree within their uncertainty, the different methods result in significant differences in the inferred spatial distribution of C_{ant}, particularly at high latitudes.

The uptake rate corresponding to the Green's function estimate of inventory is 2.3 [1.7 to 2.9] PgC yr^{-1} from 2000 to 2010, in close agreement with an independent estimate of 2.5 [1.8 to 3.2] Pg C yr^{-1} based on atmospheric O_2/N_2 measurements obtained for the same period (Ishidoya et al., 2012). The O_2/N_2 method resulted in 2.2 [1.6 to 2.8] PgC yr^{-1} for the time period 1993 to 2003 (Manning and Keeling, 2006). From surface water partial pressure (pCO_2) measurements, Gruber et al. (2009) obtained for the time period 1995–2000 a global uptake rate of 1.9 [1.2 to 2.5] PgC yr^{-1} , and Takahashi et al. (2009) found 2.0 [1.0 to 3.0] PgC yr^{-1} normalized to the year 2000. The consistency between these independent calculations provides high confidence that the ocean is taking up anthropogenic CO_2.

[INSERT FIGURE 3.15 HERE]

Figure 3.15: Compilation of the 2010 column inventories (mol m^{-2}) of anthropogenic CO_2: the global Ocean excluding the marginal seas (updated from Khatiwala et al., 2009) 150 ± 26 PgC; Arctic Ocean (Tanhua et al., 2009) 2.7–3.5 PgC; the Nordic Seas (Olsen et al., 2010) 1.0–1.6 PgC; the Mediterranean Sea (Schneider et al., 2010) 1.6–2.5 PgC; the East Sea (Sea of Japan) (Park et al., 2006) 0.40 ± 0.06 PgC. From Khatiwala et al. (2012).

The storage rate of anthropogenic carbon dioxide can also be assessed by calculating the change in C_{ant} concentration between two time periods, an approach that is less dependent on the assumption of a steady state circulation. Regional observations of the storage rate are in broad agreement with that expected from the increase in atmospheric CO_2 concentrations and with the tracer-based estimates. However, there are significant spatial and temporal variations in the degree to which the inventory of C_{ant} tracks changes in the atmosphere (Figure 3.16). The North Atlantic, in particular, is an area with high variability in circulation and deep water formation, influencing the C_{ant} inventory. As a result of the decline in Labrador Sea Water (LSW) formation since 1997 (Rhein et al., 2011), the C_{ant} increase between 1997 and 2003 was smaller in the subpolar North Atlantic than expected from the atmospheric increase, in contrast to the subtropical and equatorial Atlantic (Steinfeldt et al., 2009). Perez et al. (2010) noted the dependence of the C_{ant} storage rate in the North Atlantic on the NAO, with high C_{ant} storage rate during phases of high NAO (i.e., high LSW formation rates) and low storage during phases of low NAO (low formation). Wanninkhof et al. (2010) found a the lower inventory increase in the North Atlantic compared to the South Atlantic.

Ocean observations are insufficient to assess whether there has been a change in the rate of total (anthropogenic plus natural) carbon uptake by the global ocean. Evidence from regional ocean studies (often covering relatively short time periods), atmospheric observations and models is equivocal, with some studies suggesting the ocean uptake of total CO_2 may have declined (Le Quéré et al., 2007; McKinley et al., 2011; Sarmiento et al., 2010; Schuster and Watson, 2007b) while others conclude that a decline is rather unlikely (Gloor et al., 2010; Knorr, 2009; Sarmiento et al., 2010).

[INSERT FIGURE 3.16 HERE]

Figure 3.16: Top: Maps of storage rate distribution of anthropogenic carbon (mol m^{-2} yr^{-1}) for the three ocean basins (Left to right: Atlantic, Pacific, and Indian Ocean) averaged over 1980–2005 estimated by the Green's function approach (Khatiwala et al., 2009). Bottom: Corresponding storage rates as observed from repeat hydrography cruises. Measurements for the northern hemisphere are drawn as solid lines, the tropics as dash-dotted lines, and dashed lines for the southern hemisphere; the color schemes refer to different studies. Estimates of uncertainties are shown as vertical bars with matching colors. The solid black line represents the basin average storage rate using the same Green function approach (Khatiwala et al., 2009). Data sources as indicated in the legend are: 1) Wanninkhof et al. (2010), 2) Murata et al. (2008), 3) Friis et al. (2005), 4) Tanhua et al. (2007), 5) Olsen et al. (2006), 6) Rios et al. (2012), 7) Pérez et al. (2008), 8) Murata et al. (2007), 9) Murata et al. (2009), 10) Sabine et al. (2008), 11) Peng et al. (2003), 12) Wakita et al. (2010), 13) Matear and McNeil (2003), 14) Waters et al. (2011), 15) Peng et al. (1998), and 16) Murata et al. (2010). From Khatiwala et al. (2012).

In summary, the high agreement between multiple lines of independent evidence for increases in the ocean inventory and ocean uptake underpins the conclusion that it *is virtually certain* that the ocean is sequestering anthropogenic carbon dioxide.

3.8.2 Anthropogenic Ocean Acidification

The uptake of carbon dioxide by the ocean changes the chemical balance of seawater through the thermodynamic equilibrium of CO_2 with seawater. Dissolved CO_2 forms a weak acid and, as CO_2 in seawater increases, the pH, carbonate ion concentration [CO_3^{2-}], and $CaCO_3$ saturation state (Ω = [Ca^{2+}][CO_3^{-2}]/Ksp*) of seawater decrease. The mean pH (total scale) of surface waters ranges between 7.8 and 8.4 in the open ocean, so the ocean remains mildly basic (pH >7) at present (Feely et al., 2009; Orr et al., 2005). Ocean uptake of CO_2 results in gradual acidification of seawater; this process is termed ocean acidification (Broecker and Clark, 2001; Caldeira and Wickett, 2003). A decrease in ocean pH of 0.1 corresponds to a 26% increase in the H^+ concentration of seawater. The consequences of changes in pH, carbonate ion, and saturation states for $CaCO_3$ minerals on marine organisms and ecosystems are just beginning to be understood (see WGII Chapter 6).

Direct observations of oceanic total dissolved inorganic carbon (C_T = CO_2 + carbonate + bicarbonate) and computed partial pressure of CO_2 (pCO_2) reflect changes in both the natural carbon cycle and the uptake of anthropogenic CO_2 from the atmosphere. Ocean time-series stations in the North Atlantic and North Pacific record decreasing pH (Figure 3.17) with rates ranging between –0.0015 and –0.0024 per year (Bates, 2007; Bates, 2012; Dore et al., 2009; González-Dávila et al., 2010; Olafsson et al., 2009; Santana-Casiano et al., 2007). The greatest change occurs in the western subtropical North Atlantic and in the Iceland Sea during winter. Directly measured pH differences in the surface mixed layer along repeat transects in the central North Pacific Ocean between Hawaii and Alaska showed a -0.0017 yr^{-1} decline in pH between 1991 and 2006, which is in agreement with observations at the time-series sites (Figure 3.17b, Table 3.2, Byrne et al., 2010). This rate of pH change was also consistent with the repeat transects of CO_2 and pH measurements in the western Pacific (winter: –0.0018 ± 0.0002 yr^{-1}; summer: –0.0013 ± 0.0005 yr^{-1}) (Midorikawa et al., 2010).

[INSERT FIGURE 3.17 HERE]

Figure 3.17: Long-term trends of surface seawater pCO_2 (top), pH (middle), and carbonate ion (bottom) concentration at three subtropical ocean time series in the North Atlantic and North Pacific Oceans, including: **a)** Bermuda Atlantic Time-series Study (BATS, 31°40′N, 64°10′W; **green**) and Hydrostation S (32°10′, 64°30′W) from 1983 to present (published and updated from Bates, 2007); **b)** Hawaii Ocean Time-series (HOT) at Station ALOHA (A Long-term Oligotrophic Habitat Assessment; 22°45′N, 158°00′W; **orange**) from 1988 to present (published and updated from Dore et al., 2009), and; **c)** European Station for Time series in the Ocean (ESTOC, 29°10′N, 15°30′W; **blue**) from 1994 to present (published and updated from González-Dávila et al., 2010). Atmospheric pCO_2 (**black**) from Hawaii is shown in the top panel. Lines show linear fits to the data, whereas Table 3.2 give results for harmonic fits to the data (updated from Orr, 2011).

Seawater chemistry changes at the ocean time-series sites and in the North Pacific Ocean result from uptake of anthropogenic CO_2 (Doney et al., 2009), but also include other changes imparted by local physical and biological variability. As an example, while pH changes in the mixed layer of the North Pacific Ocean can be explained solely in terms of equilibration with atmospheric CO_2, declines in pH between 800 m and the mixed layer in the time period 1991 - 2006 were attributed in approximately equal measure to anthropogenic

and natural variations (Byrne et al., 2010). Figure 3.18 (Byrne et al., 2010) shows the portion of pH changes between the surface and 1000 m that were attributed solely to the effects of anthropogenic CO_2. Summary observations which include both anthropogenic and natural variations (Table 3.2; 1988–2009 trends) show that seawater pH and $[CO_3^{2-}]$ have decreased by 0.03–0.04 and ~8–10 µmoles kg^{-1}, respectively, over the last 20 years. Over longer time periods, anthropogenic changes in ocean chemistry are *likely* to become increasingly prominent relative to changes imparted by physical and biological variability. An anthropogenically induced decrease in surface water pH of 0.08 from 1765 to 1994 for the global ocean was calculated from the estimated uptake of atmospheric CO_2 (Sabine et al., 2004), with the largest reduction (–0.10) in the northern North Atlantic and the smallest reduction (–0.05) in the subtropical South Pacific. These results are consistent with the generally lower buffer capacities of the high latitude oceans compared to lower latitudes (Egleston et al., 2010).

[START BOX 3.2 HERE]

Box 3.2: Ocean Acidification

What is ocean acidification? Ocean acidification refers to a reduction in pH of the ocean over an extended period, typically decades or longer, caused primarily by the uptake of carbon dioxide from the atmosphere. Ocean acidification can also be caused by other chemical additions or subtractions from the oceans that are natural (e.g., increased volcanic activity, methane hydrate releases, long-term changes in net respiration) or human-induced (e.g., release of nitrogen and sulfur compounds into the atmosphere). Anthropogenic ocean acidification refers to the component of pH reduction that is caused by human activity (Caldeira, 2011).

Since the beginning of the industrial era, the release of carbon dioxide (CO_2) from our collective industrial and agricultural activities has resulted in atmospheric CO_2 concentrations that have increased from approximately 280 ppm to about 392 ppm in 2012. The atmospheric concentration of CO_2 is now higher than experienced on Earth for at least the last 800,000 years and is expected to continue to rise (Luthi et al., 2008; Siegenthaler et al., 2005). The oceans have absorbed approximately 155 Pg C from the atmosphere over the last two and a half centuries (Khatiwala et al., 2012; Sabine et al., 2004). This natural process of absorption has benefited humankind by significantly reducing the greenhouse gas levels in the atmosphere and minimizing some of the impacts of global warming. However, the ocean's uptake of carbon dioxide is having a significant impact on the chemistry of seawater. The average pH of ocean surface waters has already fallen by about 0.1 units, from about 8.2 to 8.1 (total scale), since the beginning of the industrial revolution (Feely et al., 2009; Orr et al., 2005; Figure 1). Estimates of future atmospheric and oceanic carbon dioxide concentrations indicate that, by the end of this century, the average surface ocean pH could be lower than it has been for more than 20 million years (Caldeira and Wickett, 2003).

The major controls on seawater pH are atmospheric CO_2 exchange, the production and respiration of dissolved and particulate organic matter in the water column, and the formation and dissolution of calcium carbonate minerals. Oxidation of organic matter lowers dissolved oxygen concentrations, adds CO_2 to solution, reduces carbonate ion and $CaCO_3$ saturation states (Figure 2), and lowers the pH of seawater in subsurface waters (Byrne et al., 2010). As a result of these processes, minimum pH values in the oceanic water column are generally found near the depths of the oxygen minimum layer. When CO_2 reacts with seawater it forms carbonic acid, which is highly reactive and reduces the concentration of carbonate ion (Figure 2) and can affect shell formation for marine animals such as corals, plankton, and shellfish. This process could affect some of the most fundamental biological and chemical processes of the sea in coming decades (Doney et al., 2009; Fabry et al., 2008).

Anthropogenic ocean acidification may produce far-reaching consequences for marine organisms. Results from laboratory and field studies, as well as data from the geological record, clearly show that marine ecosystems are highly susceptible to the increases in oceanic CO_2 and the corresponding decreases in pH, carbonate ion and $CaCO_3$ saturation state (Doney et al., 2009; Fabry et al., 2008). While some species, such as seagrasses, appear to benefit from ocean acidification, many calcifying species such as foraminifera, clams, oysters, mussels and corals will be increasingly affected by a decreased capability to produce their shells or skeletons (Bijma et al., 2002; Kroeker et al., 2010; WGII Chapter 6). Other species of fish and shellfish will also be negatively impacted in their physiological responses due to a decrease in pH levels. Ocean acidification is an emerging scientific issue and much research is needed before all of the ecosystem

responses are well documented. However, to the limit that the scientific community understands this issue right now, the potential for environmental, economic, and societal risks is high (Cooley et al., 2009).

[INSERT BOX 3.2, FIGURE 1 HERE]

Box 3.2, Figure 1: National Center for Atmospheric Research Community Climate System Model 3.1 (CCSM3)-modeled decadal mean pH at the sea surface centered around the years 1875 (top) and 1995 (middle). Global Ocean Data Analysis Project (GLODAP)-based pH at the sea surface, nominally for 1995 (bottom). Deep and shallow-water coral reefs are indicated with magenta dots. White areas indicate regions with no data (after Feely et al., 2009).

[INSERT BOX 3.2, FIGURE 2 HERE]

Box 3.2, Figure 2: Distribution of: **a)** pH and **b)** CO_3^{2-} ion concentration in the Pacific, Atlantic, and Indian Oceans. The data are from the World Ocean Circulation Experiment/Joint Global Ocean Flux Study/Ocean Atmosphere Carbon Exchange Study global CO_2 survey (Sabine, 2005). The lines show the mean pH (solid line top panel), aragonite (solid line bottom panel), and calcite (dashed line bottom panel) saturation CO_3^{2-} concentration for each of these basins (modified from Feely et al., 2009). The shaded areas show the range of values within the ocean basins. Dissolution of aragonite and calcite shells and skeletons occurs when CO_3^{2-} concentrations decrease below the saturation level.

[END BOX 3.2 HERE]

[INSERT FIGURE 3.18 HERE]

Figure 3.18: ΔpH_{ant}: pH change attributed to the uptake of anthropogenic carbon between 1991 and 2006, at about 150°W, Pacific Ocean (from Byrne et al., 2010). The red lines show the layers of constant density.

Table 3.2: Published and updated long-term trends of atmospheric (pCO_2^{atm}) and seawater carbonate chemistry (i.e., surface-water pCO_2, pH, $[CO_3^{2-}]$, and aragonite saturation state Ω_a) at four ocean time series in the North Atlantic and North Pacific oceans: (1) Bermuda Atlantic Time-series Study (BATS, 31°40′N, 64°10′W) and Hydrostation S (32°10′N, 64°30′W) from 1983 to present (Bates, 2007); (2) Hawaii Ocean Time-series (HOT) at Station ALOHA (A Long-term Oligotrophic Habitat Assessment; 22°45′N, 158°00′W) from 1988 to present (Dore et al., 2009); (3) European Station for Time-series in the Ocean (ESTOC, 29°10′N, 15°30′W) from 1994 to present (González-Dávila et al., 2010); and (4) Iceland Sea (IS, 68.0°N, 12.67°W) from 1985 to 2006 (Olafsson et al., 2009). Trends at the first three time-series sites are from observations with the seasonal cycle removed. Also reported are the wintertime trends in the Iceland Sea as well as the pH difference trend for the North Pacific Ocean between transects in 1991 and 2006 (Byrne et al., 2010) and repeat sections in the western North Pacific between 1983 and 2008 (Midorikawa et al., 2010).

Site	Period	pCO_2^{atm} (μatm yr^{-1})	pCO_2^{sea} (μatm yr^{-1})	pH* (yr^{-1})	$[CO_3^{2-}]$ (μmol kg^{-1} yr^{-1})	Ω_a (yr^{-1})
a. published trends						
BATS	1983–2005[a]	1.78 ± 0.02	1.67 ± 0.28	–0.0017 ± 0.0003	–0.47 ± 0.09	–0.007 ± 0.002
	1983–2005[b]	1.80 ± 0.02	1.80 ± 0.13	–0.0017 ± 0.0001	–0.52 ± 0.02	–0.006 ± 0.001
ALOHA	1988–2007[c]	1.68 ± 0.03	1.88 ± 0.16	–0.0019 ± 0.0002	-	–0.0076 ± 0.0015
	1998–2007[d]	-	-	–0.0014 ± 0.0002	-	-
ESTOC	1995–2004[e]	-	1.55 ± 0.43	–0.0017 ± 0.0004	-	-
	1995–2004[f]	1.6 ± 0.7	1.55	–0.0015 ± 0.0007	–0.90 ± 0.08	–0.0140 ± 0.0018
IS	1985–2006[g]	1.69 ± 0.04	2.15 ± 0.16	–0.0024 ± 0.0002	-	–0.0072 ± 0.0007[g]
N.Pacific	1991–2006[h]	-	-	–0.0017	-	-
N.Pacific	1983–2008[i]	Summer 1.54 ± 0.08 Winter 1.65 ± 0.05	Summer 1.37 ± 0.33 Winter 1.58 ± 0.12	Summer –0.0013 ± 0.0005 Winter –0.0018 ± 0.0002		
Coast of western N.Pacific	1994–2008[k]	1.99 ± 0.02	1.54 ± 0.33	–0.0020 ± 0.0007		–0.012 ± 0.005
b.updated trends[j,l]						
BATS	1983–2009	1.66 ± 0.01	1.92 ± 0.08	–0.0019 ± 0.0001	–0.59 ± 0.04	–0.0091 ± 0.0006
	1985–2009	1.67 ± 0.01	2.02 ± 0.08	–0.0020 ± 0.0001	–0.68 ± 0.04	–0.0105 ± 0.0006
	1988–2009	1.73 ± 0.01	2.22 ± 0.11	–0.0022 ± 0.0001	–0.87 ± 0.05	–0.0135 ± 0.0008
	1995–2009	1.90 ± 0.01	2.16 ± 0.18	–0.0021 ± 0.0002	–0.80 ± 0.08	–0.0125 ± 0.0013

ALOHA	1988–2009	1.73 ± 0.01	1.82 ± 0.07	–0.0018 ± 0.0001	–0.52 ± 0.04	–0.0083 ± 0.0007
	1995–2009	1.92 ± 0.01	1.58 ± 0.13	–0.0015 ± 0.0001	–0.40 ± 0.07	–0.0061 ± 0.0028
ESTOC	1995–2009	1.88 ± 0.02	1.83 ± 0.15	–0.0017 ± 0.0001	–0.72 ± 0.05	–0.0123 ± 0.0015
IS	1985–2009[l]	1.75 ± 0.01	2.07 ± 0.15	–0.0024 ± 0.0002	–0.47 ± 0.04	–0.0071 ± 0.0006
	1988–2009[l]	1.70 ± 0.01	1.96 ± 0.22	–0.0023 ± 0.0003	–0.48 ± 0.05	–0.0073 ± 0.0008
	1995–2009[l]	1.90 ± 0.01	2.01 ± 0.37	–0.0022 ± 0.0004	–0.40 ± 0.08	–0.0062 ± 0.0012

Notes:
* pH on the total scale
(a) Bates (2007, Table 1) - simple linear fit
(b) Bates (2007, Table 2) - seasonally detrended (including linear term for time)
(c) Dore et al. (2009) - linear fit with calculated pH and pCO_2 from measured DIC and TA(full time series); corresponding Ω_a from Feely et al. (2009)
(d) Dore et al. (2009) - linear fit with measured pH (partial time series)
(e) Santana-Casiano et al. (2007) - seasonal detrending (including linear terms for time and temperature)
(f) González-Dávila et al. (2010) - seasonal detrending (including linear terms for time, temperature, and mixed-layer depth)
(g) Olafsson et al. (2009) - multivariable linear regression (linear terms for time and temperature) for winter data only
(h) Byrne et al. (2010) - meridional section originally occupied in 1991 and repeated in 2006
(i) Midorikawa et al. (2010) - winter and summer observations along 137°E
(j) Trends are for linear time term in seasonal detrending with harmonic periods of 12, 6, and 4 months. Harmonic analysis made after interpolating data to regular monthly grids (except for IS, which was sampled much less frequently):
1983–2009 = Sep 1983 to Dec 2009 (BATS/Hydrostation S sampling period),
1985–2009 = Feb 1985 to Dec 2009 (IS sampling period),
1988–2009 = Nov 1988 to Dec 2009 (ALOHA/HOT sampling period), and
1995–2009 = Sep 1995 to Dec 2009 (ESTOC sampling period).
(k) Ishii et al (2011) - time-series observations in the coast of western N. Pacific, with the seasonal cycle removed
(l) Atmospheric pCO_2 trends computed from same harmonic analysis (12-, 6-, and 4-month periods) on the GLOBALVIEW-CO_2 (2010) data product for the marine boundary layer referenced to the latitude of the nearest atmospheric measurement station (BME for Bermuda, MLO for ALOHA, IZO for ESTOC, and ICE for Iceland)
(l) Winter ocean data, collected during dark period (between 19 January and 7 March), as per Olafsson et al. (2009) to reduce scatter from large interannual variations in intense short-term bloom events, undersampled in time, fit linearly (y=at+bT+c)

3.8.3 Oxygen

The assessment of long-term changes in dissolved oxygen is limited by data quality issues, and the general sparseness of marine observations. Nevertheless, thanks to the early introduction of standardized methods and the relatively wide interest in the distribution of dissolved oxygen, the historical record of marine oxygen observations is richer than that of nearly all other biogeochemical parameters. To date, the most thorough assessment of global-scale dissolved oxygen changes in open ocean environments reveals a general decreasing trend in the last decades since 1960, i.e., a large-scale deoxygenation of the ocean's thermocline at a rate of about 3–5 μmol kg^{-1} $decade^{-1}$, but with strong regional differences (Keeling et al., 2010). From 1970 to 1990, the mean annual global oxygen loss between 100m and 1000m was calculated to be 0.55 ± 0.13 × 10^{14} mol per year (Helm et al., 2011).

The long-term deoxygenation of the open ocean thermocline is consistent with the expectation that warmer waters can hold less dissolved oxygen (solubility effect), and that warming-induced stratification leads to a decrease in the resupply of dissolved oxygen into the thermocline from near surface waters (stratification effect). There is also evidence for deoxygenation from anthropogenic atmospheric nitrogen deposition (Duce et al., 2008). Models suggest a heat uptake to dissolved oxygen loss ratio of about 6 to 7 nmol O_2 per joule of warming, which is about twice the value expected from the reduction of the oxygen solubility alone. The means that increased stratification is of about equal importance as the solubility effect (Deutsch et al., 2005; Frölicher et al., 2009; Matear and Hirst, 2003). From oxygen observations between 1970 and 1990, however, about 15% of the oxygen decline was explained by warming, the remainder by reduced ventilation due to increased stratification (Helm et al., 2011).

Detailed analysis of time-series records from a few selected spots with sufficient data coverage in the tropical ocean reveals negative trends for the last 50 years in all ocean basins (Helm et al., 2011; Keeling et al., 2010; Ono et al., 2001; Stramma et al., 2008), resulting in a substantial expansion of the dissolved oxygen minimum zones there. A more spatially expansive analysis conducted by comparing data between 1960 and 1974 with those from 1990 to 2008 supports the spot analysis in that it identified oxygen decreases in most tropical regions with an average rate of 2–3 μmol kg^{-1} per decade (Stramma et al., 2010). Also, many observations from the high latitudes tend to suggest decreasing dissolved oxygen levels (Helm et al., 2011; Keeling et al., 2010). Observations from one of the longest time-series sites in the subpolar North Pacific (Station Papa, 50°N, 145°W) reveal a persistent declining trend in the thermocline for the last 50 years (Whitney et al., 2007), although this trend is superimposed on oscillations with time-scales of a few years to two decades. Several tropical open ocean regions in the Atlantic, Indian, and Pacific have also experienced a decrease in dissolved oxygen in the thermocline (Stramma et al., 2010; Figure 3.19). Stendardo and Gruber (2012) found dissolved oxygen decreases in upper water masses of the North Atlantic and increases in intermediate water masses. The changes were caused by changes in solubility as well as changes in ventilation and circulation over time.

[INSERT FIGURE 3.19 HERE]

Figure 3.19: Dissolved oxygen (DO) distributions (in μmol kg^{-1}) between 40°S and 40°N for: **a)** the climatological mean (Boyer et al., 2006) at 200 dbar, as well as changes between 1960 and 1974 and 1990 and 2008 of **b)** dissolved oxygen (ΔDO) at 200 dbar, and **c)** ΔDO vertically-averaged over 200–700 dbar. In **b)-c)** increases are red and decreases blue, and areas with differences below the 95% confidence interval are shaded by black horizontal lines (after Stramma et al., 2010).

Coastal regions have also experienced long-term dissolved oxygen changes. Bograd et al. (2008) reported a substantial reduction of the thermocline oxygen content in the southern part of the California Current from 1984 until 2002, resulting in a shoaling of the hypoxic boundary (60 μmol kg^{-1}). Off the Oregon coast, previously unreported hypoxic conditions have been observed on the inner shelf since 2000, with hypoxia being especially severe in 2006 (Chan et al., 2008). These changes along the west coast of North America appear to have been largely caused by the open ocean dissolved oxygen decrease and local processes associated with decreased vertical dissolved oxygen transport following near-surface warming and increased stratification. Gilbert et al. (2010) found evidence for much greater dissolved oxygen decline rates in the coastal ocean than in the open ocean depending on location.

In nearshore areas, the analysis of oxygen changes has largely been driven by the observation of a strong increase in the number of hypoxic zones since the 1960s (Diaz and Rosenberg, 2008). The formation of hypoxic zones has been exacerbated by the increase of primary production and consequent worldwide coastal eutrophication resulting from riverine runoff of fertilizers and the burning of fossil fuels.

3.8.4 Regional and Long-Term Trends in Nutrient Distributions in the Oceans

Human impacts and shifting physical processes are altering the supply of nutrients to the upper oceans, thereby exerting a control on the magnitude and variability of the ocean's biological carbon pump. The large-scale warming of the surface oceans has increased stratification (Section 3.2), thereby decreasing ventilation (Section 3.5) and the upward vertical flux of nutrients and, in low latitudes, reducing primary production. Satellite observations of chlorophyll found that oligotrophic gyres in four of the world's major oceans expanded at average rates of 0.8% to 4.3% yr^{-1} from 1998 to 2006, consistent with reduced nutrient availability.

Superimposed on the long-term trends are large interannual and multi-decadal fluctuations in nutrients. Modeling and observational studies demonstrate that these fluctuations are coupled with variability of mode water and the NAO in the Atlantic Ocean (Cianca et al., 2007; Pérez et al., 2010), climate modes of variability in the Pacific Ocean (Di Lorenzo et al., 2009; Wong et al., 2007); and variability of subtropical gyre circulation in the Indian Ocean (Álvarez et al., 2011). As a *likely* consequence, recent changes in global net primary production have been dominated by natural, multi-year oscillations (e.g., ENSO) and clearly show the close coupling between ocean ecology and climate (Behrenfeld et al., 2006; Chavez et al., 2011).

3.8.5 Summary

Based on high agreement between estimates using different approaches (e.g., oceanic carbon, nutrient, or tracer data), there is *very high confidence* that the global ocean inventory of anthropogenic carbon (C_{ant}) increased from 1994 to 2010. The C_{ant} inventory was estimated to be between 93–137 PgC in 1994, and 155 ± 30 PgC in 2010. The 2010 inventory corresponds to an annual global uptake rate of 2.3 ± 0.6 PgC yr^{-1}, consistent with carbon uptake rates, calculated from atmospheric O_2/N_2 measurements.

There is *very high confidence* that oceanic uptake of anthropogenic CO_2 results in gradual acidification of seawater and decreasing pH (i.e., anthropogenic ocean acidification) in surface waters. The observed pH trends range between –0.0015 and –0.0024 per year. In the ocean interior, pH can also be modified by natural physical and biological processes over decadal time scales.

Analyses of the limited oxygen observations available since 1960 shows *high agreement* that since 1960 over much of the open ocean oxygen concentrations in the thermocline decreased. The rate of decrease was about 3–5 μmol kg^{-1} $decade^{-1}$, with strong regional differences. This is consistent with the expectation that warmer waters can hold less oxygen, and that warming-induced stratification leads to a decrease in the supply of oxygen to the thermocline from near surface waters. It is *likely* that the tropical oxygen minimum zones have expanded in recent decades.

3.9 Synthesis

Substantial progress has been made since AR4 in documenting and understanding change in the ocean. The major findings of this chapter are largely consistent with those in AR4, but in many cases statements can now be made with a greater degree of confidence. The level of confidence has increased because more data are available, biases in historical data have been identified and reduced, and new analytical approaches have been applied.

Significant changes have been observed in a number of ocean properties of relevance to climate (Figure 3.20). It is *virtually certain* that global mean sea level and the ocean inventory of anthropogenic carbon dioxide have increased since at least 1950, and that ocean heat content has increased since 1971 (when sufficient observations became available to make global estimates). It is *likely* that sea surface salinity has increased in regions where the salinity exceeds the global mean surface salinity and decreased in regions where salinity is less than the global mean value. The amplification of the contrast between regions of high and low sea surface salinity is consistent with expectations of an intensification of the global water cycle in a warming climate.

[INSERT FIGURE 3.20 HERE]

Figure 3.20: Time series of changes in large-scale ocean climate properties. Global ocean inventory of anthropogenic carbon dioxide is updated from Khatiwala et al. (2009). Global upper ocean heat content anomaly is updated from Domingues et al. (2008). Global mean sea level (GMSL) is from Church and White (2011). “High salinity” refers to the salinity averaged over regions where the sea surface salinity is greater than the global mean sea surface salinity from Boyer et al. (2009) and "Low Salinity" to an average over regions with values below the global mean.

Trends have been detected in a number of subsurface water properties, with varying levels of confidence (Figure 3.21). There is compelling and robust evidence that most of the upper ocean has warmed over at least the last forty years, with the strongest warming observed near the sea surface. There is high confidence in the rate and pattern of sea level rise since 1993 (top panel, Figure 3.20) based on near-global coverage of satellite altimetry and the agreement with independent measurements from tide gauges and estimates of thermal expansion. While salinity observations are less abundant than temperature observations, the high agreement on the large-scale patterns between different analyses provides medium confidence that subsurface salinity has changed, with water masses formed and subducted in the precipitation-dominated mid- to high-latitudes becoming fresher, while water masses formed in the evaporation-dominated subtropics becoming saltier. Anthropogenic carbon dioxide is accumulating in surface waters and being carried into the interior, primarily by water masses formed in the North Atlantic and Southern Oceans. The accumulation of anthropogenic CO_2 is *virtually certain* to have caused the observed decline of pH and $CO_3^{=}$ in surface waters. As a result of changes in the temperature and salinity of surface waters, the density of the surface ocean has decreased, strengthening the stratification in the upper ocean. Observations of a decline in oxygen in thermocline waters in much of the global ocean are consistent with a reduction in ventilation caused by the increase in stratification, although the more limited oxygen data set means we have lower confidence in

oxygen changes than for temperature and salinity. It is *likely* that the tropical oxygen minimum zones have expanded in recent decades.

[INSERT FIGURE 3.21 HERE]

Figure 3.21: Summary of observed changes in zonal averages of global ocean properties. Temperature trends (°C decade^{-1}) are indicated in color (red = warming, blue = cooling); salinity trends are indicated by contour lines (dashed = fresher; solid = saltier) for the upper 2000 m of the water column (50-year trends from data set of Durack and Wijffels (2010); trends significant at >90% confidence are shown). Arrows indicate primary ventilation pathways. The top panel shows the zonal mean trend in sea level from 1993–2007 from satellite altimetry (Merrifield et al., 2009). Changes in other physical and chemical properties are summarised to the right of the figure, for each depth range (broken axes symbols delimit changes in vertical scale). Increases are shown in red, followed by a plus sign; decreases are shown in blue, followed by a minus sign; the number of + and–signs indicates the level of confidence associated with the observation of change (+++ = high confidence; ++ = medium confidence; + = low confidence). T = temperature, S = salinity, Strat = stratification, C_{ANT} = anthropogenic carbon, $CO_3^{=}$ = carbonate ion, NA = North Atlantic, SO = Southern Ocean, AABW = Antarctic Bottom Water. $S > \overline{S}$ refers to the salinity averaged over regions where the sea surface salinity is greater than the global mean sea surface salinity; $S < \overline{S}$ refers to the average over regions with values below the global mean.

The largest changes in the ocean inventory of heat, freshwater, anthropogenic carbon dioxide and other properties are observed along known ventilation pathways, where surface waters are transferred to the ocean interior, or in regions where changes in ocean circulation (e.g., contraction or expansion of gyres, or a southward shift of the Antarctic Circumpolar Current) result in large anomalies. The fact that the changes observed in a number of independent variables are consistent with each other and with well-understood dynamics of ocean circulation enhances confidence in the conclusion that the ocean state has changed.

For other properties of the ocean, the short and incomplete observational record is not sufficient to detect trends. For example, there is no observational evidence for or against a change in the strength of the AMOC, based on the short records presently available. However, recent observations have strengthened evidence for variability in major ocean circulation systems and water mass properties on time scales from years to decades. Much of the variability observed in ocean currents and in water masses can be linked to changes in surface forcing, including wind changes associated with the major modes of climate variability such as the NAO, SAM, ENSO, and the PDO.

Taken together, the observations summarised here give very high confidence that the physical and biogeochemical state of the oceans has changed. The spatial patterns of change are consistent with changes in the surface ocean (warming, changes in salinity, and an increase in C_{ant}) and the subsequent propagation of anomalies into the ocean interior along ventilation pathways.

While improvements in the quality and quantity of ocean observations strengthen and extend conclusions reached in AR4, substantial uncertainties remain. In many cases, the observational record is still too short or incomplete to detect trends in the presence of energetic variability on time-scales of years to decades. Recent improvements in the ocean observing system, most notably the Argo profiling float array, mean that temperature and salinity are now being sampled routinely in most of the ocean above 2000 m depth for the first time. However, sparse sampling of the deep ocean and of many biogeochemical variables continues to limit our ability to detect and understand changes in the global ocean. Sustained global-scale observations will increase confidence in the assessment of ocean change, improve the ability to detect and attribute climate change, and provide guidance for improvement of climate models.

[START FAQ 3.1 HERE]

FAQ 3.1: Is the Ocean Warming?

Yes, the ocean is warming, although neither everywhere, nor constantly. The signature of warming emerges most clearly when considering global averages over time spans of a decade or more.

Since 1970, there has been sufficient data coverage to estimate global average temperatures of the upper ocean, and those data indicate that these waters are indeed warming. Observations also suggest that, since 1990 at least, the deepest and coldest waters of the world ocean have generally been warming too.

However, ocean temperature at any given location can vary greatly with the seasons. It can also fluctuate substantially from year to year–or even decade to decade–because of variations in ocean currents and the exchange of heat between ocean and atmosphere.

Ocean temperatures have been recorded for centuries, but it was not until around 1970 that measurements were sufficiently comprehensive to estimate global upper ocean temperature for any given year confidently. In fact, before Argo–an international array of over 3000 profiling floats measuring temperature and salinity in the upper 2000 metres of the ocean–first achieved global coverage in 2004, the global average upper ocean temperature for any given year was sensitive to the methodology used to estimate it. Despite large uncertainty in most yearly means, the observed increase of the global mean over decadal time scales since 1970 is a robust result.

Temperature anomalies enter the subsurface ocean by paths in addition to mixing from above (FAQ3.1, Figure 1). Colder waters from high latitudes can sink from the surface, then spread toward the equator under warmer waters at lower latitudes. As these sinking waters themselves warm with time, they increase temperatures in the ocean interior, much more quickly than would downward mixing of surface heating alone.

At a few locations–in the northern North Atlantic Ocean and the Southern Ocean around Antarctica–ocean water is cooled so much that it sinks to great depths, even to the sea floor. This water then spreads out to fill much of the rest of the deep ocean. In the North Atlantic, the temperature of these deep waters varies from decade to decade–sometimes warming, sometimes cooling–depending on prevailing winter atmospheric patterns. Around Antarctica, bottom waters appear to have been warming detectably since at least 1990, perhaps due to the strengthening and southward shift of the westerly winds around the Southern Ocean over the last several decades.

[INSERT FAQ 3.1, FIGURE 1 HERE]

FAQ 3.1, Figure 1: Ocean heat uptake pathways. The ocean is stratified, with the coldest water in the deep ocean (upper panels, use map at top for orientation). Antarctic Bottom Water (dark blue) sinks around Antarctica and spreads northward along the ocean floor into the central Pacific (upper left panel, red arrows fading to white indicating stronger warming of the most recently-ventilated water) and western Atlantic oceans (upper right panel), as well as the Indian Ocean (not shown). North Atlantic Deep Water (lighter blue), slightly warmer and lighter, sinks in the northern North Atlantic Ocean (upper right panel, red and blue arrow indicating decadal warming and cooling) and spreads south above the Antarctic Bottom Water. Similarly, in the upper ocean (lower left panel shows Pacific Ocean detail, lower right panel the Atlantic) still-warmer Intermediate Waters (cyan) sink in sub-polar regions (red arrows fading to white indicating warming with time), then spread toward the equator under even warmer Subtropical Waters (green), which in turn sink (red arrows fading to white indicating stronger warming of the most recently-ventilated water) and spread toward the equator under tropical waters, the warmest and lightest (orange) in all three oceans. Excess heat or cold entering at the ocean surface (top straight red arrows) also mixes slowly downward (lower squiggly red arrows).

Estimates of historical changes in global average ocean temperature have become more accurate over the past several years, largely thanks to recognition and reduction of systematic measurement errors. By carefully comparing less accurate measurements with sparser, more accurate ones at adjacent locations and similar times, scientists have reduced some spurious instrumental biases in the historical record. With these biases ameliorated, it is now apparent that the global average ocean temperature has increased much more steadily from year to year than was reported prior to 2008. However, the global average warming rate may not be uniform in time. In some years, it still appears faster than average; in others, it seems to slow to almost nothing.

In the upper 60 metres of the ocean, the global average warming trend has been around 0.1°C per decade between 1971 and 2010. The global average upper ocean warming trend generally gets smaller from the surface to mid-depth, reducing to about 0.04°C per decade by 200 metres, and less than 0.02°C per decade by 500 metres.

Deep warming rates are generally less pronounced than ocean surface rates (around 0.03ºC per decade since the 1990s in the deep and bottom waters around Antarctica, and smaller in many other locations). However,

they occur over a large volume, so the deep ocean warming contributes significantly to the total increase in ocean heat.

The ocean's large mass and high heat capacity allow it to store huge amounts of energy–more than 1000 times that in the atmosphere for an equivalent increase in temperature. The Earth is absorbing more heat than it is emitting back into space, and nearly all this excess heat is entering the oceans, and being stored there. The ocean has absorbed roughly nine tenths of the total heat gain by the combined warmed air, sea, land, and melted ice between 1971 and 2010.

The ocean's huge heat capacity and the long time scales of ocean circulation mean that the ocean has significant thermal inertia. It takes about a decade for near-surface ocean temperatures to adjust in response to climate forcing, such as changes in greenhouse gas concentrations. It will take centuries to millennia for deep ocean temperatures to warm in response to today's surface conditions. Thus, even if greenhouse gas concentrations were held at present levels into the future, Earth's surface would continue to warm substantially for about a decade–and slightly more in subsequent decades–because of the ocean's thermal inertia. Furthermore, sea levels would continue to rise for centuries to millennia, because the deep oceans would continue to warm and expand.

[END FAQ 3.1 HERE]

[START FAQ 3.2 HERE]

FAQ 3.2: How Does Anthropogenic Ocean Acidification Relate to Climate Change?

Both, climate change and anthropogenic ocean acidification are caused by increasing carbon dioxide concentrations in the atmosphere. Rising levels of CO_2, along with other greenhouse gases, indirectly alter the climate system by trapping heat as it is reflected back from the Earth's surface. Anthropogenic ocean acidification is a direct consequence of rising CO_2 concentrations as seawater absorbs CO_2 from the atmosphere.

Anthropogenic ocean acidification refers to an increase in the ocean's hydrogen ion concentration (in other words, a lowering of pH or increase in acidity) caused by human activities, including the uptake of atmospheric carbon dioxide (CO_2) derived from the burning of fossil fuels, land-use changes, and cement production. Ocean acidification describes the direction of pH change rather than the end point; that is, ocean pH is decreasing but is not expected to become acidic (pH<7). Implicit with the pH change are the associated changes in the concentrations of the dissolved carbon species ($CO_{2(aq)}$, H_2CO_3, HCO_3^-, CO_3^{2-}). Measurements from the atmosphere and ocean time series stations at Hawaii illustrate the increase of pCO_2 and decrease in pH associated with the increase of CO_2 in the atmosphere (Figure 1). Results from laboratory, field, and modelling studies, as well as evidence from the geological record, clearly indicate that marine ecosystems are highly susceptible to the increases in oceanic CO_2 and the corresponding decreases in pH.

[INSERT FAQ 3.2, FIGURE 1 HERE]

FAQ 3.2, Figure 1: Time series of atmospheric pCO_2 at the atmospheric Mauna Loa Observatory (top), surface ocean pCO_2 (middle), and surface ocean pH (bottom) on the island of Hawaii and Station ALOHA in the subtropical North Pacific north of Hawaii, 1988–2008 (after Doney et al., 2009; data from Dore et al., 2009).

Climate change and anthropogenic ocean acidification do not act independently, as both processes affect the exchange of CO_2 between the atmosphere and ocean. The CO_2 that is taken up by the ocean does not contribute to greenhouse warming. Ocean warming, however, reduces the solubility of carbon dioxide in seawater; and thus reduces the amount of CO_2 the oceans can absorb from the atmosphere. For example, under doubled preindustrial CO_2 concentrations and a 2°C temperature increase, seawater absorbs about 10% less CO_2 than it would with no temperature increase (see columns 4 and 6 in Table 1), but the decrease in pH (i.e., the increase in hydrogen ion concentration) remains almost unchanged. Thus, a warmer ocean has less capacity to remove carbon dioxide from the atmosphere, yet still experiences ocean acidification.

FAQ 3.2, Table 1: Oceanic pH and carbon system parameter changes for a CO_2 doubling from the preindustrial atmosphere without and with a 2°C warming.

Parameter	preindustrial (280 ppmv) 20°C	2 × preindustrial (560 ppmv) 20°C	*(% change relative to preindustrial)*	2 × preindustrial (560 ppmv) 22°C	*(% change relative to preindustrial)*
pH	8.1714	7.9202	-	7.9207	-
H^+ (µmol kg^{-1})	$6.739e^{-9}$	$1.202e^{-8}$	*(78.4)*	$1.200e^{-8}$	*(78.1)*
CO_2(aq) (µmol kg^{-1})	9.10	18.10	*(98.9)*	17.2	*(89.0)*
HCO_3^- (µmol kg^{-1})	1723.4	1932.8	*(12.15)*	1910.4	*(10.9)*
CO_3^{2-} (µmol kg^{-1})	228.3	143.6	*(-37.1)*	152.9	*(–33.0)*
C_T (µmol kg^{-1})	1960.8	2094.5	*(6.82)*	2080.5	*(6.10)*

[END FAQ 3.2 HERE]

[START FAQ 3.3 HERE]

FAQ 3.3: Is There Evidence for Changes in the Earth's Water Cycle?

The Earth's water cycle involves evaporation and precipitation of moisture at the Earth's surface. Changes in the water vapour content of the atmosphere provide strong evidence that the water cycle is already responding to a warming climate. Further evidence comes from changes in the distribution of ocean salinity, which, given the lack of long-term observations of rain and evaporation over the global oceans, becomes an important proxy rain gauge.

The water cycle is expected to intensify in a warmer climate, because warmer air can be moister: the atmosphere can hold about 7% more water vapour for each °C of warming. Observations of the atmosphere since the 1970s do indeed show increases in surface and lower atmosphere water vapour, at a rate consistent with observed warming.

Changes recorded in ocean salinity in the last 50 years also provide strong evidence that the global water cycle is increasing in intensity as the Earth warms. Changes in surface salinity have reinforced the mean salinity pattern: the evaporation-dominated subtropical regions have become saltier, while the precipitation-dominated subpolar and tropical regions have become fresher (FAQ 3.3, Figure 1).

Seawater contains both salts and fresh water. 'Salinity' refers to the weight of dissolved salts in a kilogram of seawater. Because the total amount of salt–which comes from the weathering of rocks–does not change, seawater's salinity can only be changed by addition or removal of fresh water.

The distribution of salinity at the ocean surface largely mirrors the distribution of evaporation minus precipitation, runoff from land, and sea ice processes. High salinity occurs in the subtropics, where evaporation exceeds rainfall, whereas low salinity occurs at high latitudes and in the tropics, where there is more rainfall than evaporation (FAQ 3.3, Figure 1b, d). The Atlantic, the saltiest ocean basin, loses more freshwater through evaporation than it gains from precipitation, while the reverse is true for the Pacific. Transport of moisture as water vapour in the atmosphere connects the ocean's regions of net fresh water loss to those of fresh water gain.

A warmer atmosphere is projected to drive increases in precipitation, evaporation, and extreme hydrological events, although not necessarily at the same rate as it will drive increases in water vapour content. Observing such changes directly and globally is difficult, because most of the exchange of freshwater between the atmosphere and the surface takes place over the 70% of the Earth's surface that is covered by ocean. Long-term measurements of precipitation are only available over land, and long-term measurements of evaporation are not available.

Land-based precipitation observations show increases in some regions and decreases in others, making it difficult to construct a globally-integrated picture. From land-based observations, it is *likely* that there have been more extreme precipitation events, and more flooding associated with earlier snow melt at high

latitudes, but there is strong regionality in the trends: land-based observations are not sufficient to provide evidence of changes in drought extremes.

Ocean salinity, on the other hand, acts as a sensitive and effective rain gauge, because it naturally integrates the net freshwater flux resulting from the difference between precipitation and evaporation. Ocean salinity can also be affected by water run-off from the continents, and by the melting and freezing of sea ice or floating glacial ice. Freshwater added by melting glaciers and ice sheets on land will change global-averaged salinity, but changes to date are orders of magnitude smaller than can be detected from ocean observations.

Ocean salinity has been observed well enough over the past 50 years to state that changes are statistically significant at the 99% level of confidence over more than 40% of the global ocean surface.

[INSERT FAQ 3.3, FIGURE 1 HERE]

FAQ 3.3, Figure 1: Changes in sea surface salinity are related to the atmospheric patterns of Evaporation minus Precipitation (E-P) and trends in total precipitable water: a) Linear trend (1988 to 2010) in total precipitable water from Special Sensor Microwave Imager (after Wentz et al., 2007) (blues wetter; yellows drier). b) The 1979–2005 climatological mean net E-P (cm yr^{-1}) from NCEP (reds: net evaporation; blues: net precipitation). c) Trend (1950 to 2010) in surface salinity (after Durack and Wijffels, 2010) (blues freshening; yellows-reds saltier). d) The climatological-mean surface salinity (blues <35; yellows-reds >35).

[END FAQ 3.3 HERE]

References

Abeysirigunawardena, D. S., and I. J. Walker, 2008: Sea level responses to climatic variability and change in northern british columbia. *Atmosphere-Ocean*, **46**, 277-296. doi:10.3137/ao.460301

Ablain, M., A. Cazenave, S. Guinehut, and G. Valladeau, 2009: A new assessment of global mean sea level from altimeters highlights a reduction of global slope from 2005 to 2008 in agreement with in-situ measurements. *Ocean Sciences*, **5**, 193 - 201

Alory, G., S. Wijffels, and G. Meyers, 2007: Observed temperature trends in the indian ocean over 1960-1999 and associated mechanisms. *Geophys. Res. Lett.*, **34**. doi:10.1029/2006gl028044

Álvarez, M., T. Tanhua, H. Brix, C. Lo Monaco, N. Metzl, E. L. McDonagh, and H. L. Bryden, 2011: Decadal biogeochemical changes in the subtropical indian ocean associated with subantarctic mode water. *J. Geophys. Res.-Oceans*, **116**. doi:10.1029/2010jc006475

Andersson, A., C. Klepp, K. Fennig, S. Bakan, H. Grassl, and J. Schulz, 2011: Evaluation of hoaps-3 ocean surface freshwater flux components. *Journal of Applied Meteorology and Climatology*, **50**, 379-398. doi:10.1175/2010jamc2341.1

Aoki, S., S. R. Rintoul, S. Ushio, S. Watanabe, and N. L. Bindoff, 2005: Freshening of the adelie land bottom water near 140 degrees e. *Geophys. Res. Lett.*, **32**. doi:10.1029/2005gl024246

Bates, N. R., 2007: Interannual variability of the oceanic co2 sink in the subtropical gyre of the north atlantic ocean over the last 2 decades. *J. Geophys. Res.-Oceans*, **112**. doi:10.1029/2006JC003759

Bates, N. R., 2012: Multi-decadal uptake of carbon dioxide into subtropical mode water of the north atlantic ocean. *Biogeosciences*, **9**, 2649-2659. doi:10.5194/bg-9-2649-2012

Beckley, B. D., et al., 2010: Assessment of the jason-2 extension to the topex/poseidon, jason-1 sea-surface height time series for global mean sea level monitoring. *Marine Geodesy*, **33**, 447-471. doi:10.1080/01490419.2010.491029

Behrenfeld, M. J., et al., 2006: Climate-driven trends in contemporary ocean productivity. *Nature*, **444**, 752-755. doi:10.1038/nature05317

Beltrami, H., J. E. Smerdon, H. N. Pollack, and S. P. Huang, 2002: Continental heat gain in the global climate system. *Geophys. Res. Lett.*, **29**, 3. doi:10.1029/2001gl014310

Bersch, M., I. Yashayaev, and K. P. Koltermann, 2007: Recent changes of the thermohaline circulation in the subpolar north atlantic. *Ocean Dynamics*, **57**, 223-235. doi:10.1007/s10236-007-0104-7

Bijma, J., B. Honisch, and R. E. Zeebe, 2002: Impact of the ocean carbonate chemistry on living foraminiferal shell weight: Comment on "carbonate ion concentration in glacial-age deep waters of the caribbean sea" by w. S. Broecker and e. Clark. *Geochemistry, Geophysics, Geosystems*, **3**. doi:10.1029/2002GC000388

Bindoff, N. L., and T. J. McDougall, 1994: Diagnosing climate-change and ocean ventilation using hydrographic data. *Journal of Physical Oceanography*, **24**, 1137-1152

Bindoff, N. L., et al., 2007: Observations: Oceanic climate change and sea level. *Climate change 2007: The physical science basis. Contribution of working group i to the fourth assessment report of the intergovernmental panel on climate change*, S. Solomon, et al., Eds., Cambridge University Press.

Bingham, R. J., and C. W. Hughes, 2009: Signature of the atlantic meridional overturning circulation in sea level along the east coast of north america. *Geophys. Res. Lett.*, **36**. doi:10.1029/2008gl036215

Boening, C., J. K. Willis, F. W. Landerer, R. S. Nerem, and J. Fasullo, 2012: The 2011 la niña: So strong, the oceans fell. *Geophys. Res. Lett.*, **submitted**

Bograd, S. J., C. G. Castro, E. Di Lorenzo, D. M. Palacios, H. Bailey, W. Gilly, and F. P. Chavez, 2008: Oxygen declines and the shoaling of the hypoxic boundary in the california current. *Geophys. Res. Lett.*, **35**. doi:10.1029/2008gl034185

Böning, C. W., A. Dispert, M. Visbeck, S. R. Rintoul, and F. U. Schwarzkopf, 2008: The response of the antarctic circumpolar current to recent climate change. *Nat. Geosci.*, **1**, 864-869. doi:10.1038/ngeo362

Boyer, T., S. Levitus, J. Antonov, R. Locarnini, A. Mishonov, H. Garcia, and S. A. Josey, 2007: Changes in freshwater content in the north atlantic ocean 1955-2006. *Geophys. Res. Lett.*, **34**. doi:10.1029/2007gl030126

Boyer, T. P., S. Levitus, J. I. Antonov, R. A. Locarnini, and H. E. Garcia, 2005: Linear trends in salinity for the world ocean, 1955-1998. *Geophysical Research Letters NZ*, **32**. doi:10.1029/2004gl021791

Boyer, T. P., et al., 2006: Introduction. *World Ocean Database 2005 (dvd), NOAA Atlas NESDIS, vol. 60*, S. Levitus, Ed., US Government Printing Office, 15-37.

Boyer, T. P., et al., 2009: World ocean database 2009, 216 pp.

Broecker, W., and E. Clark, 2001: A dramatic atlantic dissolution event at the onset of the last glaciation. *Geochemistry Geophysics Geosystems*, **2**

Bromirski, P. D., A. J. Miller, R. E. Flick, and G. Auad, 2011: Dynamical suppression of sea level rise along the pacific coast of north america: Indications for imminent acceleration. *J. Geophys. Res.-Oceans*, **116**. doi:10.1029/2010jc006759

Bryden, H. L., H. R. Longworth, and S. A. Cunningham, 2005: Slowing of the atlantic meridional overturning circulation at 25°n. *Nature*, **438**, 655-657. doi:10.1038/nature04385

Byrne, R. H., S. Mecking, R. A. Feely, and X. W. Liu, 2010: Direct observations of basin-wide acidification of the north pacific ocean. *Geophys. Res. Lett.*, **37**. doi:10.1029/2009gl040999

Cai, W., 2006: Antarctic ozone depletion causes an intensification of the southern ocean super-gyre circulation. *Geophys. Res. Lett.*, **33**. doi:10.1029/2005gl024911

Calafat, F. M., D. Chambers, and M. Tsimplis, 2012: Mechanisms of decadal sea level variability in the eastern north atlantic and the mediterranean sea. *Journal of Geophysical Research - Oceans*, **submitted**

Caldeira, K., 2011: Glossary entry for "ocean acidification". *IPCC Workshop on Impacts of Ocean Acidification on Marine Biology and Ecosystems*, Bankoku Shinryokan, Okinawa, Japan, IPCC WG I and II Technical Support Units, 37.

Caldeira, K., and M. E. Wickett, 2003: Anthropogenic carbon and ocean ph. *Nature*, **425**, 365-365. doi:10.1038/425365a

Carson, M., and D. E. Harrison, 2010: Regional interdecadal variability in bias-corrected ocean temperature data. *Journal of Climate*, **23**, 2847-2855. doi:10.1175/2010jcli3121.1

Carton, J. A., and A. Santorelli, 2008: Global decadal upper-ocean heat content as viewed in nine analyses. *Journal of Climate*, **21**, 6015-6035. doi:10.1175/2008jcli2489.1

Carton, J. A., B. S. Giese, and S. A. Grodsky, 2005: Sea level rise and the warming of the oceans in the simple ocean data assimilation (soda) ocean reanalysis. *J. Geophys. Res.-Oceans*, **110**. doi:10.1029/2004jc002817

Cazenave, A., et al., 2009: Sea level budget over 2003–2008: A re-evaluation from grace space gravimetry, satellite altimetry and argo. *Marine Geodesy*, **65**, 447 - 471

Cazenave, A., et al., 2012: Estimating enso influence on the global mean sea level over 1993-2010. *Marine Geodesy*, **in press**

Cermak, J., M. Wild, R. Knutti, M. I. Mishchenko, and A. K. Heidinger, 2010: Consistency of global satellite-derived aerosol and cloud data sets with recent brightening observations. *Geophys. Res. Lett.*, **37**. doi:10.1029/2010gl044632

Chambers, D. P., J. Wahr, and R. S. Nerem, 2004: Preliminary observations of global ocean mass variations with grace. *Geophys. Res. Lett.*, **31**. doi:10.1029/2004gl020461

Chambers, D. P., M. A. Merrifield, and R. S. Nerem, 2012: Is there a 60-year oscillation in global mean sea level? *Geophys. Res. Lett.*, **submitted**

Chambers, D. P., J. Wahr, M. E. Tamisiea, and R. S. Nerem, 2010: Ocean mass from grace and glacial isostatic adjustment. *Journal of Geophysical Research-Solid Earth*, **115**. doi:10.1029/2010jb007530

Chan, F., J. A. Barth, J. Lubchenco, A. Kirincich, H. Weeks, W. T. Peterson, and B. A. Menge, 2008: Emergence of anoxia in the california current large marine ecosystem. *Science*, **319**, 920-920. doi:10.1126/science.1149016

Chavez, F. P., M. Messié, and J. T. Pennington, 2011: Marine primary production in relation to climate variability and change. *Annual Review of Marine Science*, **3**, 227-260. doi:10.1146/annurev.marine.010908.163917

Church, J. A., and N. J. White, 2006: A 20th century acceleration in global sea-level rise. *Geophys. Res. Lett.*, **33**. doi:10.1029/2005gl024826

Church, J. A., and N. J. White, 2011: Sea-level rise from the late 19th to the early 21st century. *Surveys in Geophysics*, **32**, 585-602. doi:10.1007/s10712-011-9119-1

Church, J. A., J. R. Hunter, K. L. McInnes, and N. J. White, 2006: Sea-level rise around the australian coastline and the changing frequency of extreme sea-level events. *Australian Meteorological Magazine*, **55**, 253-260

Church, J. A., N. J. White, R. Coleman, K. Lambeck, and J. X. Mitrovica, 2004: Estimates of the regional distribution of sea level rise over the 1950-2000 period. *Journal of Climate*, **17**, 2609-2625

Church, J. A., et al., 2011: Revisiting the earth's sea-level and energy budgets from 1961 to 2008. *Geophys. Res. Lett.*, **38**, 8. doi:L18601, 10.1029/2011gl048794

Cianca, A., P. Helmke, B. Mourino, M. J. Rueda, O. Llinas, and S. Neuer, 2007: Decadal analysis of hydrography and in situ nutrient budgets in the western and eastern north atlantic subtropical gyre. *J. Geophys. Res.-Oceans*, **112**. doi:10.1029/2006jc003788

Cooley, S. R., H. L. Kite-Powell, and S. C. Doney, 2009: Ocean acidification's potential to alter global marine ecosystem services. *Oceanography*, **22**, 172-181

Cravatte, S., T. Delcroix, D. X. Zhang, M. McPhaden, and J. Leloup, 2009: Observed freshening and warming of the western pacific warm pool. *Clim. Dyn.*, **33**, 565-589. doi:10.1007/s00382-009-0526-7

Cummins, P. F., and H. J. Freeland, 2007: Variability of the north pacific current and its bifurcation. *Prog. Oceanogr.*, **75**, 253-265. doi:10.1016/j.pocean.2007.08.006

Cunningham, S. A., S. G. Alderson, B. A. King, and M. A. Brandon, 2003: Transport and variability of the antarctic circumpolar current in drake passage. *J. Geophys. Res.-Oceans*, **108**. doi:10.1029/2001jc001147

Cunningham, S. A., et al., 2007: Temporal variability of the atlantic meridional overturning circulation at 26.5 degrees n. *Science*, **317**, 935-938. doi:10.1126/science.1141304

Curry, R., and C. Mauritzen, 2005: Dilution of the northern north atlantic ocean in recent decades. *Science*, **308**, 1772-1774. doi:10.1126/science.1109477

Curry, R., B. Dickson, and I. Yashayaev, 2003: A change in the freshwater balance of the atlantic ocean over the past four decades. *Nature*, **426**, 826-829. doi:10.1038/nature02206

D'Onofrio, E. E., M. M. E. Fiore, and J. L. Pousa, 2008: Changes in the regime of storm surges at buenos aires, argentina. *Journal of Coastal Research*, **24**, 260-265. doi:10.2112/05-0588.1

Delcroix, T., S. Cravatte, and M. J. McPhaden, 2007: Decadal variations and trends in tropical pacific sea surface salinity since 1970. *J. Geophys. Res.-Oceans*, **112**. doi:10.1029/2006jc003801

Deng, Z. W., and Y. M. Tang, 2009: Reconstructing the past wind stresses over the tropical pacific ocean from 1875 to 1947. *Journal of Applied Meteorology and Climatology*, **48**, 1181-1198. doi:10.1175/2008jamc2049.1

Deutsch, C., S. Emerson, and L. Thompson, 2005: Fingerprints of climate change in north pacific oxygen. *Geophys. Res. Lett.*, **32**. doi:10.1029/2005gl023190

Di Lorenzo, E., et al., 2009: Nutrient and salinity decadal variations in the central and eastern north pacific. *Geophys. Res. Lett.*, **36**. doi:10.1029/2009gl038261

Diaz, R. J., and R. Rosenberg, 2008: Spreading dead zones and consequences for marine ecosystems. *Science*, **321**, 926-929. doi:10.1126/science.1156401

Dickson, B., I. Yashayaev, J. Meincke, B. Turrell, S. Dye, and J. Holfort, 2002: Rapid freshening of the deep north atlantic ocean over the past four decades. *Nature*, **416**, 832-837

Dickson, R. R., et al., 2008: The overflow flux west of iceland: Variability, origins and forcing. *Arctic-subarctic ocean fluxes*, R. R. Dickson, J. Meincke, and P. B. Rhines, Eds., Springer Verlag.

Dmitrenko, I. A., et al., 2008: Toward a warmer arctic ocean: Spreading of the early 21st century atlantic water warm anomaly along the eurasian basin margins. *J. Geophys. Res.-Oceans*, **113**, 13. doi:10.1029/2007jc004158

Dodet, G., X. Bertin, and R. Taborda, 2010: Wave climate variability in the north-east atlantic ocean over the last six decades. *Ocean Modelling*, **31**, 120-131. doi:10.1016/j.ocemod.2009.10.010

Dohan, K., et al., 2010: Measuring the global ocean surface circulation with satellite and in situ observations. *Proceedings of OceanObs'09: Sustained Ocean Observations and Information for Society (Vol. 2)*, Venice, Italy.

Domingues, C. M., J. A. Church, N. J. White, P. J. Gleckler, S. E. Wijffels, P. M. Barker, and J. R. Dunn, 2008: Improved estimates of upper-ocean warming and multi-decadal sea-level rise. *Nature*, **453**, 1090-U1096. doi:10.1038/nature07080

Doney, S. C., V. J. Fabry, R. A. Feely, and J. A. Kleypas, 2009: Ocean acidification: The other co2 problem. *Annual Review of Marine Science*, **1**, 169-192. doi:10.1146/annurev.marine.010908.163834

Dore, J. E., R. Lukas, D. W. Sadler, M. J. Church, and D. M. Karl, 2009: Physical and biogeochemical modulation of ocean acidification in the central north pacific. *Proceedings of the National Academy of Sciences of the United States of America*, **106**, 12235-12240. doi:10.1073/pnas.0906044106

Douglas, B. C., 2001: Sea level change in the era of the recording tide gauge. *Sea level rise: History and consequences*, B. C. Douglas, M. S. Kearney, and S. P. Leatherman, Eds., Academic Press, 37–64.

Douglass, E., D. Roemmich, and D. Stammer, 2006: Interannual variability in northeast pacific circulation. *J. Geophys. Res.-Oceans*, **111**. doi:10.1029/2005jc003015

Dragani, W. C., P. B. Martin, C. G. Simionato, and M. I. Campos, 2010: Are wind wave heights increasing in south-eastern south american continental shelf between 32°s and 40°s? *Continental Shelf Research*, **30**, 481-490. doi:10.1016/j.csr.2010.01.002

Duce, R. A., et al., 2008: Impacts of atmospheric anthropogenic nitrogen on the open ocean. *Science*, **320**, 893-897. doi:10.1126/science.1150369

Ducet, N., P. Y. Le Traon, and G. Reverdin, 2000: Global high-resolution mapping of ocean circulation from topex/poseidon and ers-1 and-2. *J. Geophys. Res.-Oceans*, **105**, 19477-19498

Durack, P. J., and S. E. Wijffels, 2010: Fifty-year trends in global ocean salinities and their relationship to broad-scale warming. *Journal of Climate*, **23**, 4342-4362. doi:10.1175/2010jcli3377.1

Durack, P. J., S. E. Wijffels, and R. J. Matear, 2012: Ocean salinities reveal strong global water cycle intensification during 1950 to 2000. *Science*, **336**, 455-458. doi:10.1126/science.1212222

Egleston, E. S., C. L. Sabine, and F. M. M. Morel, 2010: Revelle revisited: Buffer factors that quantify the response of ocean chemistry to changes in dic and alkalinity. *Global Biogeochemical Cycles*, **24**. doi:10.1029/2008gb003407

Ekman, M., 1988: The world's longest continued series of sea-level observations. *Pure and Applied Geophysics*, **127**, 73-77. doi:10.1007/bf00878691

Eldevik, T., J. E. O. Nilsen, D. Iovino, K. A. Olsson, A. B. Sando, and H. Drange, 2009: Observed sources and variability of nordic seas overflow. *Nat. Geosci.*, **2**, 405-409. doi:10.1038/ngeo518

Fabry, V. J., B. A. Seibel, R. A. Feely, and J. C. Orr, 2008: Impacts of ocean acidification on marine fauna and ecosystem processes. *Ices Journal of Marine Science*, **65**, 414-432. doi:10.1093/icesjms/fsn048

Fahrbach, E., M. Hoppema, G. Rohardt, O. Boebel, O. Klatt, and A. Wisotzki, 2011: Warming of deep and abyssal water masses along the greenwich meridian on decadal time scales: The weddell gyre as a heat buffer. *Deep-Sea Research Part Ii-Topical Studies in Oceanography*, **58**, 2509-2523. doi:10.1016/j.dsr2.2011.06.007

Farneti, R., T. L. Delworth, A. J. Rosati, S. M. Griffies, and F. Zeng, 2010: The role of mesoscale eddies in the rectification of the southern ocean response to climate change. *Journal of Physical Oceanography*, **40**, 1539-1557. doi:10.1175/2010jpo4353.1

Feely, R. A., S. C. Doney, and S. R. Cooley, 2009: Ocean acidification: Present conditions and future changes in a high-co2 world. *Oceanography*, **22**, 36-47

Feely, R. A., T. Takahashi, R. Wanninkhof, M. J. McPhaden, C. E. Cosca, S. C. Sutherland, and M. E. Carr, 2006: Decadal variability of the air-sea co2 fluxes in the equatorial pacific ocean. *J. Geophys. Res.-Oceans*, **111**, -

Fischer, J., M. Visbeck, R. Zantopp, and N. Nunes, 2010: Interannual to decadal variability of outflow from the labrador sea. *Geophys. Res. Lett.*, **37**. doi:10.1029/2010gl045321

Freeland, H., et al., 2010: Argo - a decade of progress. *Proceedings of OceanObs'09: Sustained Ocean Observations and Information for Society (Vol. 2)*, Venice, Italy.

Friis, K., A. Körtzinger, J. Pätsch, and D. W. R. Wallace, 2005: On the temporal increase of anthropogenic co2 in the subpolar north atlantic. *Deep-Sea Research I*, **52**, 681-698

Frölicher, T. L., F. Joos, G. K. Plattner, M. Steinacher, and S. C. Doney, 2009: Natural variability and anthropogenic trends in oceanic oxygen in a coupled carbon cycle-climate model ensemble. *Global Biogeochemical Cycles*, **23**. doi:10.1029/2008gb003316

Fusco, G., V. Artale, Y. Cotroneo, and G. Sannino, 2008: Thermohaline variability of mediterranean water in the gulf of cadiz, 1948-1999. *Deep-Sea Res. Part I-Oceanogr. Res. Pap.*, **55**, 1624-1638. doi:10.1016/j.dsr.2008.07.009

Garabato, A. C. N., L. Jullion, D. P. Stevens, K. J. Heywood, and B. A. King, 2009: Variability of subantarctic mode water and antarctic intermediate water in the drake passage during the late-twentieth and early-twenty-first centuries. *Journal of Climate*, **22**, 3661-3688. doi:10.1175/2009jcli2621.1

Giese, B. S., G. A. Chepurin, J. A. Carton, T. P. Boyer, and H. F. Seidel, 2011: Impact of bathythermograph temperature bias models on an ocean reanalysis. *Journal of Climate*, **24**, 84-93. doi:10.1175/2010JCLI3534.1

Gilbert, D., N. N. Rabalais, R. J. Diaz, and J. Zhang, 2010: Evidence for greater oxygen decline rates in the coastal ocean than in the open ocean. *Biogeosciences*, **7**, 2283-2296. doi:10.5194/bg-7-2283-2010

Gille, S. T., 2008: Decadal-scale temperature trends in the southern hemisphere ocean. *Journal of Climate*, **21**, 4749-4765. doi:10.1175/2008jcli2131.1

Gladyshev, S. V., M. N. Koshlyakov, and R. Y. Tarakanov, 2008: Currents in the drake passage based on observations in 2007. *Oceanology*, **48**, 759-770. doi:10.1134/s0001437008060015

Gloor, M., J. L. Sarmiento, and N. Gruber, 2010: What can be learned about carbon cycle climate feedbacks from the co2 airborne fraction? *Atmos. Chem. Phys.*, **10**, 7739-7751

Goni, G. J., F. Bringas, and P. N. DiNezio, 2011: Observed low frequency variability of the brazil current front. *J. Geophys. Res.-Oceans*, **116**. doi:10.1029/2011jc007198

González-Dávila, M., J. M. Santana-Casiano, M. J. Rueda, and O. Llinas, 2010: The water column distribution of carbonate system variables at the estoc site from 1995 to 2004. *Biogeosciences*, **7**, 3067-3081. doi:10.5194/bg-7-3067-2010

Gouretski, V., and K. P. Koltermann, 2007: How much is the ocean really warming? *Geophys. Res. Lett.*, **34**, 5. doi:10.1029/2006gl027834

Gouretski, V., and F. Reseghetti, 2010: On depth and temperature biases in bathythermograph data: Development of a new correction scheme based on analysis of a global ocean database. *Deep-Sea Res. Part I-Oceanogr. Res. Pap.*, **57**, 812-833. doi:10.1016/j.dsr.2010.03.011

Griffies, S. M., et al., 2009: Coordinated ocean-ice reference experiments (cores). *Ocean Modelling*, **26**. doi:10.1016/j.ocemod.2008.08.007

Grist, J. P., R. Marsh, and S. A. Josey, 2009: On the relationship between the north atlantic meridional overturning circulation and the surface-forced overturning streamfunction. *Journal of Climate*, **22**, 4989-5002. doi:10.1175/2009jcli2574.1

Gruber, N., et al., 2009: Oceanic sources, sinks, and transport of atmospheric co2. *Global Biogeochemical Cycles*, **23**. doi:10.1029/2008gb003349

Gu, G. J., R. F. Adler, G. J. Huffman, and S. Curtis, 2007: Tropical rainfall variability on interannual-to-interdecadal and longer time scales derived from the gpcp monthly product. *Journal of Climate*, **20**, 4033-4046. doi:10.1175/jcli4227.1

Gulev, S., T. Jung, and E. Ruprecht, 2007: Estimation of the impact of sampling errors in the vos observations on air-sea fluxes. Part ii: Impact on trends and interannual variability. *Journal of Climate*, **20**, 302-315. doi:10.1175/jcli4008.1

Gulev, S., et al., 2010: Surface energy and co2 fluxes in the global ocean-atmosphere-ice system. *OceanObs'09: Sustained Ocean Observations and Information for Society*, Venice, Italy, 20 pp.

Gulev, S. K., and V. Grigorieva, 2006: Variability of the winter wind waves and swell in the north atlantic and north pacific as revealed by the voluntary observing ship data. *Journal of Climate*, **19**, 5667-5685

Haigh, I., R. Nicholls, and N. Wells, 2010: Assessing changes in extreme sea levels: Application to the english channel, 1900-2006. *Continental Shelf Research*, **30**, 1042-1055. doi:10.1016/j.csr.2010.02.002

Häkkinen, S., P. B. Rhines, and D. L. Worthen, 2011: Atmospheric blocking and atlantic multidecadal ocean variability. *Science*, **334**, 655-659. doi:10.1126/science.1205683

Hallberg, R., and A. Gnanadesikan, 2006: The role of eddies in determining the structure and response of the wind-driven southern hemisphere overturning: Results from the modeling eddies in the southern ocean (meso) project. *Journal of Physical Oceanography*, **36**, 2232-2252. doi:10.1175/jpo2980.1

Hansen, B., and S. Osterhus, 2007: Faroe bank channel overflow 1995-2005. *Prog. Oceanogr.*, **75**, 817-856. doi:10.1016/j.pocean.2007.09.004

Hansen, B., H. Hatun, R. Kristiansen, S. M. Olsen, and S. Osterhus, 2010: Stability and forcing of the iceland-faroe inflow of water, heat, and salt to the arctic. *Ocean Sci.*, **6**, 1013-1026. doi:10.5194/os-6-1013-2010

Hansen, J., M. Sato, P. Kharecha, and K. von Schuckmann, 2011: Earth's energy imbalance and implications. *Atmospheric Chemistry and Physics*, **11**, 13421-13449. doi:10.5194/acp-11-13421-2011

Hatun, H., A. B. Sando, H. Drange, B. Hansen, and H. Valdimarsson, 2005: Influence of the atlantic subpolar gyre on the thermohaline circulation. *Science*, **309**, 1841-1844. doi:10.1126/science.1114777

Held, I. M., and B. J. Soden, 2006: Robust responses of the hydrological cycle to global warming. *Journal of Climate*, **19**, 5686-5699. doi:10.1175/jcli3990.1

Helm, K. P., N. L. Bindoff, and J. A. Church, 2010: Changes in the global hydrological-cycle inferred from ocean salinity. *Geophys. Res. Lett.*, **37**. doi:10.1029/2010gl044222

Helm, K. P., N. L. Bindoff, and J. A. Church, 2011: Observed decreases in oxygen content of the global ocean. *Geophys. Res. Lett.*, **38**. doi:10.1029/2011gl049513

Hemer, M. A., 2010: Historical trends in southern ocean storminess: Long-term variability of extreme wave heights at cape sorell, tasmania. *Geophys. Res. Lett.*, **37**. doi:10.1029/2010gl044595

Hemer, M. A., J. A. Church, and J. R. Hunter, 2010: Variability and trends in the directional wave climate of the southern hemisphere. *International Journal of Climatology*, **30**, 475-491. doi:10.1002/joc.1900

Hill, K. L., S. R. Rintoul, R. Coleman, and K. R. Ridgway, 2008: Wind forced low frequency variability of the east australia current. *Geophys. Res. Lett.*, **35**. doi:10.1029/2007gl032912

Hinkelman, L. M., P. W. Stackhouse, B. A. Wielicki, T. P. Zhang, and S. R. Wilson, 2009: Surface insolation trends from satellite and ground measurements: Comparisons and challenges. *Journal of Geophysical Research-Atmospheres*, **114**. doi:10.1029/2008jd011004

Holgate, S. J., 2007: On the decadal rates of sea level change during the twentieth century. *Geophys. Res. Lett.*, **34**. doi:10.1029/2006gl028492

Holland, P. R., A. Jenkins, and D. M. Holland, 2008: The response of ice shelf basal melting to variations in ocean temperature. *Journal of Climate*, **21**, 2558-2572. doi:10.1175/2007jcli1909.1

Holliday, N., et al., 2008: Reversal of the 1960s to 1990s freshening trend in the northeast north atlantic and nordic seas. *Geophys. Res. Lett.*, **35**, -. doi:10.1029/2007GL032675

Hong, B. G., W. Sturges, and A. J. Clarke, 2000: Sea level on the us east coast: Decadal variability caused by open ocean wind-curl forcing. *Journal of Physical Oceanography*, **30**, 2088-2098. doi:10.1175/1520-0485(2000)030<2088:slotus>2.0.co;2

Hood, M., et al., 2010: Ship-based repeat hydrography: A strategy for a sustained global program. *Proceedings of OceanObs'09: Sustained Ocean Observations and Information for Society (Vol. 2)*, Venice, Italy.

Hosoda, S., T. Suga, N. Shikama, and K. Mizuno, 2009: Global surface layer salinity change detected by argo and its implication for hydrological cycle intensification. *Journal of Oceanography*, **65**, 579-586

Houston, J. R., and R. G. Dean, 2011: Sea-level acceleration based on us tide gauges and extensions of previous global-gauge analyses. *Journal of Coastal Research*, **27**, 409-417. doi:10.2112/jcoastres-d-10-00157.1

Hughes, C. W., P. L. Woodworth, M. P. Meredith, V. Stepanov, T. Whitworth, and A. R. Pyne, 2003: Coherence of antarctic sea levels, southern hemisphere annular mode, and flow through drake passage. *Geophys. Res. Lett.*, **30**. doi:10.1029/2003gl017240

Huhn, O., M. Rhein, M. Hoppema, and S. van Heuven, 2012: Decline of deep and bottom water ventilation and slowing down of anthropogenic carbon storage in the weddell sea, 1984-2011. *Deep-Sea Research I*, **submitted**

Ingvaldsen, R. B., L. Asplin, and H. Loeng, 2004: Velocity field of the western entrance to the barents sea. *J. Geophys. Res.-Oceans*, **109**. doi:10.1029/2003jc001811

Ishidoya, S., S. Aoki, D. Goto, T. Nakazawa, S. Taguchi, and P. K. Patra, 2012: Time and space variations of the o2/n2 ratio in the troposphere over japan and estimation of the global co2 budget for the period 2000-2010. *Tellus B*, **64**. doi:10.3402/tellusb.v64i0.18964

Ishii, M., and M. Kimoto, 2009: Reevaluation of historical ocean heat content variations with time-varying xbt and mbt depth bias corrections. *Journal of Oceanography*, **65**, 287-299. doi:10.1007/s10872-009-0027-7

Ishii, M., N. Kosugi, D. Sasano, S. Saito, T. Midorikawa, and H. Y. Inoue, 2011: Ocean acidification off the south coast of japan: A result from time series observations of co(2) parameters from 1994 to 2008. *J. Geophys. Res.-Oceans*, **116**. doi:10.1029/2010jc006831

Ishii, M., et al., 2009: Spatial variability and decadal trend of the oceanic co2 in the western equatorial pacific warm/fresh water. *Deep-Sea Research Part Ii-Topical Studies in Oceanography*, **56**. doi:10.1016/j.dsr2.2009.01.002

Jackson, J. M., E. C. Carmack, F. A. McLaughlin, S. E. Allen, and R. G. Ingram, 2010: Identification, characterization, and change of the near-surface temperature maximum in the canada basin, 1993-2008. *J. Geophys. Res.-Oceans*, **115**, 16. doi:10.1029/2009jc005265

Jacobs, S. S., and C. F. Giulivi, 2010: Large multidecadal salinity trends near the pacific-antarctic continental margin. *Journal of Climate*, **23**, 4508-4524. doi:10.1175/2010jcli3284.1

Jacobs, S. S., A. Jenkins, C. F. Giulivi, and P. Dutrieux, 2011: Stronger ocean circulation and increased melting under pine island glacier ice shelf. *Nat. Geosci.*, **4**, 519-523. doi:10.1038/ngeo1188

Jevrejeva, S., A. Grinsted, J. C. Moore, and S. Holgate, 2006: Nonlinear trends and multiyear cycles in sea level records. *J. Geophys. Res.-Oceans*, **111**. doi:10.1029/2005jc003229

Jevrejeva, S., J. C. Moore, A. Grinsted, and P. L. Woodworth, 2008: Recent global sea level acceleration started over 200 years ago? *Geophys. Res. Lett.*, **35**. doi:10.1029/2008gl033611

Jevrejeva, S., J. C. Moore, A. Grinsted, and A. Matthews, 2012: Trends and acceleration in global and regional sea levels since 1807. *Journal of Geophysical Research*, **submitted**

Jochumsen, K., D. Quadfasel, H. Valdimarsson, and S. Jonsson, 2012: Variability of the denmark strait overflow: Moored time series from 1996-2011. *Journal of Geophysical Research*, **submitted**

Johns, W. E., et al., 2011: Continuous, array-based estimates of atlantic ocean heat transport at 26.5 degrees n. *Journal of Climate*, **24**, 2429-2449. doi:10.1175/2010jcli3997.1

Johnson, G. C., S. G. Purkey, and J. M. Toole, 2008a: Reduced antarctic meridional overturning circulation reaches the north atlantic ocean. *Geophys. Res. Lett.*, **35**. doi:10.1029/2008gl035619

Johnson, G. C., S. G. Purkey, and J. L. Bullister, 2008b: Warming and freshening in the abyssal southeastern indian ocean. *Journal of Climate*, **21**, 5351-5363. doi:10.1175/2008jcli2384.1

Jónsson, S., and H. Valdimarsson, 2012: Water mass transport variability to the north icelandic shelf, 1994–2010. *ICES Journal of Marine Science*. doi:10.1093/icesjms/fss024

Josey, S. A., 2011: Air-sea fluxes of heat, freshwater and momentum. *Operational oceanography in the 21st century*, A. Schiller, and G. B. Brassington, Eds., Springer, 155-184.

Josey, S. A., J. P. Grist, and R. Marsh, 2009: Estimates of meridional overturning circulation variability in the north atlantic from surface density flux fields. *J. Geophys. Res.-Oceans*, **114**. doi:10.1029/2008jc005230

Joyce, T. M., and R. Zhang, 2010: On the path of the gulf stream and the atlantic meridional overturning circulation. *Journal of Climate*, **23**, 3146-3154. doi:10.1175/2010jcli3310.1

Kanzow, T., U. Send, and M. McCartney, 2008: On the variability of the deep meridional transports in the tropical north atlantic. *Deep-Sea Res. Part I-Oceanogr. Res. Pap.*, **55**, 1601-1623. doi:10.1016/j.dsr.2008.07.011

Kanzow, T., et al., 2009: Basinwide integrated volume transports in an eddy-filled ocean. *Journal of Physical Oceanography*, **39**, 3091-3110. doi:10.1175/2009jpo4185.1

Kanzow, T., et al., 2007: Observed flow compensation associated with the moc at 26.5 degrees n in the atlantic. *Science*, **317**, 938-941. doi:10.1126/science.1141293

Kanzow, T., et al., 2010: Seasonal variability of the atlantic meridional overturning circulation at 26.5 degrees n. *Journal of Climate*, **23**, 5678-5698. doi:10.1175/2010jcli3389.1

Katsumata, K., and H. Yoshinari, 2010: Uncertainties in global mapping of argo drift data at the parking level. *Journal of Oceanography*, **66**, 553-569

Kawai, Y., T. Doi, H. Tomita, and H. Sasaki, 2008: Decadal-scale changes in meridional heat transport across 24 degrees n in the pacific ocean. *J. Geophys. Res.-Oceans*, **113**. doi:10.1029/2007jc004525

Kawano, T., T. Doi, H. Uchida, S. Kouketsu, M. Fukasawa, Y. Kawai, and K. Katsumata, 2010: Heat content change in the pacific ocean between the 1990s and 2000s. *Deep-Sea Research Part II-Topical Studies in Oceanography*, **57**, 1141-1151. doi:10.1016/j.dsr2.2009.12.003

Kazmin, A. S., 2012: Variability of the large-scale frontal zones: Analysis of the global satellite information. *Modern problems of remote sensing of Earth from space*, **9**, 213-218 (in Russian)

Keeling, C. D., H. Brix, and N. Gruber, 2004: Seasonal and long-term dynamics of the upper ocean carbon cycle at station aloha near hawaii. *Global Biogeochemical Cycles*, **18**, -

Keeling, R. F., A. Kortzinger, and N. Gruber, 2010: Ocean deoxygenation in a warming world. *Annual Review of Marine Science*, **2**, 199-229. doi:10.1146/annurev.marine.010908.163855

Khatiwala, S., F. Primeau, and T. Hall, 2009: Reconstruction of the history of anthropogenic co2 concentrations in the ocean. *Nature*, **462**, 346-U110

Khatiwala, S., et al., 2012: Global ocean storage of anthropogenic carbon. *Biogeosciences Discussions*, **9**, 8931-8988. doi:10.5194/bgd-9-8931-2012

Kieke, D., M. Rhein, L. Stramma, W. M. Smethie, D. A. LeBel, and W. Zenk, 2006: Changes in the cfc inventories and formation rates of upper labrador sea water, 1997-2001. *Journal of Physical Oceanography*, **36**, 64-86. doi:10.1175/jpo2814.1

Kieke, D., M. Rhein, L. Stramma, W. Smethie, J. Bullister, and D. LeBel, 2007: Changes in the pool of labrador sea water in the subpolar north atlantic. *Geophys. Res. Lett.* doi:ARTN L06605, 10.1029/2006GL028959

Knorr, W., 2009: Is the airborne fraction of anthropogenic co2 emissions increasing? *Geophys. Res. Lett.*, **36**. doi:10.1029/2009gl040613

Komar, P. D., and J. C. Allan, 2008: Increasing hurricane-generated wave heights along the us east coast and their climate controls. *Journal of Coastal Research*, **24**, 479-488. doi:10.2112/07-0894.1

Koshlyakov, M. N., Lisina, II, E. G. Morozov, and R. Y. Tarakanov, 2007: Absolute geostrophic currents in the drake passage based on observations in 2003 and 2005. *Oceanology*, **47**, 451-463. doi:10.1134/s0001437007040029

Koshlyakov, M. N., S. V. Gladyshev, R. Y. Tarakanov, and D. A. Fedorov, 2011: Currents in the western drake passage by the observations in january 2010. *Oceanology*, **51**, 187-198. doi:10.1134/S000143701102007X

Kouketsu, S., et al., 2009: Changes in water properties and transports along 24 degrees n in the north pacific between 1985 and 2005. *J. Geophys. Res.-Oceans*, **114**. doi:10.1029/2008jc004778

Kouketsu, S., et al., 2011: Deep ocean heat content changes estimated from observation and reanalysis product and their influence on sea level change. *J. Geophys. Res.-Oceans*, **116**. doi:10.1029/2010jc006464

Kroeker, K. J., R. L. Kordas, R. N. Crim, and G. G. Singh, 2010: Meta-analysis reveals negative yet variable effects of ocean acidification on marine organisms. *Ecology Letters*, **13**, 1419-1434. doi:10.1111/j.1461-0248.2010.01518.x

Kwok, R., G. F. Cunningham, M. Wensnahan, I. Rigor, H. J. Zwally, and D. Yi, 2009: Thinning and volume loss of the arctic ocean sea ice cover: 2003-2008. *J. Geophys. Res.-Oceans*, **114**. doi:C07005, 10.1029/2009jc005312

Large, W. G., and S. G. Yeager, 2009: The global climatology of an interannually varying air-sea flux data set. *Clim. Dyn.*, **33**, 341-364. doi:10.1007/s00382-008-0441-3

Le Quéré, C., T. Takahashi, E. T. Buitenhuis, C. Roedenbeck, and S. C. Sutherland, 2010: Impact of climate change and variability on the global oceanic sink of co2. *Global Biogeochemical Cycles*, **24**. doi:10.1029/2009gb003599

Le Quéré, C., et al., 2007: Saturation of the southern ocean co2 sink due to recent climate change. *Science*, **316**. doi:10.1126/science.1136188

LeBel, D. A., et al., 2008: The formation rate of north atlantic deep water and eighteen degree water calculated from cfc-11 inventories observed during woce. *Deep-Sea Res. Part I-Oceanogr. Res. Pap.*, **55**, 891-910. doi:10.1016/j.dsr.2008.03.009

Letetrel, C., M. Marcos, B. M. Miguez, and G. Woppelmann, 2010: Sea level extremes in marseille (nw mediterranean) during 1885-2008. *Continental Shelf Research*, **30**, 1267-1274. doi:10.1016/j.csr.2010.04.003

Leuliette, E. W., and L. Miller, 2009: Closing the sea level rise budget with altimetry, argo, and grace. *Geophys. Res. Lett.*, **36**. doi:10.1029/2008gl036010

Leuliette, E. W., and R. Scharroo, 2010: Integrating jason-2 into a multiple-altimeter climate data record. *Marine Geodesy*, **33**, 504-517. doi:10.1080/01490419.2010.487795

Leuliette, E. W., and J. K. Willis, 2011: Balancing the sea level budget. *Oceanography*, **24**, 122-129

Levitus, S., J. I. Antonov, T. P. Boyer, R. A. Locarnini, H. E. Garcia, and A. V. Mishonov, 2009: Global ocean heat content 1955-2008 in light of recently revealed instrumentation problems. *Geophys. Res. Lett.*, **36**, 5. doi:10.1029/2008gl037155

Levitus, S., et al., 2012: World ocean heat content and thermosteric sea level change (0-2000). *Geophys. Res. Lett.*, **in press**. doi:10.1029/2012GL051106

Li, G., B. Ren, J. Zheng, and C. Yang, 2011: Trend singular value decomposition analysis and its application to the global ocean surface latent heat flux and sst anomalies. *Journal of Climate*, **24**, 2931-2948. doi:10.1175/2010jcli3743.1

Llovel, W., S. Guinehut, and A. Cazenave, 2010: Regional and interannual variability in sea level over 2002-2009 based on satellite altimetry, argo float data and grace ocean mass. *Ocean Dynamics*, **60**, 1193-1204. doi:10.1007/s10236-010-0324-0

Llovel, W., B. Meyssignac, and A. Cazenave, 2011: Steric sea level variations over 2004-2010 as a function of region and depth: Inference on the mass component variability in the north atlantic ocean. *Geophys. Res. Lett.*, **38**. doi:10.1029/2011gl047411

Llovel, W., A. Cazenave, P. Rogel, A. Lombard, and M. B. Nguyen, 2009: Two-dimensional reconstruction of past sea level (1950-2003) from tide gauge data and an ocean general circulation model. *Climate of the Past*, **5**, 217-227

Lowe, J. A., and J. M. Gregory, 2006: Understanding projections of sea level rise in a hadley centre coupled climate model. *J. Geophys. Res.-Oceans*, **111**. doi:10.1029/2005jc003421

Lowe, J. A., et al., 2010: Past and future changes in extreme sea levels and waves. *Understanding sea-level rise and variability*, J. A. Church, P. L. Woodworth, T. Aarup, and W. S. Wilson, Eds., Wiley-Blackwell.

Lozier, M. S., and N. M. Stewart, 2008: On the temporally varying northward penetration of mediterranean overflow water and eastward penetration of labrador sea water. *Journal of Physical Oceanography*, **38**, 2097-2103. doi:10.1175/2008jpo3908.1

Lumpkin, R., and K. Speer, 2007: Global ocean meridional overturning. *Journal of Physical Oceanography*, **37**, 2550-2562. doi:10.1175/jpo3130.1

Lumpkin, R., and S. Garzoli, 2011: Interannual to decadal changes in the western south atlantic's surface circulation. *J. Geophys. Res.-Oceans*, **116**. doi:10.1029/2010jc006285

Luthi, D., et al., 2008: High-resolution carbon dioxide concentration record 650,000-800,000 years before present. *Nature*, **453**, 379-382. doi:10.1038/nature06949

Lyman, J. M., and G. C. Johnson, 2008: Estimating annual global upper-ocean heat content anomalies despite irregular in situ ocean sampling. *Journal of Climate*, **21**, 5629-5641. doi:10.1175/2008jcli2259.1

Lyman, J. M., et al., 2010: Robust warming of the global upper ocean. *Nature*, **465**, 334-337. doi:10.1038/nature09043

Macrander, A., U. Send, H. Valdimarsson, S. Jonsson, and R. H. Kase, 2005: Interannual changes in the overflow from the nordic seas into the atlantic ocean through denmark strait. *Geophys. Res. Lett.*, **32**. doi:10.1029/2004gl021463

Manning, A. C., and R. F. Keeling, 2006: Global oceanic and land biotic carbon sinks from the scripps atmospheric oxygen flask sampling network. *Tellus Series B-Chemical and Physical Meteorology*, **58**, 95-116

Marcos, M., M. N. Tsimplis, and A. G. P. Shaw, 2009: Sea level extremes in southern europe. *J. Geophys. Res.-Oceans*, **114**. doi:10.1029/2008jc004912

Marsh, R., 2000: Recent variability of the north atlantic thermohaline circulation inferred from surface heat and freshwater fluxes. *Journal of Climate*, **13**, 3239-3260

Marshall, G. J., 2003: Trends in the southern annular mode from observations and reanalyses. *Journal of Climate*, **16**, 4134-4143

Masuda, S., et al., 2010: Simulated rapid warming of abyssal north pacific waters. *Science*, **329**, 319-322. doi:10.1126/science.1188703

Matear, R. J., and A. C. Hirst, 2003: Long-term changes in dissolved oxygen concentrations in the ocean caused by protracted global warming. *Global Biogeochemical Cycles*, **17**. doi:10.1029/2002gb001997

Matear, R. J., and B. I. McNeil, 2003: Decadal accumulation of anthropogenic co2 in the southern ocean: A comparison of cfc-age derived estimates to multiple-linear regression estimates. *Global Biogeochemical Cycles*, **17**. doi:10.1029/2003GB002089

Mauritzen, C., A. Melsom, and R. T. Sutton, 2012: Recent heat uptake in the north atlantic ocean. *Nature Geosciences*, **submitted**

Mauritzen, C., et al., 2011: Closing the loop - approaches to monitoring the state of the arctic mediterranean during the international polar year 2007-2008. *Prog. Oceanogr.*, **90**, 62-89. doi:10.1016/j.pocean.2011.02.010

McCarthy, G., E. McDonagh, and B. King, 2011: Decadal variability of thermocline and intermediate waters at 24°s in the south atlantic. *Journal of Physical Oceanography*, **41**, 157-165. doi:10.1175/2010jpo4467.1

McCarthy, G., et al., 2012: Observed interannual variability of the atlantic meridional overturning circulation at 26.5°n. *Geophys. Res. Lett.*, **submitted**

McKinley, G. A., A. R. Fay, T. Takahashi, and N. Metzl, 2011: Convergence of atmospheric and north atlantic carbon dioxide trends on multidecadal timescales. *Nat. Geosci.*, **4**, 606-610. doi:10.1038/ngeo1193

McPhee, M. G., A. Proshutinsky, J. H. Morison, M. Steele, and M. B. Alkire, 2009: Rapid change in freshwater content of the arctic ocean. *Geophys. Res. Lett.*, **36**. doi:10.1029/2009gl037525

Mears, C. A., and F. J. Wentz, 2009a: Construction of the remote sensing systems v3.2 atmospheric temperature records from the msu and amsu microwave sounders. *J. Atmos. Ocean. Technol.*, **26**, 1040-1056. doi:10.1175/2008jtecha1176.1

——, 2009b: Construction of the rss v3.2 lower-tropospheric temperature dataset from the msu and amsu microwave sounders. *J. Atmos. Ocean. Technol.*, **26**, 1493-1509. doi:10.1175/2009jtecha1237.1

Meijers, A. J. S., N. L. Bindoff, and S. R. Rintoul, 2011: Frontal movements and property fluxes: Contributions to heat and freshwater trends in the southern ocean. *J. Geophys. Res.-Oceans*, **116**. doi:10.1029/2010jc006832

Meinen, C. S., M. O. Baringer, and R. F. Garcia, 2010: Florida current transport variability: An analysis of annual and longer-period signals. *Deep-Sea Res. Part I-Oceanogr. Res. Pap.*, **57**, 835-846. doi:10.1016/j.dsr.2010.04.001

Menendez, M., and P. L. Woodworth, 2010: Changes in extreme high water levels based on a quasi-global tide-gauge data set. *J. Geophys. Res.-Oceans*, **115**. doi:10.1029/2009jc005997

Menendez, M., F. J. Mendez, I. J. Losada, and N. E. Graham, 2008: Variability of extreme wave heights in the northeast pacific ocean based on buoy measurements. *Geophys. Res. Lett.*, **35**. doi:10.1029/2008gl035394

Meredith, M. P., P. L. Woodworth, C. W. Hughes, and V. Stepanov, 2004: Changes in the ocean transport through drake passage during the 1980s and 1990s, forced by changes in the southern annular mode. *Geophys. Res. Lett.*, **31**. doi:10.1029/2004gl021169

Merrifield, M. A., 2011: A shift in western tropical pacific sea level trends during the 1990s. *Journal of Climate*, **24**, 4126-4138. doi:10.1175/2011jcli3932.1

Merrifield, M. A., and M. E. Maltrud, 2011: Regional sea level trends due to a pacific trade wind intensification. *Geophys. Res. Lett.*, **38**. doi:10.1029/2011gl049576

Merrifield, M. A., S. T. Merrifield, and G. T. Mitchum, 2009: An anomalous recent acceleration of global sea level rise. *Journal of Climate*, **22**, 5772-5781. doi:10.1175/2009jcli2985.1

Merrifield, M. A., P. R. Thompson, and M. Lander, 2012: Multidecadal sea level anomalies and trends in the western tropical pacific. *Geophys. Res. Lett.*, **39**. doi:10.1029/2012GL052032

Metzl, N., 2009: Decadal increase of oceanic carbon dioxide in southern indian ocean surface waters (1991-2007). *Deep-Sea Research Part Ii-Topical Studies in Oceanography*, **56**, 607-619. doi:10.1016/j.dsr2.2008.12.007

Meyssignac, B., M. Becker, W. Llovel, and A. Cazenave, 2012: An assessment of two-dimensional past sea level reconstructions over 1950–2009 based on tide-gauge data and different input sea level grids. *Surveys in Geophysics*. doi:10.1007/s10712-011-9171-x

Midorikawa, T., K. Nemoto, H. Kamiya, M. Ishii, and H. Y. Inoue, 2005: Persistently strong oceanic co2 sink in the western subtropical north pacific. *Geophys. Res. Lett.*, **32**. doi:10.1029/2004gl021952

Midorikawa, T., et al., 2010: Decreasing ph trend estimated from 25-year time series of carbonate parameters in the western north pacific. *Tellus Series B-Chemical and Physical Meteorology*, **62**, 649-659. doi:10.1111/j.1600-0889.2010.00474.x

Mikaloff-Fletcher, S. E., et al., 2006: Inverse estimates of anthropogenic co2 uptake, transport, and storage by the ocean. *Global Biogeochemical Cycles*, **20**

Miller, L., and B. C. Douglas, 2007: Gyre-scale atmospheric pressure variations and their relation to 19th and 20th century sea level rise. *Geophys. Res. Lett.*, **34**. doi:10.1029/2007gl030862

Mishchenko, M. I., and I. V. Geogdzhayev, 2007: Satellite remote sensing reveals regional tropospheric aerosol trends. *Optics Express*, **15**, 7423-7438

Mitas, C. M., and A. Clement, 2005: Has the hadley cell been strengthening in recent decades? *Geophys. Res. Lett.*, **32**. doi:10.1029/2004gl021765

Mitchum, G. T., R. S. Nerem, M. A. Merrifield, and W. R. Gehrels, 2010: Modern sea-level-change estimates. *Understanding sea-level rise and variability*, J. A. Church, P. L. Woodworth, T. Aarup, and W. S. Wilson, Eds., Wiley-Blackwell.

Morison, J., R. Kwok, C. Peralta-Ferriz, M. Alkire, I. Rigor, R. Andersen, and M. Steele, 2012: Changing arctic ocean freshwater pathways. *Nature*, **481**, 66-70. doi:10.1038/nature10705

Murata, A., Y. Kumamoto, S. Watanabe, and M. Fukasawa, 2007: Decadal increases of anthropogenic co2 in the south pacific subtropical ocean along 32 degrees s. *J. Geophys. Res.-Oceans*, **112**. doi:10.1029/2005JC003405

Murata, A., Y. Kumamoto, K. Sasaki, S. Watanabe, and M. Fukasawa, 2008: Decadal increases of anthropogenic co2 in the subtropical south atlantic ocean along 30 degrees s. *J. Geophys. Res.-Oceans*, **113**. doi:10.1029/2007JC004424

Murata, A., Y. Kumamoto, K.-i. Sasaki, S. Watanabe, and M. Fukasawa, 2010: Decadal increases in anthropogenic co2 along 20°s in the south indian ocean. *J. Geophys. Res.*, **115**. doi:10.1029/2010JC006250

Murata, A., Y. Kumamoto, K. Sasaki, ichi, S. Watanabe, and M. Fukasawa, 2009: Decadal increases of anthropogenic co2 along 149°e in the western north pacific. *J. Geophys. Res.*, **114**. doi:10.1029/2008JC004920

Myers, P. G., and C. Donnelly, 2008: Water mass transformation and formation in the labrador sea. *Journal of Climate*, **21**, 1622-1638. doi:10.1175/2007jcli1722.1

Nakano, T., I. Kaneko, T. Soga, H. Tsujino, T. Yasuda, H. Ishizaki, and M. Kamachi, 2007: Mid-depth freshening in the north pacific subtropical gyre observed along the jma repeat and woce hydrographic sections. *Geophys. Res. Lett.*, **34**. doi:10.1029/2007gl031433

Nakanowatari, T., K. Ohshima, and M. Wakatsuchi, 2007: Warming and oxygen decrease of intermediate water in the northwestern north pacific, originating from the sea of okhotsk, 1955-2004. *Geophys. Res. Lett.*, **34**. doi:10.1029/2006GL028243

Nerem, R. S., D. P. Chambers, C. Choe, and G. T. Mitchum, 2010: Estimating mean sea level change from the topex and jason altimeter missions. *Marine Geodesy*, **33**, 435-446. doi:10.1080/01490419.2010.491031

Nerem, R. S., D. P. Chambers, E. W. Leuliette, G. T. Mitchum, and B. S. Giese, 1999: Variations in global mean sea level associated with the 1997-1998 enso event: Implications for measuring long term sea level change. *Geophys. Res. Lett.*, **26**, 3005-3008. doi:10.1029/1999gl002311

Olafsson, J., S. R. Olafsdottir, A. Benoit-Cattin, M. Danielsen, T. S. Arnarson, and T. Takahashi, 2009: Rate of iceland sea acidification from time series measurements. *Biogeosciences*, **6**, 2661-2668

Olsen, A., A. M. Omar, E. Jeansson, L. G. Anderson, and R. G. J. Bellerby, 2010: Nordic seas transit time distributions and anthropogenic co2. *J. Geophys. Res.*, **115**, C05005

Olsen, A., et al., 2006: Magnitude and origin of the anthropogenic co2 increase and c-13 suess effect in the nordic seas since 1981. *Global Biogeochemical Cycles*, **20**. doi:10.1029/2005GB002669

Olsen, S. M., B. Hansen, D. Quadfasel, and S. Osterhus, 2008: Observed and modelled stability of overflow across the greenland-scotland ridge. *Nature*, **455**, 519-U535. doi:10.1038/nature07302

Ono, T., T. Midorikawa, Y. W. Watanabe, K. Tadokoro, and T. Saino, 2001: Temporal increases of phosphate and apparent oxygen utilization in the subsurface waters of western subarctic pacific from 1968 to 1998. *Geophys. Res. Lett.*, **28**, 3285-3288. doi:10.1029/2001gl012948

Orr, J. C., 2011: Recent and future changes in ocean carbonate chemistry. *Ocean acidification*, J.-P. Guttuso, and L. Hansson, Eds., Oxford University Press, 41-66.

Orr, J. C., S. Pantoja, and H. O. Portner, 2005: Introduction to special section: The ocean in a high-co2 world. *J. Geophys. Res.-Oceans*, **110**. doi:10.1029/2005jc003086

Orsi, A. H., G. C. Johnson, and J. L. Bullister, 1999: Circulation, mixing, and production of antarctic bottom water. *Prog. Oceanogr.*, **43**, 55-109

Østerhus, S., W. R. Turrell, S. Jonsson, and B. Hansen, 2005: Measured volume, heat, and salt fluxes from the atlantic to the arctic mediterranean. *Geophys. Res. Lett.*, **32**. doi:10.1029/2004gl022188

Palmer, M., and P. Brohan, 2011: Estimating sampling uncertainty in fixed-depth and fixed-isotherm estimates of ocean warming. *International Journal of Climatology*, **31**, 980-986. doi:10.1002/joc.2224

Palmer, M., K. Haines, S. Tett, and T. Ansell, 2007: Isolating the signal of ocean global warming. *Geophys. Res. Lett.*, **34**. doi:10.1029/2007GL031712|10.1029/2007GL031712

Park, G. H., et al., 2006: Large accumulation of anthropogenic co2 in the east (japan) sea and its significant impact on carbonate chemistry. *Global Biogeochemical Cycles*, **20**, -

Peltier, W. R., 2001: Global glacial isostatic adjustment and modern instrumental records of relative sea level history. *Sea level rise*, B. C. Douglas, M. S. Kearney, and S. P. Leatherman, Eds., Elsevier, 65-95.

——, 2004: Global glacial isostasy and the surface of the ice-age earth: The ice-5g (vm2) model and grace. *Annual Review of Earth and Planetary Sciences*, **32**, 111-149. doi:10.1146/annurev.earth.32.082503.144359

Peltier, W. R., R. Drummond, and K. Roy, 2012: Comments on the paper by chambers et al, 2010 concerning the interpretation of grace time-dependent gravity observations and the influence upon them of rotational feedback in glacial isostatic adjustment. *Journal of Geophysical Research*, **submitted**

Pena-Molino, B., T. M. Joyce, and J. M. Toole, 2011: Recent changes in the labrador sea water within the deep western boundary current southeast of cape cod. *Deep-Sea Res. Part I-Oceanogr. Res. Pap.*, **58**, 1019-1030. doi:10.1016/j.dsr.2011.07.006

Peng, T.-H., R. Wanninkhof, and R. A. Feely, 2003: Increase of anthropogenic co2 in the pacific ocean over the last two decades. *Deep-Sea Research A*, **50**, 3065-3082

Peng, T.-H., R. Wanninkhof, J. L. Bullister, R. A. Feely, and T. Takahashi, 1998: Quantification of decadal anthropogenic co2 uptake in the ocean based on dissolved inorganic carbon measurements. *Nature*, **396**, 560-563

Pérez, F. F., V.-R. M., E. Louarn, X. A. Padín, H. Mercier, and A. F. Ríos, 2008: Temporal variability of the anthropogenicv co2 storage in the irminger sea. *Biogeosciences*, **5**, 1669-1679

Pérez, F. F., M. Vázquez-Rodríguez, H. Mercier, A. Velo, P. Lherminier, and A. F. RÃos, 2010: Trends of anthropogenic co2 storage in north atlantic water masses. *Biogeosciences*, **7**, 1789-1807

Pierce, D. W., T. P. Barnett, K. M. AchutaRao, P. J. Gleckler, J. M. Gregory, and W. M. Washington, 2006: Anthropogenic warming of the oceans: Observations and model results. *Journal of Climate*, **19**, 1873-1900

Polyakov, I. V., J. E. Walsh, and R. Kwok, 2012: Recent changes of arctic multiyear sea ice coverage and the likely causes. *Bull. Amer. Meteorol. Soc.*, **93**, 145-151. doi:10.1175/bams-d-11-00070.1

Polyakov, I. V., V. A. Alexeev, U. S. Bhatt, E. I. Polyakova, and X. D. Zhang, 2010a: North atlantic warming: Patterns of long-term trend and multidecadal variability. *Clim. Dyn.*, **34**, 439-457. doi:10.1007/s00382-008-0522-3

Polyakov, I. V., U. S. Bhatt, H. L. Simmons, D. Walsh, J. E. Walsh, and X. Zhang, 2005: Multidecadal variability of north atlantic temperature and salinity during the twentieth century. *Journal of Climate*, **18**, 4562-4581

Polyakov, I. V., et al., 2008: Arctic ocean freshwater changes over the past 100 years and their causes. *Journal of Climate*, **21**, 364-384. doi:10.1175/2007jcli1748.1

Polyakov, I. V., et al., 2010b: Arctic ocean warming contributes to reduced polar ice cap. *Journal of Physical Oceanography*, **40**, 2743-2756. doi:10.1175/2010jpo4339.1

Potemra, J. T., and N. Schneider, 2007: Interannual variations of the indonesian throughflow. *J. Geophys. Res.-Oceans*, **112**. doi:10.1029/2006jc003808

Pritchard, H. D., S. R. M. Ligtenberg, H. A. Fricker, D. G. Vaughan, M. R. van den Broeke, and L. Padman, 2012: Antarctic ice-sheet loss driven by basal melting of ice shelves. *Nature*, **484**, 502-505. doi:10.1038/nature10968

Proshutinsky, A., et al., 2009: Beaufort gyre freshwater reservoir: State and variability from observations. *J. Geophys. Res.-Oceans*, **114**. doi:10.1029/2008jc005104

Purkey, S. G., and G. C. Johnson, 2010: Warming of global abyssal and deep southern ocean waters between the 1990s and 2000s: Contributions to global heat and sea level rise budgets. *Journal of Climate*, **23**, 6336-6351. doi:10.1175/2010jcli3682.1

——, 2012: Global contraction of antarctic bottom water between the 1980s and 2000s. *Journal of Climate*, **in press**. doi:10.1175/JCLI-D-11-00612.1

Qiu, B., and S. Chen, 2006: Decadal variability in the large-scale sea surface height field of the south pacific ocean: Observations and causes. *Journal of Physical Oceanography*, **36**, 1751-1762

——, 2010: Interannual-to-decadal variability in the bifurcation of the north equatorial current off the philippines. *Journal of Physical Oceanography*, **40**, 2525-2538. doi:10.1175/2010jpo4462.1

Qiu, B., and S. Chen, 2012: Multi-decadal sea level and gyre circulation variability in the northwestern tropical pacific ocean. *Journal of Physical Oceanography*, **42**, 193-206. doi:10.1175/JPO-D-11-061.1

Rabe, B., et al., 2011: An assessment of arctic ocean freshwater content changes from the 1990s to the 2006-2008 period. *Deep-Sea Res. Part I-Oceanogr. Res. Pap.*, **58**, 173-185. doi:10.1016/j.dsr.2010.12.002

Rahmstorf, S., and M. Vermeer, 2011: Discussion of: Houston, j.R. And dean, r.G., 2011. Sea-level acceleration based on u.S. Tide gauges and extensions of previous global-gauge analyses. Journal of coastal research, 27(3), 409-417. *Journal of Coastal Research*, **27**, 784-787. doi:10.2112/jcoastres-d-11-00082.1

Rawlins, M. A., et al., 2010: Analysis of the arctic system for freshwater cycle intensification: Observations and expectations. *Journal of Climate*, **23**, 5715-5737. doi:10.1175/2010jcli3421.1

Ray, R. D., and B. C. Douglas, 2011: Experiments in reconstructing twentieth-century sea levels. *Prog. Oceanogr.*, **91**, 496-515. doi:10.1016/j.pocean.2011.07.021

Ren, L., and S. C. Riser, 2010: Observations of decadal time scale salinity changes in the subtropical thermocline of the north pacific ocean. *Deep-Sea Research Part Ii-Topical Studies in Oceanography*, **57**, 1161-1170. doi:10.1016/j.dsr2.2009.12.005

Reverdin, G., 2010: North atlantic subpolar gyre surface variability (1895-2009). *Journal of Climate*, **23**, 4571-4584. doi:10.1175/2010jcli3493.1

Reverdin, G., F. Durand, J. Mortensen, F. Schott, H. Valdimarsson, and W. Zenk, 2002: Recent changes in the surface salinity of the north atlantic subpolar gyre. *J. Geophys. Res.-Oceans*, **107**. doi:10.1029/2001jc001010

Rhein, M., et al., 2011: Deep water formation, the subpolar gyre, and the meridional overturning circulation in the subpolar north atlantic. *Deep-Sea Research Part Ii-Topical Studies in Oceanography*, **58**, 1819-1832. doi:10.1016/j.dsr2.2010.10.061

Rignot, E., J. L. Bamber, M. R. Van Den Broeke, C. Davis, Y. H. Li, W. J. Van De Berg, and E. Van Meijgaard, 2008: Recent antarctic ice mass loss from radar interferometry and regional climate modelling. *Nat. Geosci.*, **1**, 106-110. doi:10.1038/ngeo102

Rintoul, S. R., 2007: Rapid freshening of antarctic bottom water formed in the indian and pacific oceans. *Geophys. Res. Lett.*, **34**. doi:10.1029/2006gl028550

Rintoul, S. R., S. Sokolov, and J. Church, 2002: A 6 year record of baroclinic transport variability of the antarctic circumpolar current at 140 degrees e derived from expendable bathythermograph and altimeter measurements. *J. Geophys. Res.-Oceans*, **107**. doi:10.1029/2001jc000787

Rios, A. F., A. Velo, P. C. Pardo, M. Hoppema, and F. F. Perez, 2012: An update of anthropogenic co2 storage rates in the western south atlantic basin and the role of antarctic bottom water. *Journal of Marine Systems*, **94**. doi:10.1016/j.jmarsys.2011.11.023

Roemmich, D., and J. Gilson, 2009: The 2004-2008 mean and annual cycle of temperature, salinity, and steric height in the global ocean from the argo program. *Prog. Oceanogr.*, **82**, 81-100. doi:10.1016/j.pocean.2009.03.004

Roemmich, D., W. J. Gould, and J. Gilson, 2012: 135 years of global ocean warming between the challenger expedition and the argo programme. *Nature Climate Change*, **2**, 425-428. doi:10.1038/nclimate1461

Roemmich, D., J. Gilson, R. Davis, P. Sutton, S. Wijffels, and S. Riser, 2007: Decadal spinup of the south pacific subtropical gyre. *Journal of Physical Oceanography*, **37**, 162-173. doi:10.1175/jpo3004.1

Romanou, A., W. B. Rossow, and S. H. Chou, 2006: Decorrelation scales of high-resolution turbulent fluxes at the ocean surface and a method to fill in gaps in satellite data products. *Journal of Climate*, **19**, 3378-3393

Romanou, A., B. Liepert, G. A. Schmidt, W. B. Rossow, R. A. Ruedy, and Y. Zhang, 2007: 20th century changes in surface solar irradiance in simulations and observations. *Geophys. Res. Lett.*, **34**. doi:10.1029/2006gl028356

Ruggiero, P., P. D. Komar, and J. C. Allan, 2010: Increasing wave heights and extreme value projections: The wave climate of the us pacific northwest. *Coastal Engineering*, **57**. doi:10.1016/j.coastaleng.2009.12.005

Sabine, C. L., 2005: Global ocean data analysis project (glodap): Results and data. Carbon Dioxide Information Analysis Center, Oak Ridge National Laboratory, U.S. Department of Energy, 110 pp. plus 116 Appendices pp.

Sabine, C. L., R. A. Feely, F. Millero, A. G. Dickson, C. Langdon, S. Mecking, and D. Greeley, 2008: Decadal changes in pacific carbon. *J. Geophys. Res.-Oceans*, **113**. doi:10.1029/2007JC004577

Sabine, C. L., et al., 2004: The oceanic sink for anthropogenic co2. *Science*, **305**, 367-371

Sallengar, A. H., K. S. Doran, and P. A. Howd, 2012: Hotspot of accelerated sea level rise on the atlantic coast of north america. *Nature Climate Change*. doi:10.1038/NCLIMATE1597

Santana-Casiano, J. M., M. González-Dávila, M. J. Rueda, O. Llinas, and E. F. González-Dávila, 2007: The interannual variability of oceanic co2 parameters in the northeast atlantic subtropical gyre at the estoc site. *Global Biogeochemical Cycles*, **21**. doi:10.1029/2006gb002788

Sarafanov, A., A. Falina, A. Sokov, and A. Demidov, 2008: Intense warming and salinification of intermediate waters of southern origin in the eastern subpolar north atlantic in the 1990s to mid-2000s. *J. Geophys. Res.-Oceans*, **113**, -. doi:10.1029/2008JC004975

Sarmiento, J. L., et al., 2010: Trends and regional distributions of land and ocean carbon sinks. *Biogeosciences*, **7**, 2351-2367. doi:10.5194/bg-7-2351-2010

Sasaki, W., S. I. Iwasaki, T. Matsuura, and S. Iizuka, 2005: Recent increase in summertime extreme wave heights in the western north pacific. *Geophys. Res. Lett.*, **32**. doi:10.1029/2005gl023722

Schanze, J. J., R. W. Schmitt, and L. L. Yu, 2010: The global oceanic freshwater cycle: A state-of-the-art quantification. *Journal of Marine Research*, **68**, 569-595. doi:10.1357/002224010794657164

Schauer, U., and A. Beszczynska-Möller, 2009: Problems with estimation and interpretation of oceanic heat transport–conceptual remarks for the case of fram strait in the arctic ocean. *Ocean Sci.*, **5**, 487–494

Schmidtko, S., and G. C. Johnson, 2012: Multi-decadal warming and shoaling of antarctic intermediate water. *Journal of Climate*, **25**, 201-221. doi:10.1175/JCLI-D-11-00021.1

Schmitt, R. W., 2008: Salinity and the global water cycle. *Oceanography*, **21**, 12-19

Schneider, T., P. A. O'Gorman, and X. J. Levine, 2010: Water vapor and the dynamics of climate changes. *Reviews of Geophysics*, **48**. doi:10.1029/2009rg000302

Schuster, U., and A. J. Watson, 2007a: A variable and decreasing sink for atmospheric co2 in the north atlantic. *Journal of Geophysical Research-Oceans*, **112**, -

——, 2007b: A variable and decreasing sink for atmospheric co2 in the north atlantic. *J. Geophys. Res.-Oceans*, **112**. doi:10.1029/2006JC003941

Semedo, A., K. Suselj, A. Rutgersson, and A. Sterl, 2011: A global view on the wind sea and swell climate and variability from era-40. *Journal of Climate*, **24**, 1461-1479. doi:10.1175/2010jcli3718.1

Send, U., M. Lankhorst, and T. Kanzow, 2011: Observation of decadal change in the atlantic meridional overturning circulation using 10 years of continuous transport data. *Geophys. Res. Lett.*, **38**. doi:10.1029/2011GL049801

Shepherd, A., D. Wingham, and E. Rignot, 2004: Warm ocean is eroding west antarctic ice sheet. *Geophys. Res. Lett.*, **31**. doi:10.1029/2004gl021106

Shiklomanov, A. I., and R. B. Lammers, 2009: Record russian river discharge in 2007 and the limits of analysis. *Environmental Research Letters*, **4**. doi:10.1088/1748-9326/4/4/045015

Siegenthaler, U., et al., 2005: Stable carbon cycle-climate relationship during the late pleistocene. *Science*, **310**. doi:10.1126/science.1120130

Smith, D. M., and J. M. Murphy, 2007: An objective ocean temperature and salinity analysis using covariances from a global climate model. *J. Geophys. Res.-Oceans*, **112**, 19. doi:C02022, 10.1029/2005jc003172

Smith, R. O., H. L. Bryden, and K. Stansfield, 2008: Observations of new western mediterranean deep water formation using argo floats 2004-2006. *Ocean Sci.*, **4**, 133-149. doi:10.5194/os-4-133-2008

Smith, T. M., P. A. Arkin, and M. R. P. Sapiano, 2009: Reconstruction of near-global annual precipitation using correlations with sea surface temperature and sea level pressure. *Journal of Geophysical Research-Atmospheres*, **114**. doi:10.1029/2008jd011580

Smith, T. M., P. A. Arkin, L. Ren, and S. S. P. Shen, 2012: Improved reconstruction of global precipitation since 1900. *J. Atmos. Ocean. Technol.*, **in press**. doi:10.1175/JTECH-D-12-00001.1

Sokolov, S., and S. R. Rintoul, 2009: Circumpolar structure and distribution of the antarctic circumpolar current fronts: 2. Variability and relationship to sea surface height. *J. Geophys. Res.-Oceans*, **114**, 15. doi:10.1029/2008jc005248

Spada, G., and G. Galassi, 2012: New estimates of secular sea–level rise from tide gauge data and gia modeling. *Geophysical Journal International*, **submitted**

Speer, K. G., 1997: A note on average cross-isopycnal mixing in the north atlantic ocean. *Deep-Sea Res. Part I-Oceanogr. Res. Pap.*, **44**, 1981-1990

Spence, P., J. C. Fyfe, A. Montenegro, and A. J. Weaver, 2010: Southern ocean response to strengthening winds in an eddy-permitting global climate model. *Journal of Climate*, **23**, 5332-5343. doi:10.1175/2010jcli3098.1

Sprintall, J., S. Wijffels, T. Chereskin, and N. Bray, 2002: The jade and woce i10/ir6 throughflow sections in the southeast indian ocean. Part 2: Velocity and transports. *Deep-Sea Research Part Ii-Topical Studies in Oceanography*, **49**, 1363-1389

Sprintall, J., S. E. Wijffels, R. Molcard, and I. Jaya, 2009: Direct estimates of the indonesian throughflow entering the indian ocean: 2004-2006. *J. Geophys. Res.-Oceans*, **114**. doi:10.1029/2008jc005257

Stammer, D., et al., 2010: Multi-model ensemble ocean synthesis in support of climate diagnostics. *OceanObs'09: Sustained Ocean Observations and Information for Society*, J. Hall, D. E. Harrison, and D. Stammer, Eds., European Space Agency.

Steele, M., and W. Ermold, 2007: Steric sea level change in the northern seas. *Journal of Climate*, **20**, 403-417. doi:10.1175/jcli4022.1

Steinfeldt, R., M. Rhein, J. L. Bullister, and T. Tanhua, 2009: Inventory changes in anthropogenic carbon from 1997-2003 in the atlantic ocean between 20 degrees s and 65 degrees n. *Global Biogeochemical Cycles*, **23**, GB3010. doi:doi:10.1029/2008GB003311

Stendardo, I., and N. Gruber, 2012: Oxygen trends over five decades in the north atlantic. *Journal of Geophysical Research*, **submitted**

Sterl, A., and S. Caires, 2005: Climatology, variability and extrema of ocean waves: The web-based knmi/era-40 wave atlas. *International Journal of Climatology*, **25**, 963-977. doi:10.1002/joc.1175

Stott, P. A., R. T. Sutton, and D. M. Smith, 2008: Detection and attribution of atlantic salinity changes. *Geophys. Res. Lett.*, **35**. doi:10.1029/2008gl035874

Stramma, L., G. C. Johnson, J. Sprintall, and V. Mohrholz, 2008: Expanding oxygen-minimum zones in the tropical oceans. *Science*, **320**, 655-658. doi:10.1126/science.1153847

Stramma, L., S. Schmidtko, L. A. Levin, and G. C. Johnson, 2010: Ocean oxygen minima expansions and their biological impacts. *Deep-Sea Res. Part I-Oceanogr. Res. Pap.*, **57**, 587-595. doi:10.1016/j.dsr.2010.01.005

Straneo, F., et al., 2010: Rapid circulation of warm subtropical waters in a major glacial fjord in east greenland. *Nat. Geosci.*, **3**, 182-186. doi:10.1038/ngeo764

Sturges, W., and B. G. Hong, 1995: Wind forcing of the atlantic thermocline along 32°n at low-frequencies. *Journal of Physical Oceanography*, **25**, 1706-1715. doi:10.1175/1520-0485(1995)025<1706:wfotat>2.0.co;2

Sturges, W., and B. C. Douglas, 2011: Wind effects on estimates of sea level rise. *J. Geophys. Res.-Oceans*, **116**. doi:10.1029/2010jc006492

Sugimoto, S., and K. Hanawa, 2010: The wintertime wind stress curl field in the north atlantic and its relation to atmospheric teleconnection patterns. *Journal of the Atmospheric Sciences*, **67**, 1687-1694. doi:10.1175/2009jas3339.1

Swart, S., S. Speich, I. J. Ansorge, G. J. Goni, S. Gladyshev, and J. R. E. Lutjeharms, 2008: Transport and variability of the antarctic circumpolar current south of africa. *J. Geophys. Res.-Oceans*, **113**. doi:10.1029/2007jc004223

Takahashi, T., S. C. Sutherland, R. A. Feely, and R. Wanninkhof, 2006: Decadal change of the surface water pco(2) in the north pacific: A synthesis of 35 years of observations. *J. Geophys. Res.-Oceans*, **111**. doi:10.1029/2005jc003074

Takahashi, T., et al., 2009: Climatological mean and decadal change in surface ocean pco(2), and net sea-air co2 flux over the global oceans (vol 56, pg 554, 2009). *Deep-Sea Res. Part I-Oceanogr. Res. Pap.*, **56**, 2075-2076

Tanaka, H. L., N. Ishizaki, and A. Kitoh, 2004: Trend and interannual variability of walker, monsoon and hadley circulations defined by velocity potential in the upper troposphere. *Tellus Series a-Dynamic Meteorology and Oceanography*, **56**, 250-269

Tanhua, T., A. Koertzinger, K. Friis, D. W. Waugh, and D. W. R. Wallace, 2007: An estimate of anthropogenic co(2) inventory from decadal changes in oceanic carbon content. *Proceedings of the National Academy of Sciences of the United States of America*, **104**, 3037-3042. doi:10.1073/pnas.0606574104

Tanhua, T., E. P. Jones, E. Jeansson, S. Jutterstrom, W. M. Smethie, D. W. R. Wallace, and L. G. Anderson, 2009: Ventilation of the arctic ocean: Mean ages and inventories of anthropogenic co2 and cfc-11. *J. Geophys. Res.-Oceans*, **114**, -

Timmermann, A., S. McGregor, and F. F. Jin, 2010: Wind effects on past and future regional sea level trends in the southern indo-pacific. *Journal of Climate*, **23**, 4429-4437. doi:10.1175/2010jcli3519.1

Tokinaga, H., and S.-P. Xie, 2011: Wave- and anemometer-based sea surface wind (waswind) for climate change analysis. *Journal of Climate*, **24**, 267-285. doi:10.1175/2010jcli3789.1

Toole, J. M., R. G. Curry, T. M. Joyce, M. McCartney, and B. Pena-Molino, 2011: Transport of the north atlantic deep western boundary current about 39 degrees n, 70 degrees w: 2004-2008. *Deep-Sea Research Part Ii-Topical Studies in Oceanography*, **58**, 1768-1780. doi:10.1016/j.dsr2.2010.10.058

Trenberth, K. E., and L. Smith, 2005: The mass of the atmosphere: A constraint on global analyses. *Journal of Climate*, **18**, 864-875. doi:10.1175/jcli-3299.1

Trenberth, K. E., J. T. Fasullo, and J. Kiehl, 2009: Earth's global energy budget. *Bull. Amer. Meteorol. Soc.*, **90**, 311-+. doi:10.1175/2008bams2634.1

Trenberth, K. E., J. T. Fasullo, and J. Mackaro, 2011: Atmospheric moisture transports from ocean to land and global energy flows in reanalyses. *Journal of Climate*, **24**, 4907-4924. doi:10.1175/2011jcli4171.1

Trenberth, K. E., et al., 2007: Observations: Surface and atmospheric climate change. *Climate change 2007: The physical science basis. Contribution of working group i to the fourth assessment report of the intergovernmental panel on climate change*, S. Solomon, et al., Eds., Cambridge University Press.

Tsimplis, M. N., and A. G. P. Shaw, 2010: Seasonal sea level extremes in the mediterranean sea and at the atlantic european coasts. *Natural Hazards and Earth System Sciences*, **10**, 1457-1475. doi:10.5194/nhess-10-1457-2010

Våge, K., et al., 2009: Surprising return of deep convection to the subpolar north atlantic ocean in winter 2007-2008. *Nat. Geosci.*, 67-72. doi:10.1038/ngeo382

Vargas-Yanez, M., et al., 2010: How much is the western mediterranean really warming and salting? *J. Geophys. Res.-Oceans*, **115**. doi:10.1029/2009jc005816

Vecchi, G. A., B. J. Soden, A. T. Wittenberg, I. M. Held, A. Leetmaa, and M. J. Harrison, 2006: Weakening of tropical pacific atmospheric circulation due to anthropogenic forcing. *Nature (London)*, **441**, 73-76. doi::10.1038/nature04744

Velicogna, I., 2009: Increasing rates of ice mass loss from the greenland and antarctic ice sheets revealed by grace. *Geophys. Res. Lett.*, **36**, 4. doi:L19503, 10.1029/2009gl040222

Vilibic, I., and J. Sepic, 2010: Long-term variability and trends of sea level storminess and extremes in european seas. *Global and Planetary Change*, **71**, 1-12. doi:10.1016/j.gloplacha.2009.12.001

von Schuckmann, K., and P. Y. Le Traon, 2011: How well can we derive global ocean indicators from argo data? *Ocean Sci.*, **7**, 783-791. doi:10.5194/os-7-783-2011

Wahlin, A. K., X. Yuan, G. Bjork, and C. Nohr, 2010: Inflow of warm circumpolar deep water in the central amundsen shelf. *Journal of Physical Oceanography*, **40**, 1427-1434. doi:10.1175/2010jpo4431.1

Wainwright, L., G. Meyers, S. Wijffels, and L. Pigot, 2008: Change in the indonesian throughflow with the climatic shift of 1976/77. *Geophys. Res. Lett.*, **35**. doi:10.1029/2007gl031911

Wakita, M., S. Watanabe, A. Murata, N. Tsurushima, and M. Honda, 2010: Decadal change of dissolved inorganic carbon in the subarctic western north pacific ocean. *Tellus B*, **62**, 608-620

Wang, C. Z., S. F. Dong, and E. Munoz, 2010: Seawater density variations in the north atlantic and the atlantic meridional overturning circulation. *Clim. Dyn.*, **34**, 953-968. doi:10.1007/s00382-009-0560-5

Wang, X., Y. Feng, and V. R. Swail, 2012: North atlantic wave height trends as reconstructed from the twentieth century reanalysis. *Geophys. Res. Lett.*, **submitted**

Wang, X. L. L., and V. R. Swail, 2006: Climate change signal and uncertainty in projections of ocean wave heights. *Clim. Dyn.*, **26**, 109-126. doi:10.1007/s00382-005-0080-x

Wang, X. L. L., V. R. Swail, F. W. Zwiers, X. B. Zhang, and Y. Feng, 2009: Detection of external influence on trends of atmospheric storminess and northern oceans wave heights. *Clim. Dyn.*, **32**, 189-203. doi:10.1007/s00382-008-0442-2

Wanninkhof, R., W. E. Asher, D. T. Ho, C. Sweeney, and W. R. McGillis, 2009: Advances in quantifying air-sea gas exchange and environmental forcing. *Annual Review of Marine Science*, **1**, 213-244

Wanninkhof, R., S. C. Doney, J. L. Bullister, N. M. Levine, M. Warner, and N. Gruber, 2010: Detecting anthropogenic co2 changes in the interior atlantic ocean between 1989 and 2005. *J. Geophys. Res.*, **115**. doi:10.1029/2010JC006251

WASA-Group, 1998: Changing waves and storm in the northern atlantic? *Bull. Amer. Meteorol. Soc.*, **79**, 741-760

Waters, J. F., F. J. Millero, and C. L. Sabine, 2011: Changes in south pacific anthropogenic carbon. *Global Biogeochemical Cycles*, **25**. doi:10.1029/2010gb003988

Watson, A. J., et al., 2009: Tracking the variable north atlantic sink for atmospheric co2. *Science*, **326**, 1391-1393. doi:10.1126/science.1177394

Watson, P. J., 2011: Is there evidence yet of an acceleration in mean sea level rise around mainland australia? *Journal of Coastal Research*, **27**, 368–377. doi:http://dx.doi.org/10.2112/JCOASTRES-D-10-00141.1

Waugh, D. W., T. M. Hall, B. I. McNeil, R. Key, and R. J. Matear, 2006: Anthropogenic co2 in the oceans estimated using transit-time distributions. *Tellus*, **58B**, 376-389. doi:doi:10.1111/j.1600-0889.2006.00222.x

Wentz, F. J., and L. Ricciardulli, 2011: Comment on "global trends in wind speed and wave height". *Science*, **334**, 905-905. doi:10.1126/science.1210317

Wentz, F. J., L. Ricciardulli, K. Hilburn, and C. Mears, 2007: How much more rain will global warming bring? *Science*, **317**, 233-235. doi:10.1126/science.1140746

Wenzel, M., and J. Schroeter, 2010: Reconstruction of regional mean sea level anomalies from tide gauges using neural networks. *J. Geophys. Res.-Oceans*, **115**. doi:10.1029/2009jc005630

Whitney, F. A., H. J. Freeland, and M. Robert, 2007: Persistently declining oxygen levels in the interior waters of the eastern subarctic pacific. *Prog. Oceanogr.*, **75**, 179-199. doi:10.1016/j.pocean.2007.08.007

Wijffels, S. E., et al., 2008: Changing expendable bathythermograph fall rates and their impact on estimates of thermosteric sea level rise. *Journal of Climate*, **21**, 5657-5672. doi:10.1175/2008jcli2290.1

Wild, M., 2009: Global dimming and brightening: A review. *Journal of Geophysical Research-Atmospheres*, **114**. doi:10.1029/2008jd011470

Wild, M., et al., 2005: From dimming to brightening: Decadal changes in solar radiation at earth's surface. *Science*, **308**, 847-850. doi:10.1126/science.1103215

Willis, J. K., 2010: Can in situ floats and satellite altimeters detect long-term changes in atlantic ocean overturning? *Geophys. Res. Lett.*, **37**. doi:10.1029/2010gl042372

Willis, J. K., D. Roemmich, and B. Cornuelle, 2004: Interannual variability in upper ocean heat content, temperature, and thermosteric expansion on global scales. *J. Geophys. Res.-Oceans*, **109**. doi:10.1029/2003jc002260

Willis, J. K., D. P. Chambers, and R. S. Nerem, 2008: Assessing the globally averaged sea level budget on seasonal to interannual timescales. *J. Geophys. Res.-Oceans*, **113**. doi:10.1029/2007jc004517

Willis, J. K., D. P. Chambers, C.-Y. Kuo, and C. K. Shum, 2010: Global sea level rise: Recent progress and challenges for the decade to come. *Oceanography*, **23**, 26 - 35

Wong, A. P. S., N. L. Bindoff, and J. A. Church, 1999: Large-scale freshening of intermediate waters in the pacific and indian oceans. *Nature*, **400**, 440-443

Wong, C. S., L. S. Xie, and W. W. Hsieh, 2007: Variations in nutrients, carbon and other hydrographic parameters related to the 1976/77 and 1988/89 regime shifts in the sub-arctic northeast pacific. *Prog. Oceanogr.*, **75**, 326-342. doi:10.1016/j.pocean.2007.08.002

Woodworth, P. L., 1990: A search for accelerations in records of european mean sea-level. *International Journal of Climatology*, **10**, 129-143. doi:10.1002/joc.3370100203

——, 1999: High waters at liverpool since 1768: The uk's longest sea level record. *Geophys. Res. Lett.*, **26**, 1589-1592. doi:10.1029/1999gl900323

Woodworth, P. L., and D. L. Blackman, 2004: Evidence for systematic changes in extreme high waters since the mid-1970s. *Journal of Climate*, **17**, 1190-1197

Woodworth, P. L., N. Pouvreau, and G. Woeppelmann, 2010: The gyre-scale circulation of the north atlantic and sea level at brest. *Ocean Sci.*, **6**, 185-190

Woodworth, P. L., M. Menendez, and W. R. Gehrels, 2011: Evidence for century-timescale acceleration in mean sea levels and for recent changes in extreme sea levels. *Surveys in Geophysics*, **32**, 603-618. doi:10.1007/s10712-011-9112-8

Woodworth, P. L., N. J. White, S. Jevrejeva, S. J. Holgate, J. A. Church, and W. R. Gehrels, 2009: Evidence for the accelerations of sea level on multi-decade and century timescales. *International Journal of Climatology*, **29**, 777-789. doi:10.1002/joc.1771

Wöppelmann, G., et al., 2009: Rates of sea-level change over the past century in a geocentric reference frame. *Geophys. Res. Lett.*, **36**. doi:10.1029/2009gl038720

Wu, L., et al., 2012: Enhanced warming over the global subtropical western boundary currents. *Nature Climate Change*, **2**, 161-166. doi:10.1038/nclimate1353

Wunsch, C., 2010: Variability of the indo-pacific ocean exchanges. *Dynamics of Atmospheres and Oceans*, **50**, 157-173. doi:10.1016/j.dynatmoce.2009.12.001

Xue, Y., B. Huang, Z.-Z. Hu, A. Kumar, C. Wen, D. Behringer, and S. Nadiga, 2010: An assessment of oceanic variability in the ncep climate forecast system reanalysis. *Clim. Dyn.*, **37**, 2541-2550. doi:10.1007/s00382-010-0954-4

Xue, Y., et al., 2012: A comparative analysis of upper ocean heat content variability from an ensemble of operational ocean reanalyses. *Journal of Climate*, **in press**. doi:10.1175/JCLI-D-11-00542.1

Yamamoto-Kawai, M., F. A. McLaughlin, E. C. Carmack, S. Nishino, K. Shimada, and N. Kurita, 2009: Surface freshening of the canada basin, 2003-2007: River runoff versus sea ice meltwater. *J. Geophys. Res.-Oceans*, **114**. doi:10.1029/2008jc005000

Yang, X. Y., R. X. Huang, and D. X. Wang, 2007: Decadal changes of wind stress over the southern ocean associated with antarctic ozone depletion. *Journal of Climate*, **20**, 3395-3410. doi:10.1175/jcli4195.1

Yashayaev, I., 2007: Hydrographic changes in the labrador sea, 1960-2005. *Prog. Oceanogr.*, **73**, 242-276. doi:10.1016/j.pocean.2007.04.015

Yashayaev, I., and J. W. Loder, 2009: Enhanced production of labrador sea water in 2008. *Geophys. Res. Lett.*, **36**. doi:10.1029/2008gl036162

Yoshikawa-Inoue, H., and M. Ishii, 2005: Variations and trends of co2 in the surface seawater in the southern ocean south of australia between 1969 and 2002. *Tellus Series B-Chemical and Physical Meteorology*, **57**. doi:10.1111/j.1600-0889.2005.00130.x

Young, I. R., S. Zieger, and A. V. Babanin, 2011: Global trends in wind speed and wave height. *Science*, **332**, 451-455. doi:10.1126/science.1197219

Yu, L., 2011: A global relationship between the ocean water cycle and near-surface salinity. *J. Geophys. Res.-Oceans*, **116**. doi:10.1029/2010jc006937

Yu, L., and R. A. Weller, 2007: Objectively analyzed air-sea flux fields for the global ice-free oceans (1981-2005). *Bull. Amer. Meteorol. Soc.*, **88**, 527-539

Yu, L. S., 2007: Global variations in oceanic evaporation (1958-2005): The role of the changing wind speed. *Journal of Climate*, **20**, 5376-5390. doi:10.1175/2007jcli1714.1

Yu, L. S., X. Z. Jin, and R. A. Weller, 2007: Annual, seasonal, and interannual variability of air-sea heat fluxes in the indian ocean. *Journal of Climate*, **20**, 3190-3209. doi:10.1175/jcli4163.1

Zhang, X., and J. A. Church, 2012: Sea level trend, interannual and decadal variability in the pacific ocean. *Geophys. Res. Lett.*, **submitted**

Chapter 3: Observations: Ocean

Coordinating Lead Authors: Monika Rhein (Germany), Stephen R. Rintoul (Australia)

Lead Authors: Shigeru Aoki (Japan), Edmo Campos (Brazil), Don Chambers (USA), Richard Feely (USA), Sergey Gulev (Russia), Gregory C. Johnson (USA), Simon A. Josey (UK), Andrey Kostianoy (Russia), Cecilie Mauritzen (Norway), Dean Roemmich (USA), Lynne Talley (USA), Fan Wang (China)

Contributing Authors: Michio Aoyama, Molly Baringer, Nicholas R. Bates, Timothy Boyer, Robert Byrne, Sarah Cooley, Stuart Cunningham, Thierry Delcroix, Catia M. Domingues, John Dore, Scott Doney, Paul Durack, Rana Fine, Melchor González-Dávila, Simon Good, Nicolas Gruber, Mark Hemer, David Hydes, Masayoshi Ishii, Stanley Jacobs, Torsten Kanzow, David Karl, Alexander Kazmin, Samar Khatiwala, Joan Kleypas, Kitack Lee, Eric Leuliette, Calvin Mordy, Jon Olafsson, James Orr, Alejandro Orsi, Geun-Ha Park, Igor Polyakov, Sarah G. Purkey, Bo Qiu, Gilles Reverdin, Anastasia Romanou, Raymond Schmitt, Koji Shimada, Lothar Stramma, Toshio Suga, Taro Takahashi, Toste Tanhua, Sunke Schmidtko, Karina von Schuckmann, Doug Smith, Hans von Storch, Xiaolan Wang, Rik Wanninkhof, Susan Wijffels, Philip Woodworth, Igor Yashayaev, Lisan Yu

Review Editors: Howard Freeland (Canada), Silvia Garzoli (USA), Yukihiro Nojiri (Japan)

Date of Draft: 5 October 2012

Notes: TSU Compiled Version

Figures

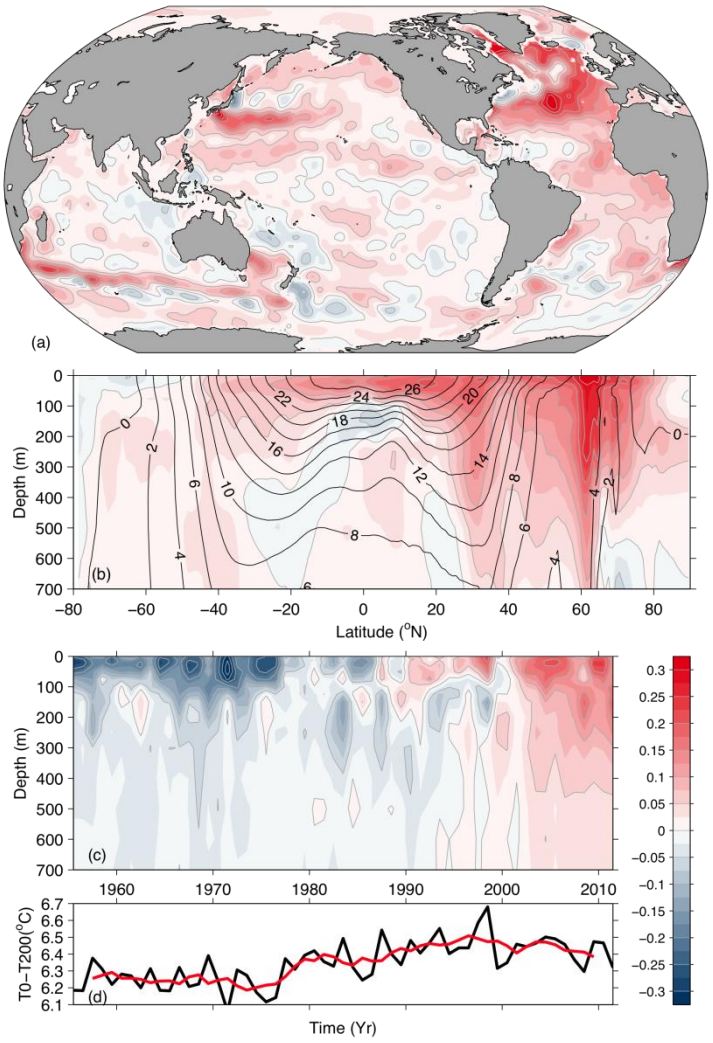

Figure 3.1: a) Depth-averaged 0–700 m temperature trend for 1971–2010 (longitude vs. latitude, colors and grey contours in °C per decade)**. b)** Zonally-averaged temperature trends (latitude versus depth, colors and grey contours in °C per decade) for 1971–2010, with zonally averaged mean temperature over-plotted (black contours in °C). **c)** Globally-averaged temperature anomaly (time versus depth, colors and grey contours in °C) relative to the 1971–2010 mean. **d)** Globally-averaged temperature difference between the ocean surface and 200-m depth (black: annual values, red: 5-year running mean). All plots are constructed from the annual analysis of Levitus et al. (2009).

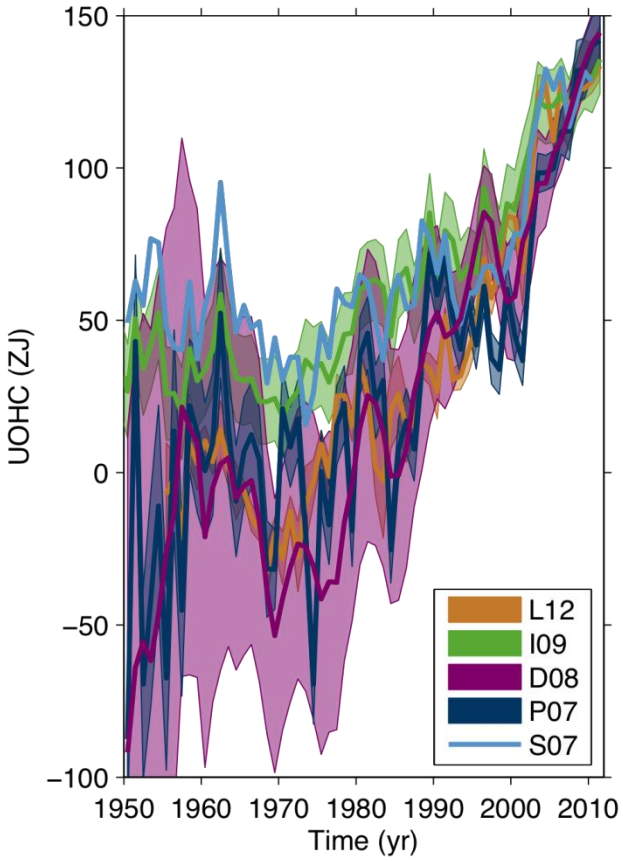

Figure 3.2: Observation-based estimates of annual global mean upper (0–700 m) ocean heat content in ZJ (1 ZJ = 10^{21} J) updated from (see legend): L12 (Levitus et al., 2012), I09 (Ishii and Kimoto, 2009), D08 (Domingues et al., 2008), P07 (Palmer et al., 2007), and S07 (Smith and Murphy, 2007), Uncertainties for each estimate (except for S07) are shaded, and plotted as published (at the one standard error level, except one standard deviation for L12, with no uncertainties provided for S07). Estimates are shifted to align for 2006–2010, 5 years of overlap well measured by Argo, and then plotted relative to the resulting mean of all curves for 1971, the starting year for trend calculations.

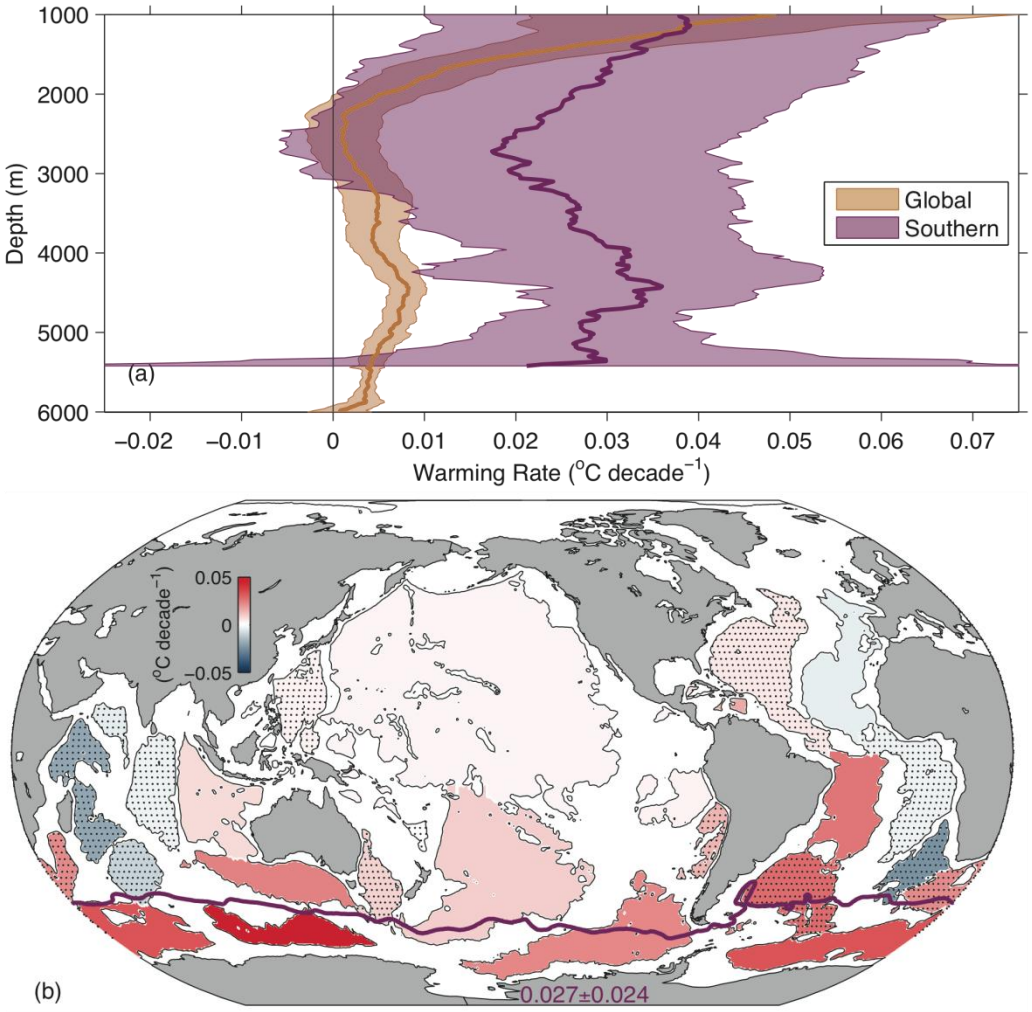

Figure 3.3: a) Areal mean warming rates versus depth (thick lines) with 95% confidence limits (shading), both global (orange) and for the Southern Ocean south of the Sub-Antarctic Front SAF (purple). **b)** Mean warming rate below 4000 m (colorbar) estimated for deep ocean basins (thin black outlines) and centred on 1992–2005. Stippled basin warming rates are not significantly different from zero at 95% confidence. The mean warming rate for 1000–4000 m south of the SAF (purple line) is also given (purple number) with its 95% confidence interval. Data from Purkey and Johnson (2010).

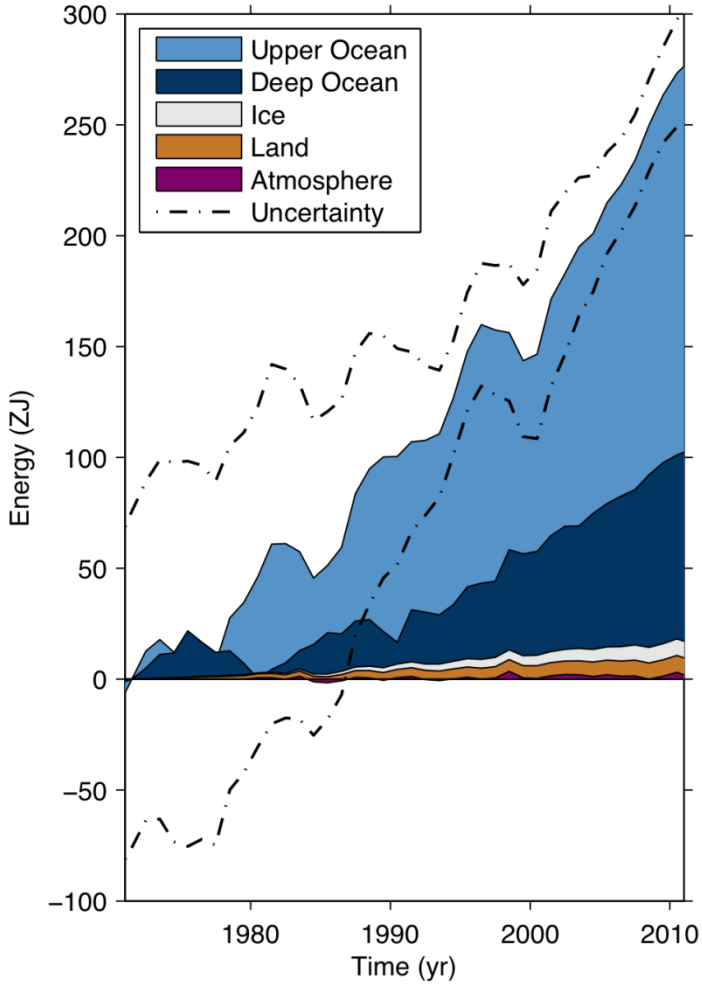

Box 3.1, Figure 1: Plot of energy change inventory in ZJ (1 ZJ = 10^{21} J) within distinct components of Earth's climate system relative to 1971 and from 1971–2010 unless otherwise indicated. See text for data sources. Ocean warming dominates, with the upper ocean (light blue, above 700 m) contributing more than the deep ocean (dark blue, below 700 m; with below 2000 m starting from 1992); ice melt (light grey; for glaciers and ice caps, Greenland starting from 1992, Antarctica starting from 1992, and Arctic sea ice from 1979–2008); continental (land) warming (orange); and atmospheric warming (purple; starting from 1979) make smaller contributions. The ocean uncertainty also dominates the total uncertainty (dot-dashed lines about the sum of all five components at 90% confidence intervals).

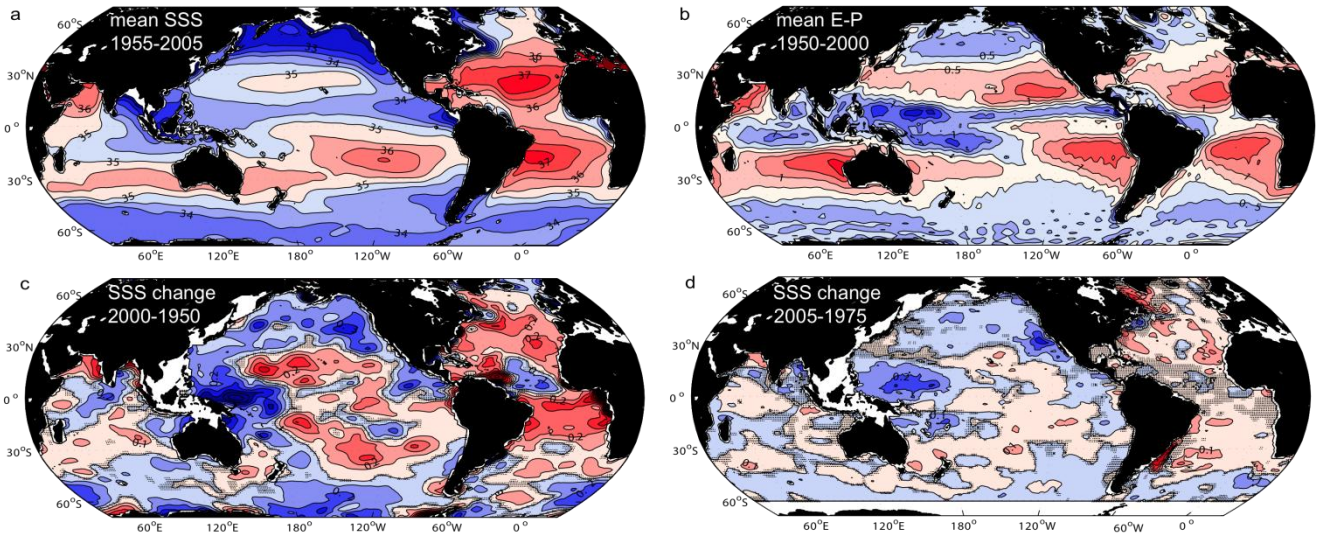

Figure 3.4: a) The 1955–2005 climatological-mean surface salinity (World Ocean Atlas 2009). Contours every 0.5 are plotted in black. **b)** Annual mean Evaporation-Precipitation averaged over the period 1950–2000 (NCEP). Contours every 0.5 m yr^{-1} are plotted in black. **c**) The 50-year (2000 minus1950) surface salinity change (Durack and Wijffels, 2010) and **d**) 30-year (2005 minus 1975) surface salinity change (Hosoda et al., 2009). Contours every 0.1 are plotted in black. Regions where the change is not significant at the 99% confidence level are stippled in grey.

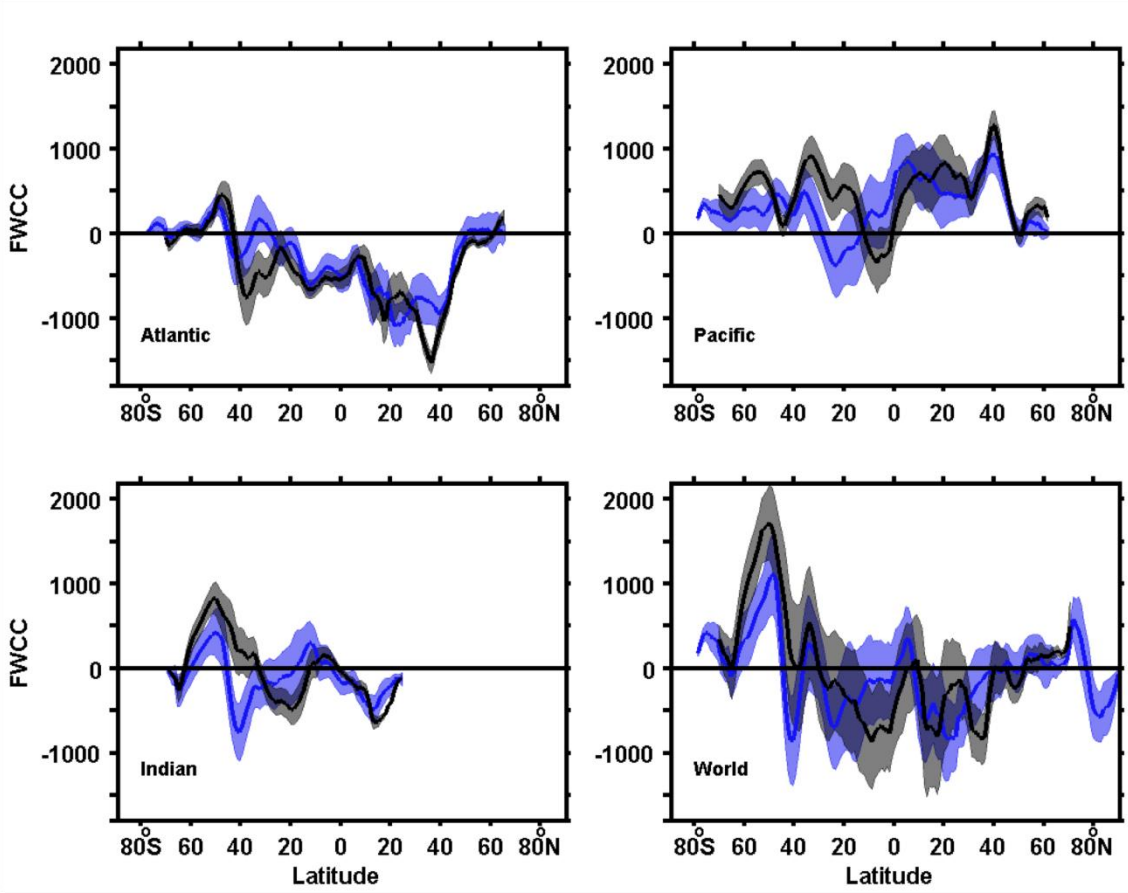

Figure 3.5: Zonally integrated freshwater content changes (km^3 per degree of latitude) for the latter half of the 20th century in the upper 500 m over the one-degree zonal belt of the Atlantic, Pacific, Indian, and World Oceans. The time period is from the late-1950s to 2000s (Boyer et al., 2005; blue lines) and 1950–2000 (Durack and Wijffels, 2010; black lines). Calculations are done according to the method of Boyer et al. (2007). Error estimates are 90% confidence intervals.

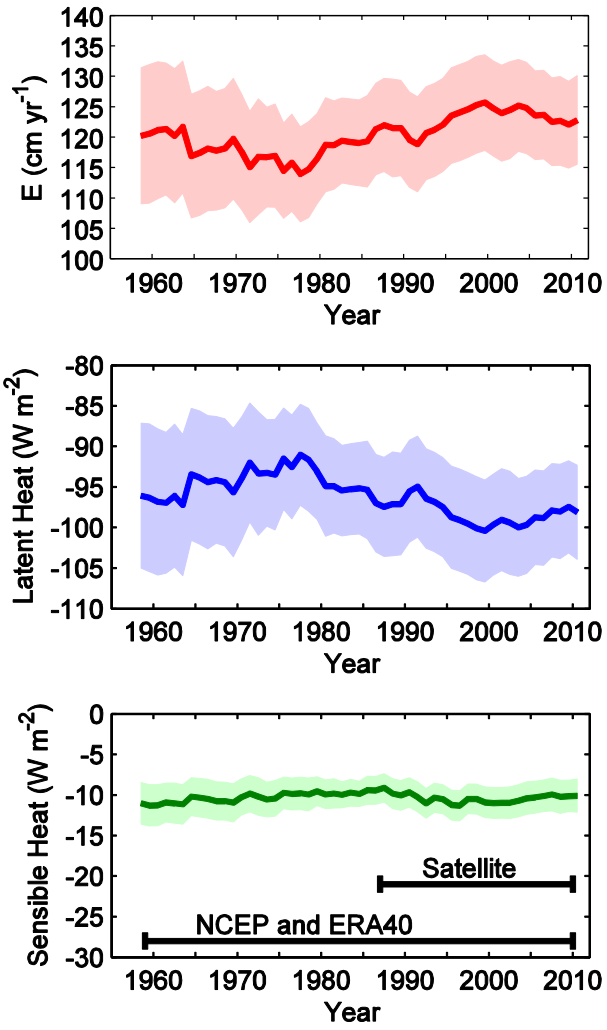

Figure 3.6: Time series of globally averaged annual mean ocean evaporation (E), latent and sensible heat flux from 1958 to 2010 determined from OAFlux. Shaded bands show uncertainty estimates; the time series have been updated to 2010 by Yu following the method described in Yu (2007). The error represents the spread of the input datasets used in the OAFlux analysis and is computed from their standard deviation. The black horizontal bars in the lower panel show the time periods for which NCEP and ERA40 reanalysis output and satellite observations were employed in the OAFlux analysis; they apply to all three panels.

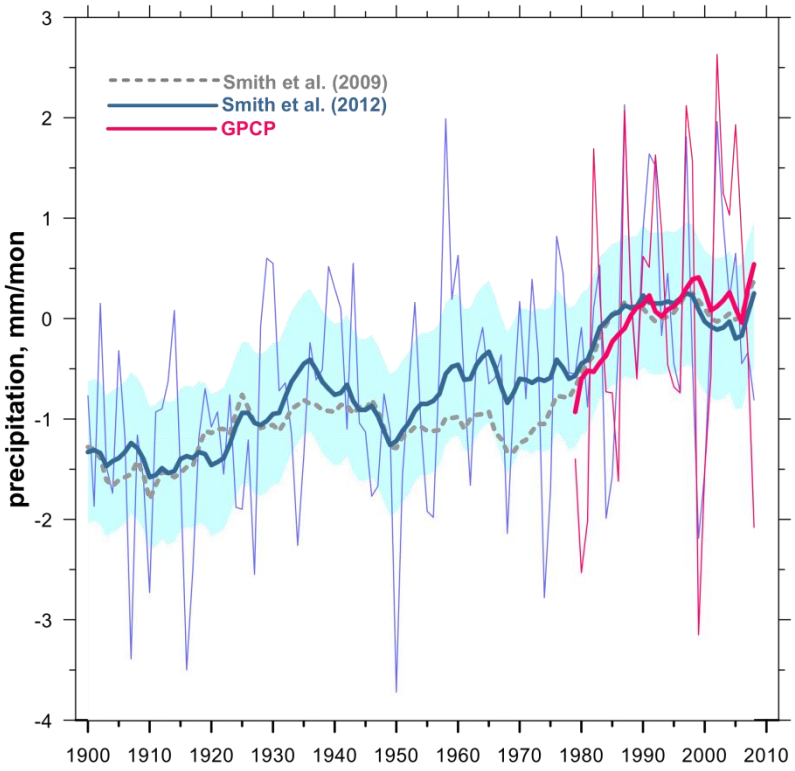

Figure 3.7: Long-term reconstruction of ocean precipitation over 75°S–75°N by Smith et al. (2012) (annual values–thin blue line, low-pass filtered data (15-year RM)–bold blue line) and Smith et al. (2009) (low-pass filtered data–dashed grey line). Also shown are GPCP-derived ocean precipitation over the same latitudinal range (annual values–thin magenta line, low-pass filtered data –bold magenta line). Precipitation anomalies were taken relative to the 1979–2008 period.

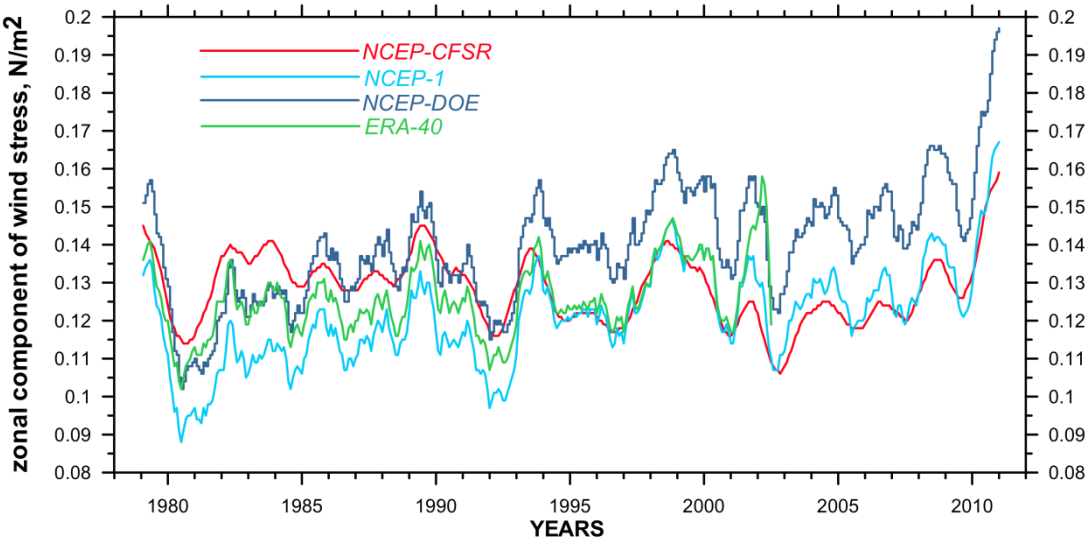

Figure 3.8: Time series of 1-year running mean of zonal mean wind stress over the Southern Ocean (45–70°S) for NCEP-CFSR (red), NCEP R1 (cyan, labelled NCEP-1), NCEP/NCAR R2 (dark blue line, labelled NCEP-DOE) and ERA-40 (green line). Units are N m^{-2} (Xue et al., 2010).

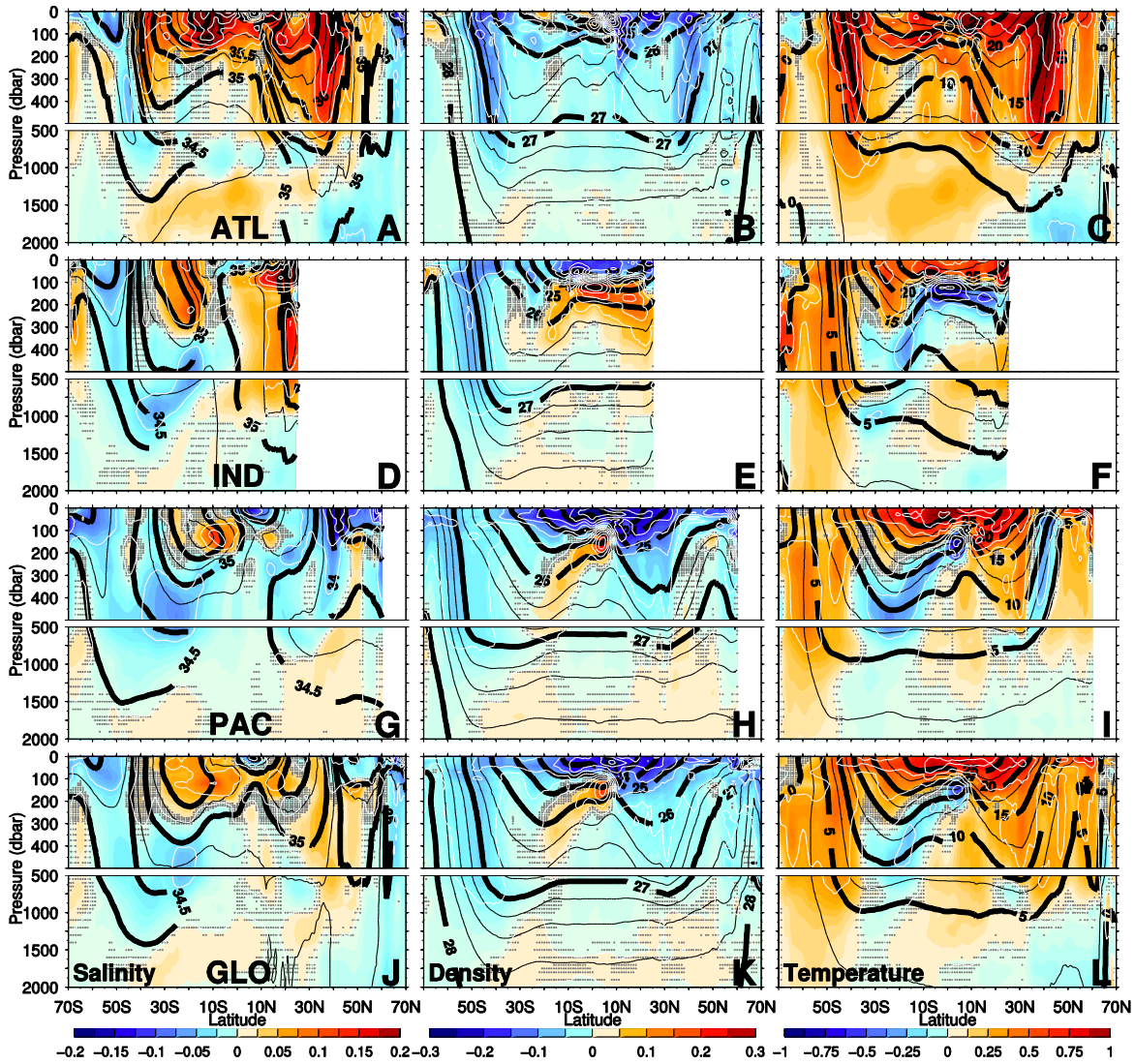

Figure 3.9: Upper 2000 m zonally averaged mean trend distribution, 1950–2000 (colours with white contours) of potential temperature (column 1), neutral density (column 2), and salinity (column 3), for the Atlantic Ocean (ATL) in row 1, Indian Ocean (IND), row 2, Pacific Ocean (PAC), row 3, and global ocean (GLO) in row 4. The mean fields are shown as black lines. Regions where the resolved linear trend is not significant at the 90% confidence level are stippled in gray.

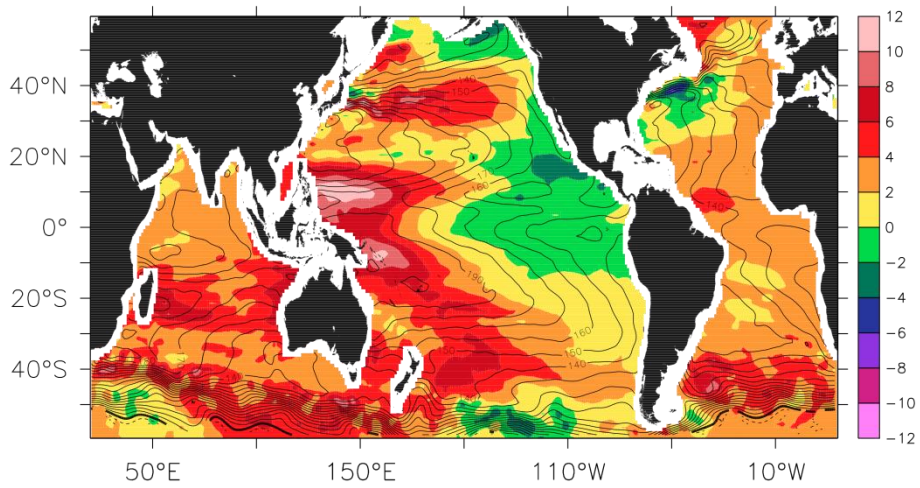

Figure 3.10: The mean SSH (black contours, 10 cm CI) for the Argo era is the sum of the geostrophic pressure field at 1000 m based on Argo trajectory data (Katsumata and Yoshinari, 2010) plus the relative pressure field (0/1000 dbar steric height) based on Argo profile data from Roemmich and Gilson (2009). The SSH trend (cm per decade, color shading) for the period 1993–2011 is based on the AVISO altimetry "reference" product (Ducet et al., 2000). Spatial gradients in the SSH trend are proportional to changes in surface geostrophic velocity.

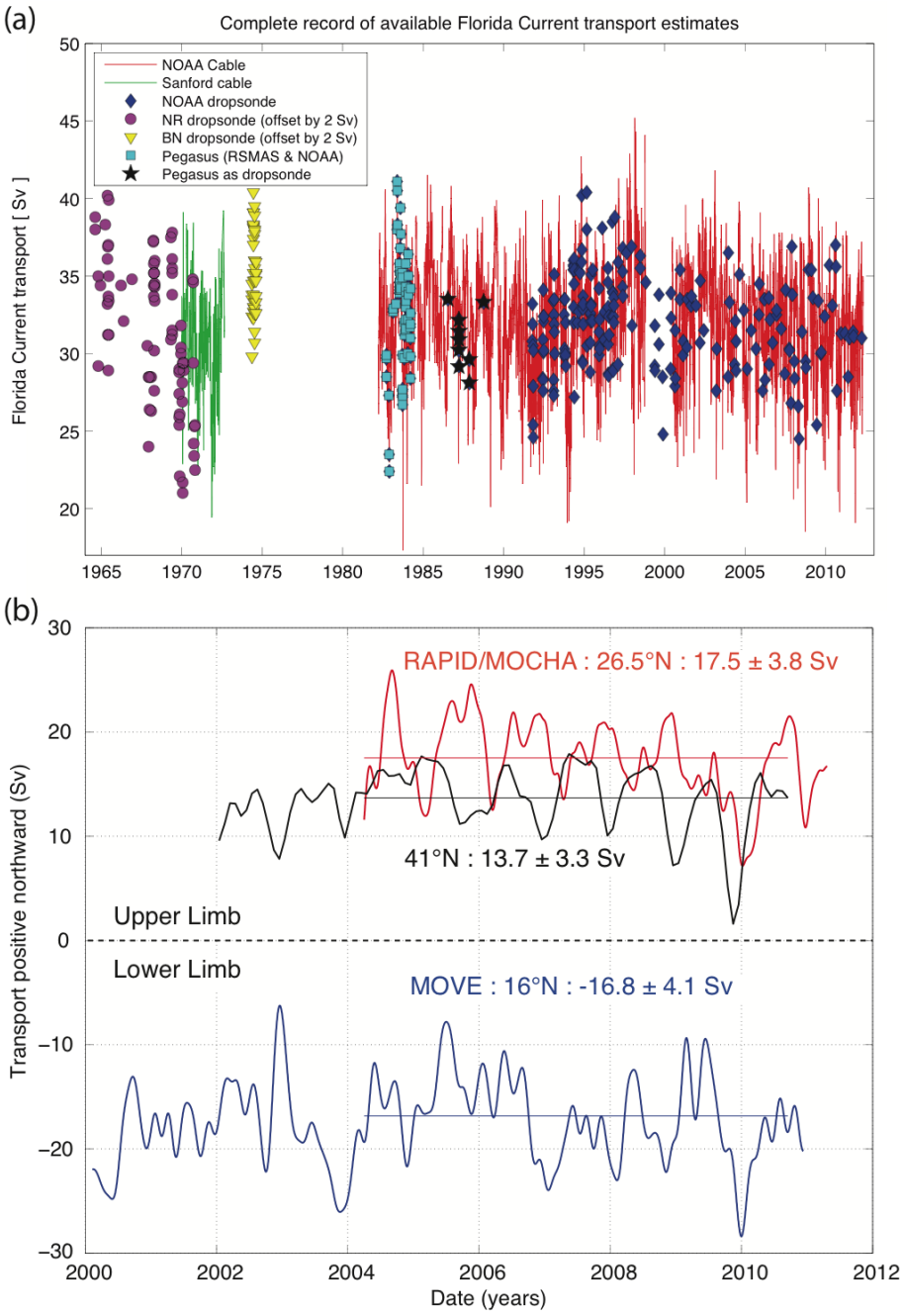

Figure 3.11: a) Volume transport of the Florida Current from dropsonde measurements (symbols) and cable voltages (continuous line), extending the time-series shown in Meinen et al. (2010) **b)** AMOC transport estimates in Sverdrups (Sv; where 1 Sv = 10^6 m^3 s^{-1}). 1. RAPID/MOCHA (Rapid Climate Change programme/Meridional Ocean Circulation and Heatflux Array) at 26.5°N (red): The array monitors the top-to-bottom Atlantic wide circulation, ensuring a closed mass balance across the section, and hence a direct measure of the upper and lower limbs of the AMOC. 2. 41°N (black): An index of maximum AMOC strength from Argo float measurements in the upper 2000 m only, combined with satellite altimeter data. The lower limb is not measured. 3. MOVE at 16°N (blue): Transport of North Atlantic Deep Water in the lower limb of the AMOC between 1100m and 4800m depth between the Caribbean and the mid-Atlantic Ridge. This transport is thought to be representative of maximum MOC variability based on model validation experiments. The temporal resolution of the three timeseries is ten days for 16°N and 26°N and one month for 41°N. In this figure the data have been three month low-pass filtered. The means and standard deviations for the common period of 2 April 2004 to 1 April 2010 are 17.5 ± 3.8 Sv, 13.7 ± 3.3 Sv and –16.8 ± 4.1 Sv for 26.5°N, 41°N and 16°N respectively. Means over this period are indicated by the horizontal line on each timeseries.

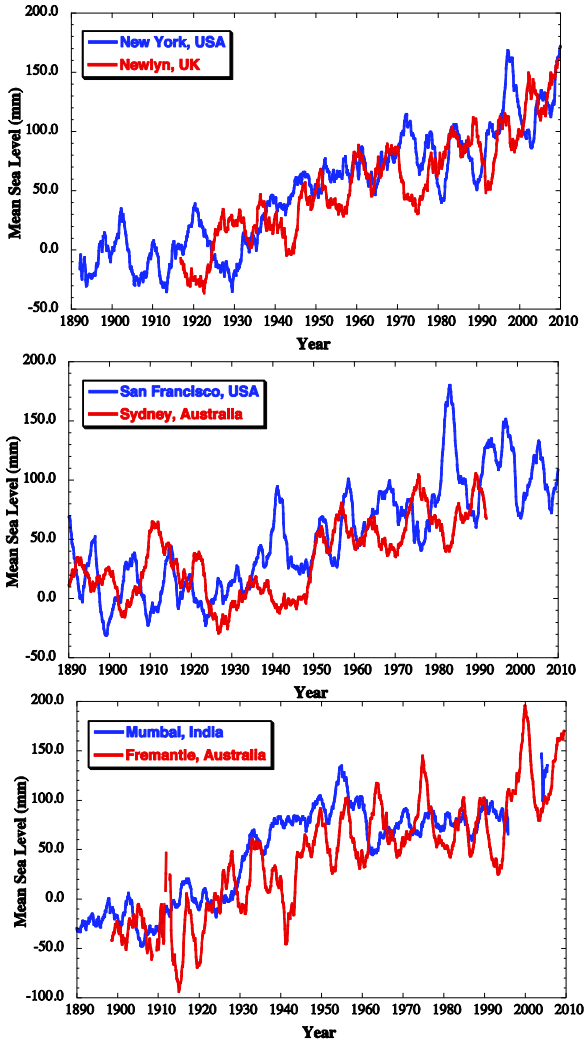

Figure 3.12: 3-year running mean sea level from long tide gauge records representing each ocean basin from the Permanent Service for Mean Sea Level (PSMSL), corrected for Glacial Isostatic Adjustment (GIA) (Peltier, 2004), after Woodworth et al. (2009).

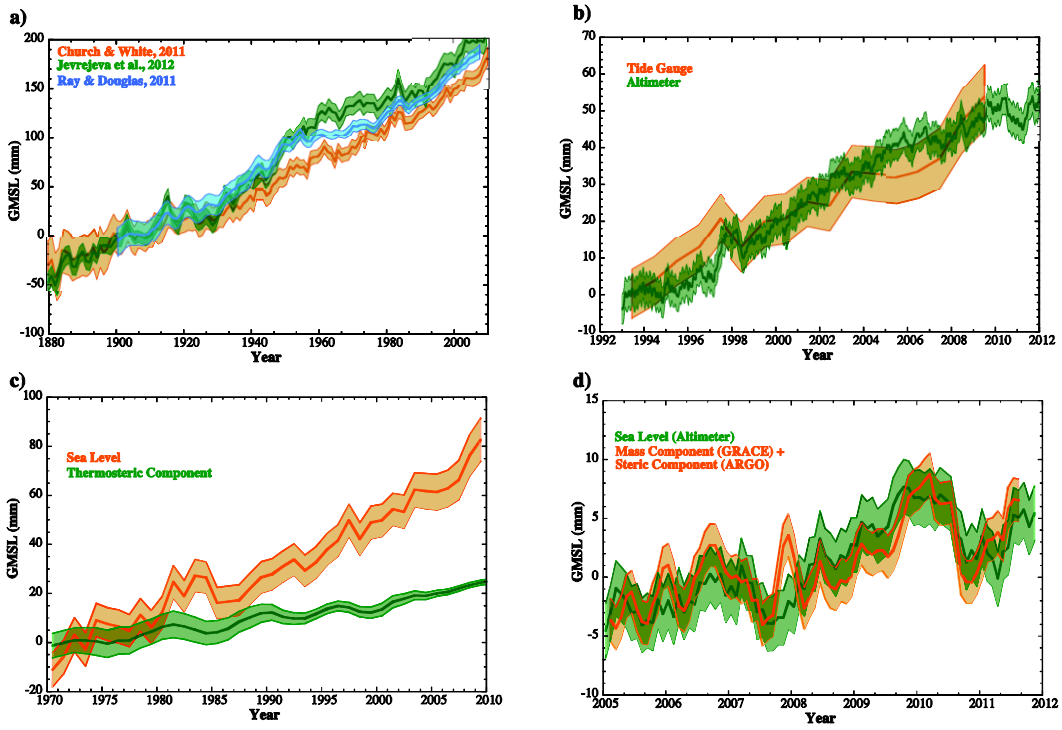

Figure 3.13: Global mean sea level from the different measuring systems as they have evolved in time. **a)** Yearly average GMSL reconstructed from tide gauges (1900–2010) by three different approaches (Church and White, 2011; Jevrejeva et al., 2012; Ray and Douglas, 2011), **b)** GMSL (1993–2010) from tide gauges, along with measurement from altimetry (Nerem et al., 2010) with seasonal variations removed and smoothed with a 60-day running mean **c)** GMSL (1970–2010) from tide gauges along with the thermosteric component, (3-year running mean) estimated from in situ temperature profiles (updated from Domingues et al., 2008), **d)** the GMSL (nonseasonal) from altimetry and that computed from the mass component (GRACE) and steric component (Argo) from 2005–2010 (Leuliette and Willis, 2011), all with a 3-month running mean filter. All uncertainty bars are one standard error as reported by the authors. The thermosteric component is just a portion of total sea level, and is not expected to agree individually with total sea level. The time-series are plotted relative to 5-year mean values that start at **a)** 1900, **b)** 1970, **c)** 1993, and **d)** 2005.

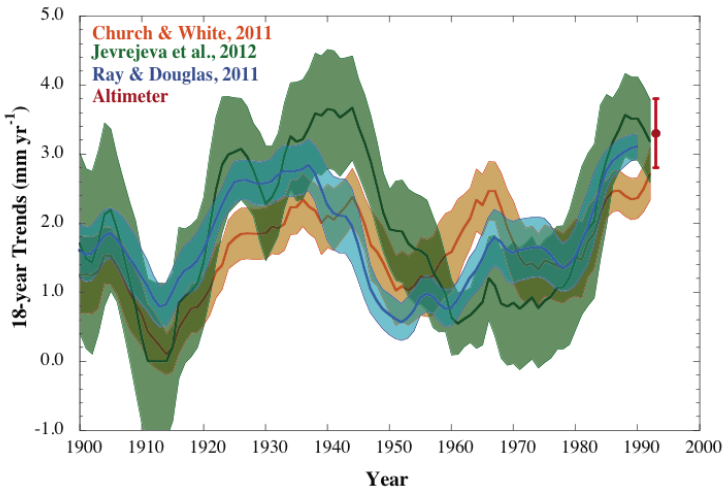

Figure 3.14: 18-year trends of GMSL rise estimated at 1-year intervals. The time is the start date of the 18-year period, and the shading represents the 90% confidence. The estimate from satellite altimetry is also given, with the 90% confidence given as an error bar.

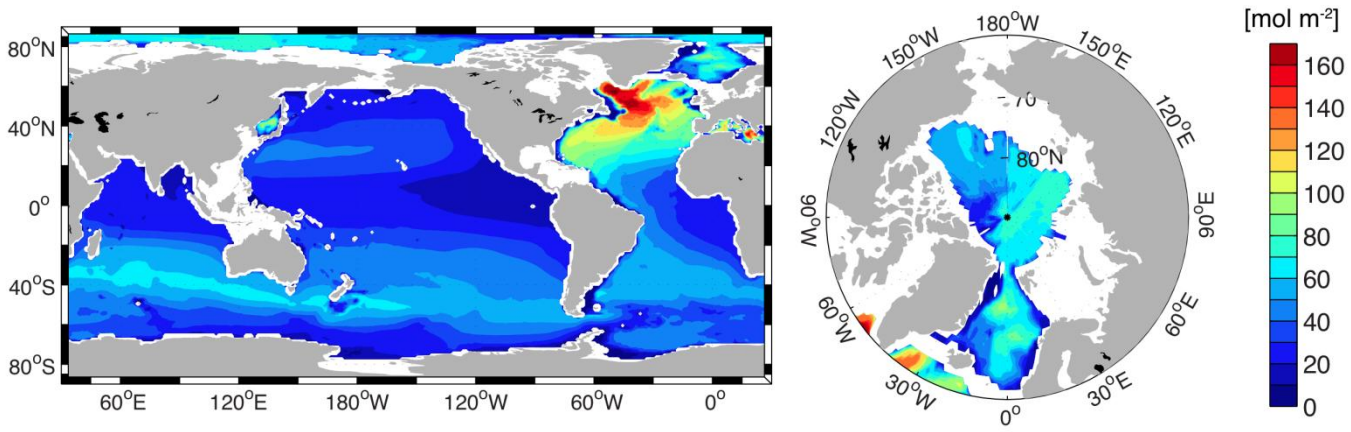

Figure 3.15: Compilation of the 2010 column inventories (mol m^{-2}) of anthropogenic CO_2: the global Ocean excluding the marginal seas (updated from Khatiwala et al., 2009) 150 ± 26 PgC; Arctic Ocean (Tanhua et al., 2009) 2.7–3.5 PgC; the Nordic Seas (Olsen et al., 2010) 1.0–1.6 PgC; the Mediterranean Sea (Schneider et al., 2010) 1.6–2.5 PgC; the East Sea (Sea of Japan) (Park et al., 2006) 0.40 ± 0.06 PgC. From Khatiwala et al. (2012).

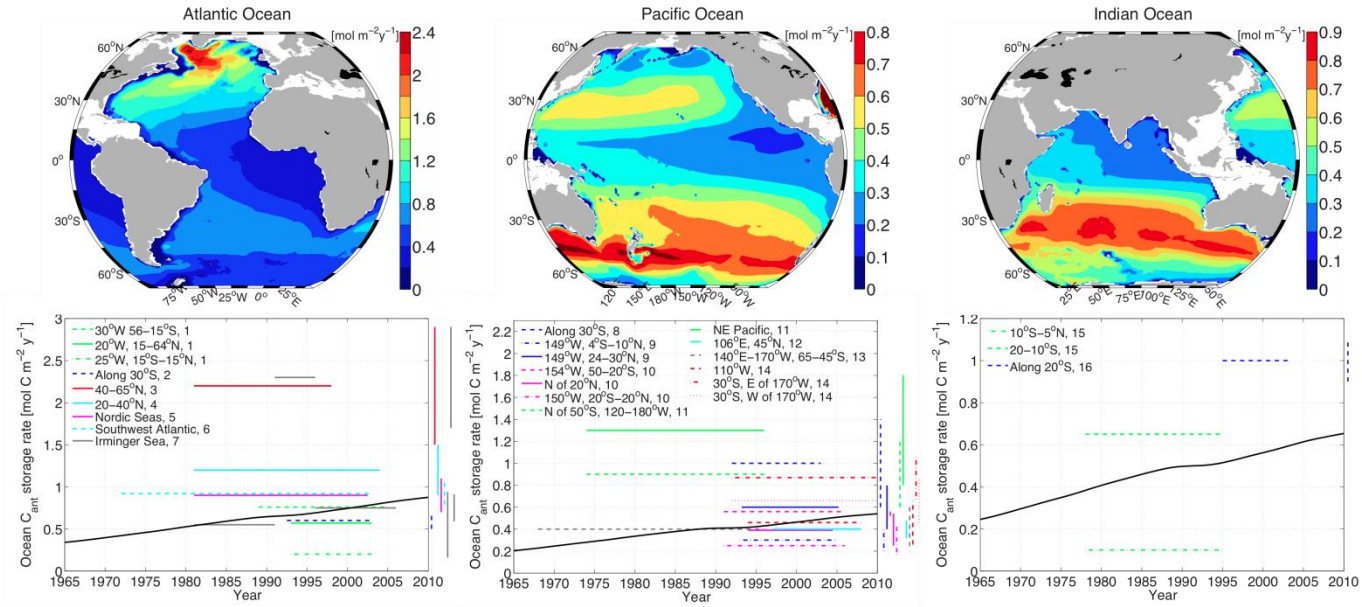

Figure 3.16: Top: Maps of storage rate distribution of anthropogenic carbon (mol m^{-2} yr^{-1}) for the three ocean basins (Left to right: Atlantic, Pacific, and Indian Ocean) averaged over 1980–2005 estimated by the Green's function approach (Khatiwala et al., 2009). Bottom: Corresponding storage rates as observed from repeat hydrography cruises. Measurements for the northern hemisphere are drawn as solid lines, the tropics as dash-dotted lines, and dashed lines for the southern hemisphere; the color schemes refer to different studies. Estimates of uncertainties are shown as vertical bars with matching colors. The solid black line represents the basin average storage rate using the same Green function approach (Khatiwala et al., 2009). Data sources as indicated in the legend are: 1) Wanninkhof et al. (2010), 2) Murata et al. (2008), 3) Friis et al. (2005), 4) Tanhua et al. (2007), 5) Olsen et al. (2006), 6) Rios et al. (2012), 7) Pérez et al. (2008), 8) Murata et al. (2007), 9) Murata et al. (2009), 10) Sabine et al. (2008), 11) Peng et al. (2003), 12) Wakita et al. (2010), 13) Matear and McNeil (2003), 14) Waters et al. (2011), 15) Peng et al. (1998), and 16) Murata et al. (2010). From Khatiwala et al. (2012).

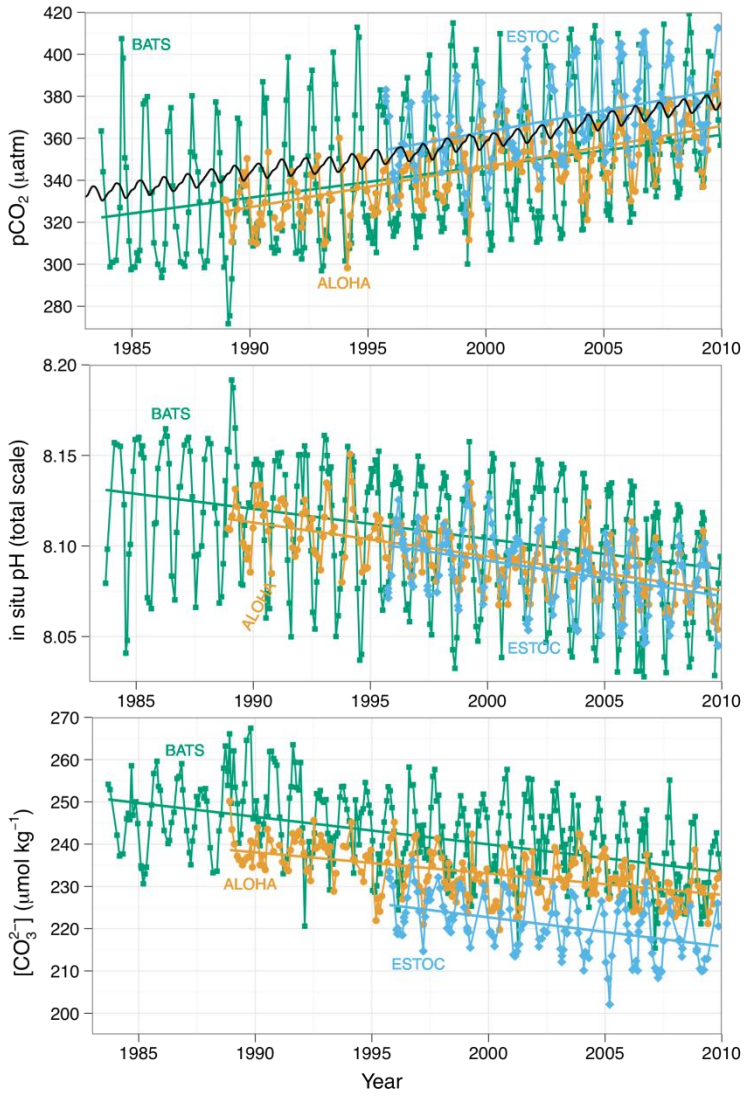

Figure 3.17: Long-term trends of surface seawater pCO_2 (top), pH (middle), and carbonate ion (bottom) concentration at three subtropical ocean time series in the North Atlantic and North Pacific Oceans, including: **a)** Bermuda Atlantic Time-series Study (BATS, 31°40′N, 64°10′W; **green**) and Hydrostation S (32°10′, 64°30′W) from 1983 to present (published and updated from Bates, 2007); **b)** Hawaii Ocean Time-series (HOT) at Station ALOHA (A Long-term Oligotrophic Habitat Assessment; 22°45′N, 158°00′W; **orange**) from 1988 to present (published and updated from Dore et al., 2009), and; **c)** European Station for Time series in the Ocean (ESTOC, 29°10′N, 15°30′W; **blue**) from 1994 to present (published and updated from González-Dávila et al., 2010). Atmospheric pCO_2 (**black**) from Hawaii is shown in the top panel. Lines show linear fits to the data, whereas Table 3.2 give results for harmonic fits to the data (updated from Orr, 2011).

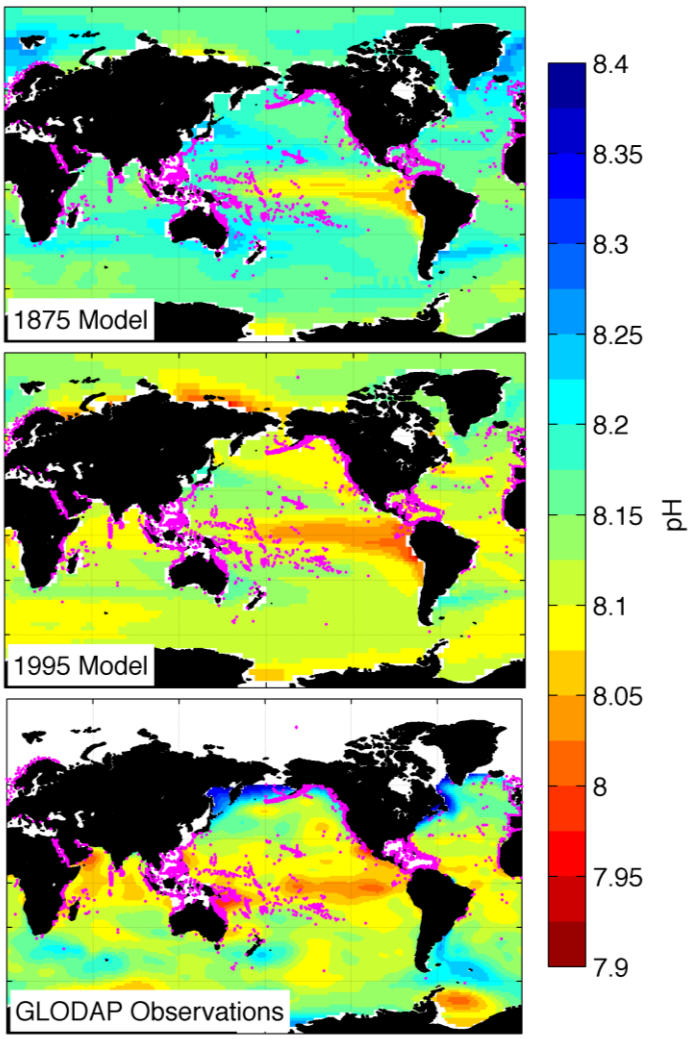

Box 3.2, Figure 1: National Center for Atmospheric Research Community Climate System Model 3.1 (CCSM3)-modeled decadal mean pH at the sea surface centered around the years 1875 (top) and 1995 (middle). Global Ocean Data Analysis Project (GLODAP)-based pH at the sea surface, nominally for 1995 (bottom). Deep and shallow-water coral reefs are indicated with magenta dots. White areas indicate regions with no data (after Feely et al., 2009).

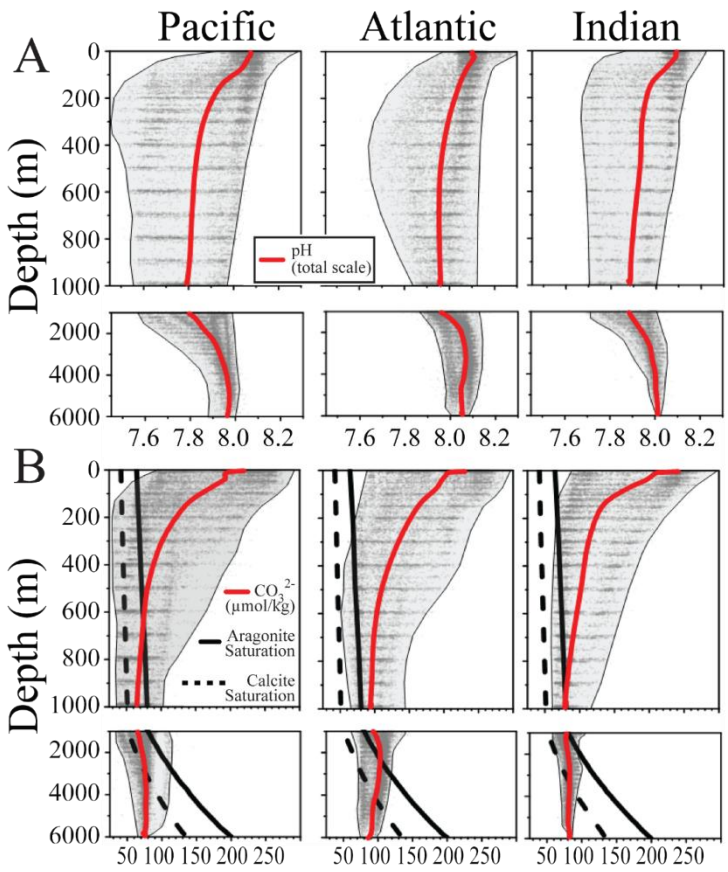

Box 3.2, Figure 2: Distribution of: **a)** pH and **b)** CO_3^{2-} ion concentration in the Pacific, Atlantic, and Indian Oceans. The data are from the World Ocean Circulation Experiment/Joint Global Ocean Flux Study/Ocean Atmosphere Carbon Exchange Study global CO_2 survey (Sabine, 2005). The lines show the mean pH (solid line top panel), aragonite (solid line bottom panel), and calcite (dashed line bottom panel) saturation CO_3^{2-} concentration for each of these basins (modified from Feely et al., 2009). The shaded areas show the range of values within the ocean basins. Dissolution of aragonite and calcite shells and skeletons occurs when CO_3^{2-} concentrations decrease below the saturation level.

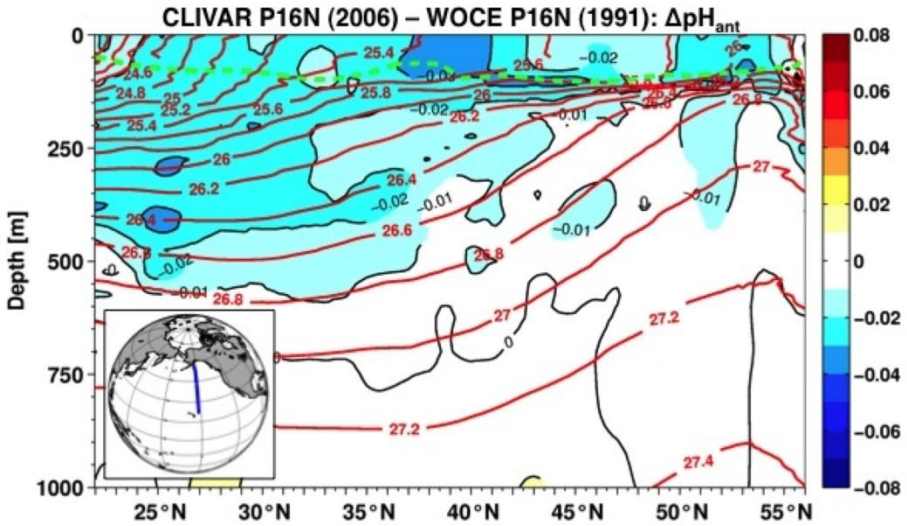

Figure 3.18: ΔpH_{ant}: pH change attributed to the uptake of anthropogenic carbon between 1991 and 2006, at about 150°W, Pacific Ocean (from Byrne et al., 2010). The red lines show the layers of constant density.

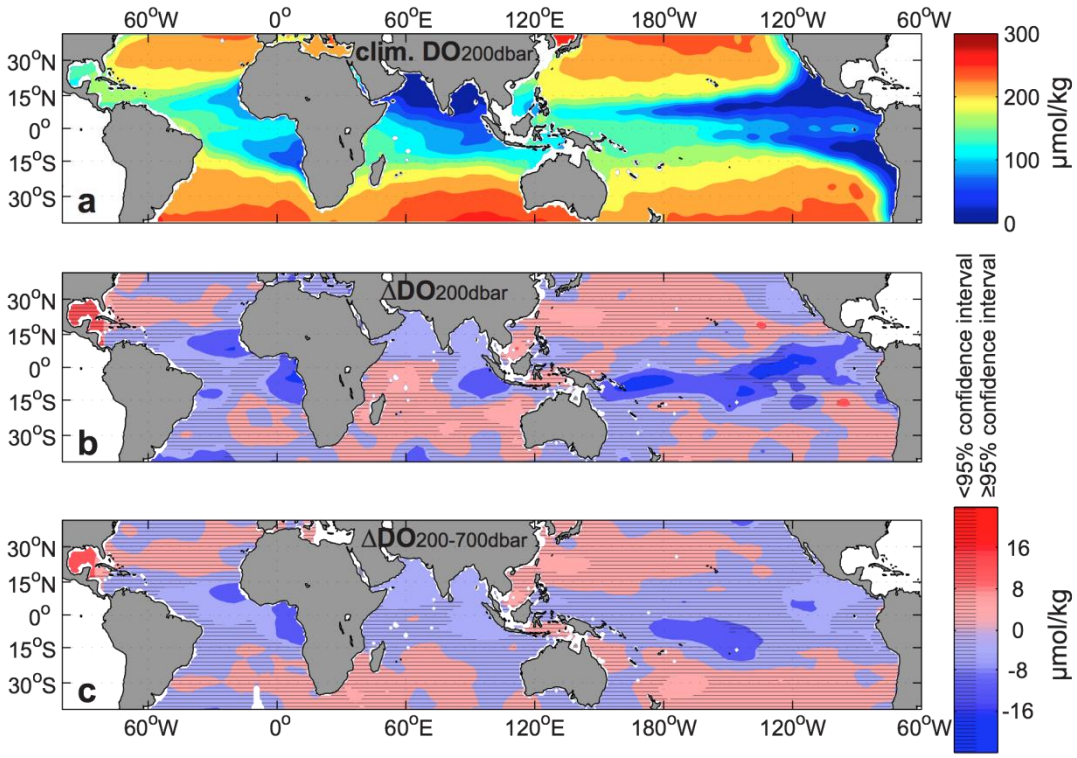

Figure 3.19: Dissolved oxygen (DO) distributions (in µmol kg^{-1}) between 40°S and 40°N for: **a)** the climatological mean (Boyer et al., 2006) at 200 dbar, as well as changes between 1960 and 1974 and 1990 and 2008 of **b)** dissolved oxygen (ΔDO) at 200 dbar, and **c)** ΔDO vertically-averaged over 200–700 dbar. In **b)-c)** increases are red and decreases blue, and areas with differences below the 95% confidence interval are shaded by black horizontal lines (after Stramma et al., 2010).

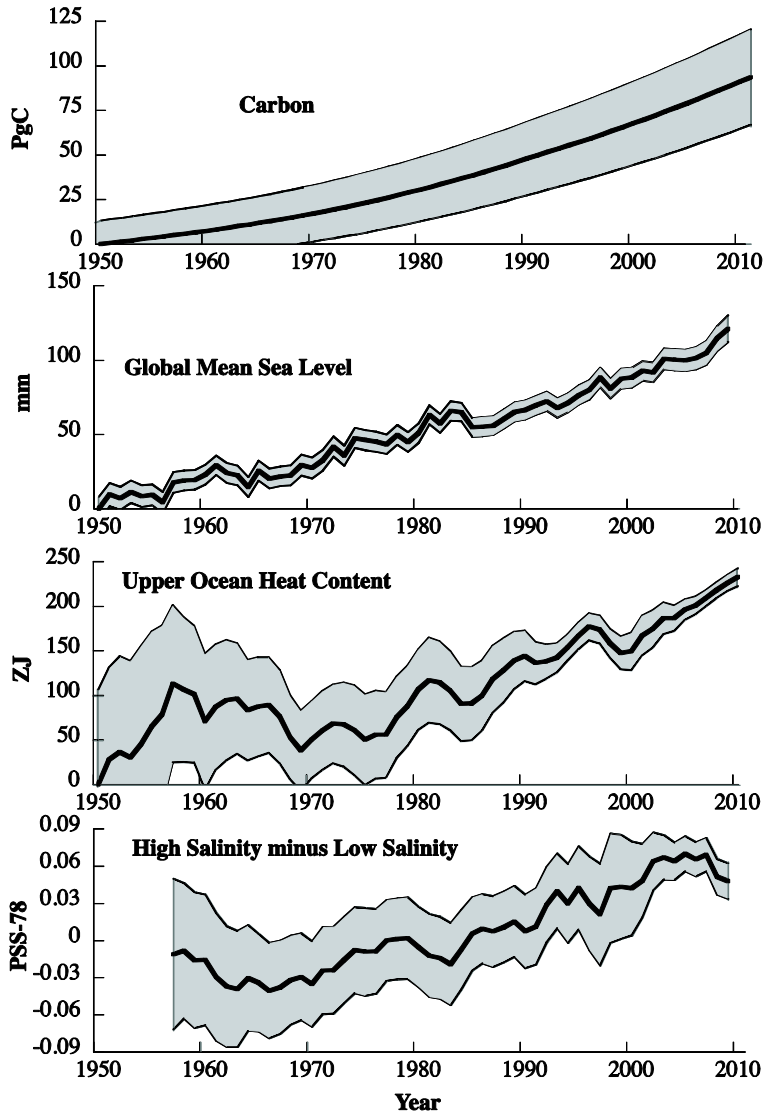

Figure 3.20: Time series of changes in large-scale ocean climate properties. Global ocean inventory of anthropogenic carbon dioxide is updated from Khatiwala et al. (2009). Global upper ocean heat content anomaly is updated from Domingues et al. (2008). Global mean sea level (GMSL) is from Church and White (2011). "High salinity" refers to the salinity averaged over regions where the sea surface salinity is greater than the global mean sea surface salinity from Boyer et al. (2009) and "Low Salinity" to an average over regions with values below the global mean.

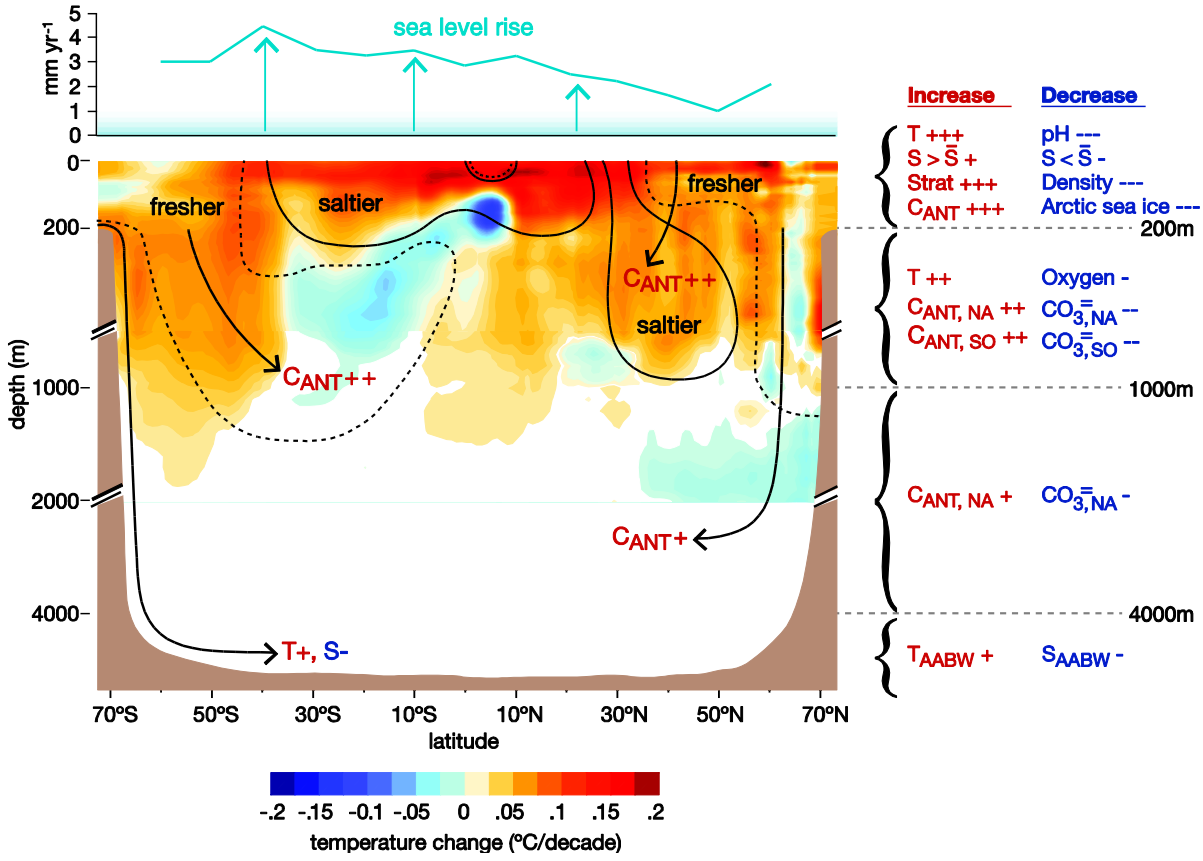

Figure 3.21: Summary of observed changes in zonal averages of global ocean properties. Temperature trends (°C decade^{-1}) are indicated in color (red = warming, blue = cooling); salinity trends are indicated by contour lines (dashed = fresher; solid = saltier) for the upper 2000 m of the water column (50-year trends from data set of Durack and Wijffels (2010); trends significant at >90% confidence are shown). Arrows indicate primary ventilation pathways. The top panel shows the zonal mean trend in sea level from 1993–2007 from satellite altimetry (Merrifield et al., 2009). Changes in other physical and chemical properties are summarised to the right of the figure, for each depth range (broken axes symbols delimit changes in vertical scale). Increases are shown in red, followed by a plus sign; decreases are shown in blue, followed by a minus sign; the number of + and–signs indicates the level of confidence associated with the observation of change (+++ = high confidence; ++ = medium confidence; + = low confidence). T = temperature, S = salinity, Strat = stratification, C_{ANT} = anthropogenic carbon, $CO_3^{=}$ = carbonate ion, NA = North Atlantic, SO = Southern Ocean, AABW = Antarctic Bottom Water. $S > \bar{S}$, refers to the salinity averaged over regions where the sea surface salinity is greater than the global mean sea surface salinity; $S < \bar{S}$, refers to the average over regions with values below the global mean.

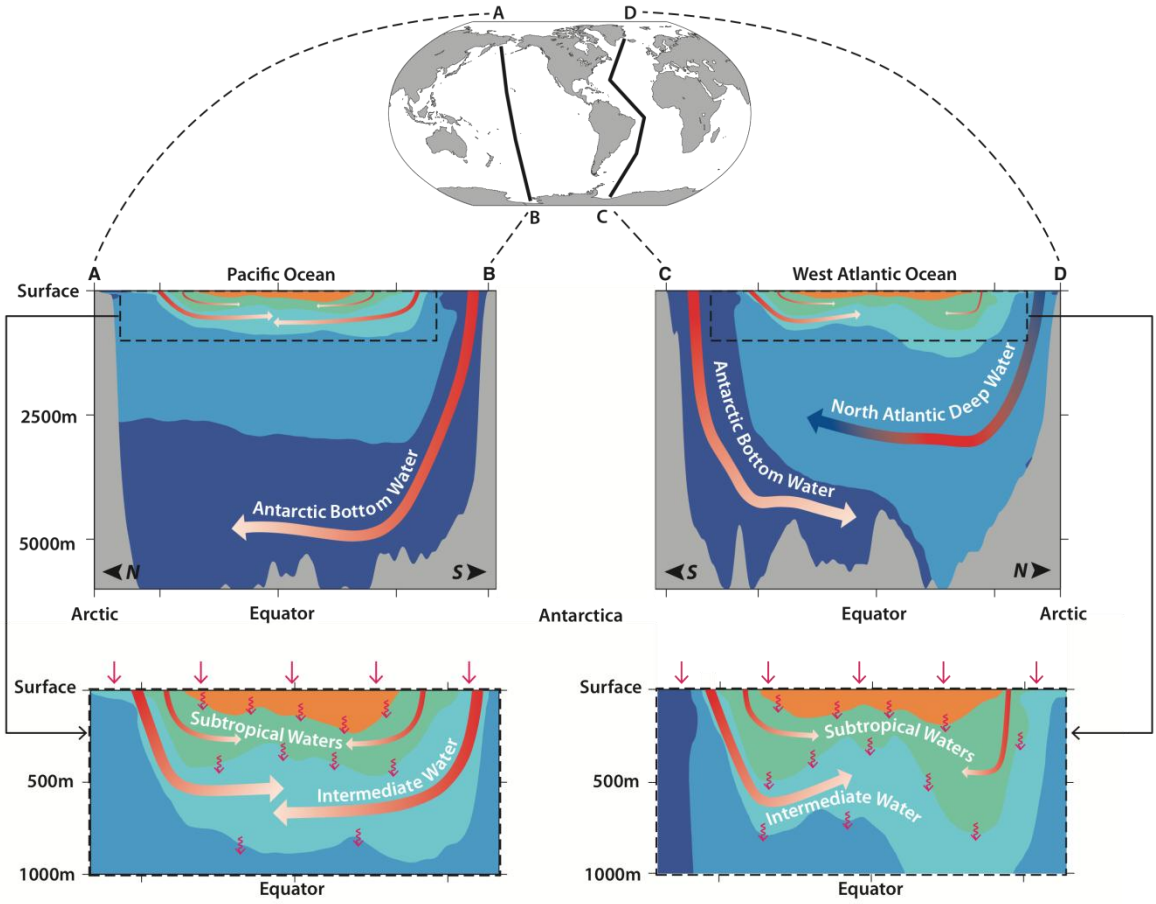

FAQ 3.1, Figure 1: Ocean heat uptake pathways. The ocean is stratified, with the coldest water in the deep ocean (upper panels, use map at top for orientation). Antarctic Bottom Water (dark blue) sinks around Antarctica and spreads northward along the ocean floor into the central Pacific (upper left panel, red arrows fading to white indicating stronger warming of the most recently-ventilated water) and western Atlantic oceans (upper right panel), as well as the Indian Ocean (not shown). North Atlantic Deep Water (lighter blue), slightly warmer and lighter, sinks in the northern North Atlantic Ocean (upper right panel, red and blue arrow indicating decadal warming and cooling) and spreads south above the Antarctic Bottom Water. Similarly, in the upper ocean (lower left panel shows Pacific Ocean detail, lower right panel the Atlantic) still-warmer Intermediate Waters (cyan) sink in sub-polar regions (red arrows fading to white indicating warming with time), then spread toward the equator under even warmer Subtropical Waters (green), which in turn sink (red arrows fading to white indicating stronger warming of the most recently-ventilated water) and spread toward the equator under tropical waters, the warmest and lightest (orange) in all three oceans. Excess heat or cold entering at the ocean surface (top straight red arrows) also mixes slowly downward (lower squiggly red arrows).

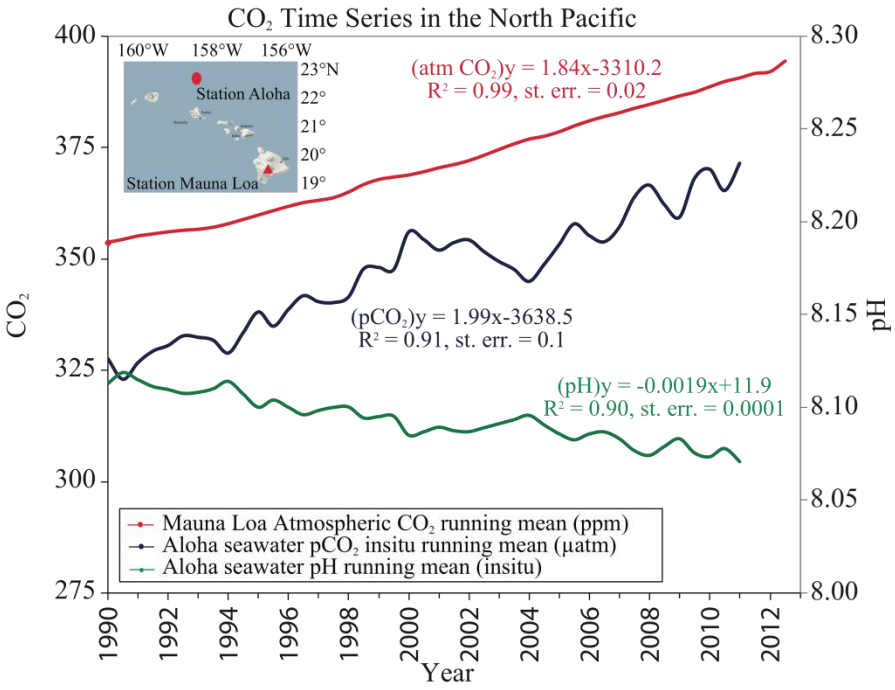

FAQ 3.2, Figure 1: Time series of atmospheric pCO_2 at the atmospheric Mauna Loa Observatory (top), surface ocean pCO_2 (middle), and surface ocean pH (bottom) on the island of Hawaii and Station ALOHA in the subtropical North Pacific north of Hawaii, 1988–2008 (after Doney et al., 2009; data from Dore et al., 2009).

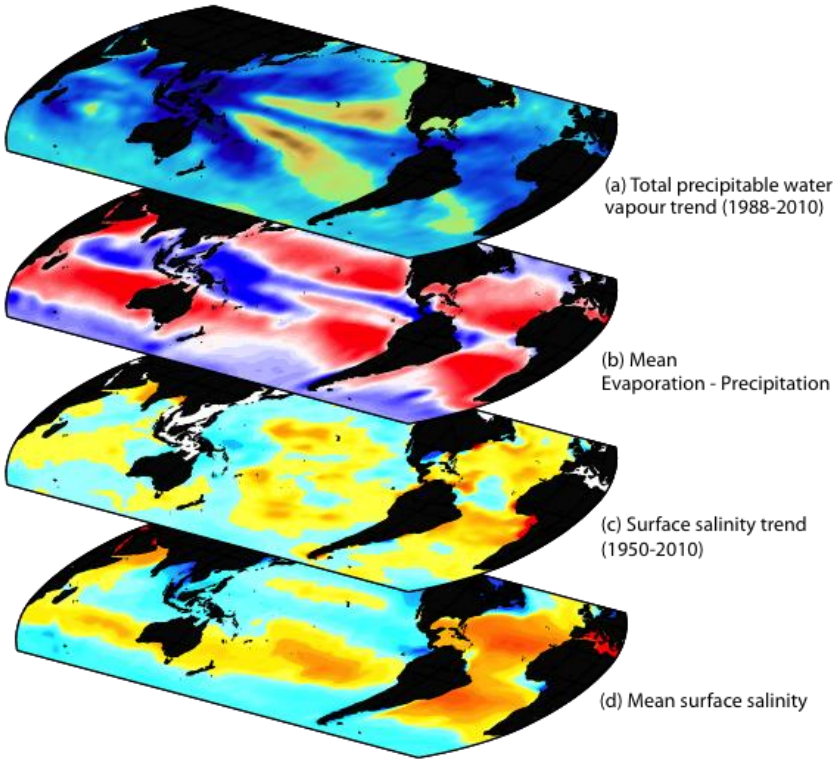

FAQ 3.3, Figure 1: Changes in sea surface salinity are related to the atmospheric patterns of Evaporation minus Precipitation (E-P) and trends in total precipitable water: a) Linear trend (1988 to 2010) in total precipitable water from Special Sensor Microwave Imager (after Wentz et al., 2007) (blues wetter; yellows drier). b) The 1979–2005 climatological mean net E-P (cm yr^{-1}) from NCEP (reds: net evaporation; blues: net precipitation). c) Trend (1950 to 2010) in surface salinity (after Durack and Wijffels, 2010) (blues freshening; yellows-reds saltier). d) The climatological-mean surface salinity (blues <35; yellows-reds >35).